Universitat Autònoma de Barcelona

STUDY AND DEVELOPMENT OF NEW BIOSENSORS BASED ON NANOPARTICLES AND NANOCHANNELS

By

Marisol Espinoza Castañeda

Thesis dissertation to apply for the PhD in Biotechnology

Department of Genetic and Microbiology

Autonomous University of Barcelona

Directors

Prof. Arben Merkoçi and Dr. Alfredo de la Escosura Muñiz

Nanobioelectronics and Biosensors Group

Institut Català de Nanociencia i Nanotecnologia (ICN2)

Tutor

Prof. Antoni Villaverde Corrales

2 0 1 4

The present thesis titled "***Study and development of new biosensors based on nanoparticles and nanochannels"*** presented by Marisol Espinoza Castañeda has been performed at the laboratories of the Nanobioelectronics and Biosensors Group at the *Institut Català de Nanociencia i Nanotecnologia* (ICN2), under the supervision of Prof. Arben Merkoçi and Dr. Alfredo de la Escosura Muñiz.

Directors

Prof. Arben Merkoçi	Dr. Alfredo de la Escosura Muñiz
ICREA Research Professor	Senior Researcher
Nanobioelectronics & Biosensors Group	Nanobioelectronics & Biosensors Group
Institut Català de Nanociència i Nanotecnologia (ICN2)	*Institut Català de Nanociència i Nanotecnologia (ICN2)*

Tutor

Prof. Antoni Villaverde Corrales

Marisol Espinoza Castañeda

Bellaterra, July 21st, 2014

Acknowledgment for the economic and logistic support

Nanobioelectronics a nd Biosensors Gr oup of the *Institut C atalà de N anociencia i Nanotecnologia* (ICN2) and also the *Ministerio de Educación Cultura y Deporte* of Spain for the grant given in the fr amework of the "*Programa de For mación de Profesorado Universitario*" (AP2010-5942) are acknowledged.

Acknowledgments are also given fo r the fina ncial supports from se veral institutions / programs: MEC (Ma drid) for the projects AGL2009-07328 a nd MAT2011 -25870 a nd the NATO Science for Peace and Security Programme's support under the project SfP98380; EU's support under FP7 contract number 246513 ''NADINE; *Hospital Sant J oan de Deù* (Barcelona, Spain); EMPA, Swiss Federal Laboratories for Materials Science and Technology (Thun, Switzerland).

HOSPITAL MATERNOINFANTIL – UNIVERSITAT DE BARCELONA

Thesis Overview

A general overview about the use of nanomaterials in electrochemical biosensing, focusing on gold nanoparticles (AuNPs), Prussian blue nanoparticles (PBNPs) and nanochannels is given in **Chapter 1**. A special emphasis is given to the approaches based on solid-state nanochannel array devices (nanoporous membranes) including the state-of-the-art of their applications in biosensing.

The general and detailed objectives of this thesis are described in **Chapter 2**.

Chapter 3 presents the results obtained for the synthesis and characterization of gold nanoparticles (AuNPs 20 nm sized) modified with k-casein derived peptides for the fimbriae bacteria recognition and quantification, taking advantage of the peptide effect as bacterial adhesion inhibitor. This peptide-based nanoparticle assay takes advantage of the dual character of the AuNPs: as carrier of the biorecognition molecule and as electrocatalytic label, allowing the evaluation of the pathogen bacteria-peptide interaction in a simple and rapid way through the chronoamperometric monitoring of the hydrogen evolution reaction (HER) on screen-printed carbon electrodes.

Chapter 4 describes the study of a novel, cheap, disposable and single-use assembled nanoparticles-based nanochannel platform for label-free immunosensing. This sensing device is based on the deposition of a homogeneous monolayer of carboxylated polystyrene nanospheres onto the working area of homemade screen-printed ITO/PET electrodes by dip-coating. The spaces between the self-assembled nanospheres generate well-ordered

nanochannels, which are blocked upon the immunocomplex formation. Proteins are detected through the monitoring of the blockage in the channels, which is evaluated by the decrease in the voltammetric signal of a typical red-ox indicator. The developed device represents an integrated and simple biodetection system which overcomes many of the limitations of previously reported nanochannels-based approaches representing a really disposable biosensing device for a one-step sensing application. The work described in this chapter is done in collaboration with EMPA (Swiss Federal Laboratories for Materials Science and Technology).

The development and study of a novel nanochannel array device, that operates through Prussian blue nanoparticles (PBNPs) as red-ox indicator for sensitive label free immunodetection of a cancer biomarker is presented in **Chapter 5**. Stable and narrow-sized (around 4 nm) PBNPs, protected by polyvinylpyrrolidone, exhibit a well-defined and reproducible red-ox behavior and are successfully applied for the voltammetric evaluation of the nanochannels (20 nm pore sized) blockage due to the immunocomplex formation. This novel and effective technology for the detection of small proteins captured inside the nanochannels is successfully applied for the quantification of a cancer biomarker (parathyroid hormone-related protein, PTHrP).

In **Chapter 6** the general conclusions and the future perspectives are discussed

Finally, in the context of the development of nanochannel array-based integrated systems, **Annex 1** describes the preliminary results related to the use of nanoimprint lithography (NIL) for the nanochannels creation onto ITO/PET electrodes. In addition, **Annex 2** describes preliminary studies related to the *in-situ* detection of protein biomarkers secreted by cells cultured onto nanoporous membranes.

Resumen

En el **capítulo 1**, se presenta una introducción general sobre el uso de nanomateriales en sistemas de biosensores electroquímicos, centrada principalmente en nanopartículas de oro y de Azul de Prusia así como en nanocanales. En este capítulo se detallan también en profundidad las aplicaciones de los sistemas basados en nanocanales de estado sólido (membranas nanoporosas).

En el **capítulo 2** se detallan los objetivos generales y específicos de esta tesis.

En el **capítulo** 3 se muestran los resultados obtenidos sobre la síntesis y caracterización de nanopartículas de oro (20 nm) modificadas con péptidos derivados de k-caseina para su uso en el reconocimiento y cuantificación de bacterias patógenas, aprovechando sus propiedades como inhibidores de la adhesión bacteriana. En este trabajo se aprovecha la capacidad que tienen las AuNPs para actuar tanto como portadores del péptido como de marcadores electroactivos, permitiendo la evaluación de la interacción bacteria patógena-péptido de un modo simple y rápido gracias a la medición cronoamperométrica de la reacción de evolución de hidrógeno sobre electrodos serigrafiados de carbono.

En el **capítulo 4** se describe el estudio de una nueva plataforma nanoporosa basada en el ensamblaje de nanoesferas, para el desarrollo de inmunosensores electroquímicos que no requieren el uso de marcadores. El sistema sensor se prepara mediante la deposición recubrimiento por inmersión, sobre la superficie de electrodos serigrafiados ITO/PET, formando una monocapa homogénea de nanoesferas de poliestireno carboxiladas. Los

espacios entre las nanopartículas generan nanocanales bien ordenados, que se bloquean a través de la formación de inmunocomplejos. Las proteínas se detectan midiendo el descenso en la señal electroquímica de un indicador red-ox convencional ($Fe^{2/3}$), debido al bloqueo de los nanocanales. El sistema desarrollado es simple, rápido y altamente integrado, permitiendo superar las limitaciones de sistemas basados en nanocanales propuestos anteriormente.

En el **capítulo 5** se presenta un biosensor novedoso basado en el uso de nanocanales en combinación con nanopartículas de azul de Prusia como indicadores redox para la detección de proteínas biomarcadoras de cáncer, sin necesidad del uso de marcadores. La suspensión estable y homogénea de nanopartículas de azul de Prusia (4 nm) obtenidas, protegidas por polivinilpirrolidona, muestran un par de picos re-dox bien definidos y reproducibles, por lo que estas nanopartículas se aplican con éxito para la evaluación voltamperométrica del bloqueo de los nanocanales (20 nm de diámetro de poro) debido a la formación del immunocomplejo. Esta novedosa tecnología permite la captura de proteínas de bajo peso molecular dentro de los canales y su posterior detección a niveles de ng/mL, como es el caso del biomarcador de cáncer PTHrP, por sus siglas en ingles, (proteína vinculada a la hormona paratiroidea).

En el **capítulo 6** se discuten las conclusiones generales de la tesis y las perspectivas futuras.

Finalmente, en el contexto del desarrollo de sistemas biosensores integrados basados en nanocanales de estado sólido, en el **anexo 1** se muestran los resultados preliminares relacionados con la detección *in-situ* de proteínas biomarcadoras secretadas por células cultivadas sobre la superficie de membranas nanoporosas. Por otro lado, en el **anexo 2** se

muestran los resultados preliminares relacionados con el uso de litografía de nanoimpresión para la creación de nanocanales en electrodos de ITO/PET.

Index

Chapter 1.

Introduction

Chapter 1. Introduction

1.1. Electrochemical biosensors and nanomaterials

Biosensing represents the recognition of an analyte (chemical or biochemical) through the use of an immobilized (bio)receptor (ex. enzyme, antibody, cell etc.). The possible change during the recognition event (occurring at the transducer) can be optical, electrical, mass etc. Between various kinds of the generated signals the electrical/electrochemical one shows advantages of related instruments simplicity, moderate cost and portability. The purpose of the electrochemical transducer is to convert the biological recognition event between the analyte and the receptor into a useful electrical signal that can be easily transformed to a quantitative or qualitative analytical one [1].

Electrochemical devices have traditionally received the major share of the attention in biosensor development [2] and recently are getting an increased attention with the advances in nanoscience and nanotechnologies in general and especially recent development in nanomaterials (NMs) field.

A wide variety of NMs, especially nanoparticles (normally in the range of 1 - 100 nm) with different properties have found broad application in analytical methods [3]. NMs are being increasingly used for the development of electrochemical biosensors, due to their interesting qualities ranging from unique electrocatalytic properties shown in nanoscale, capability to be easily linked with various polymers and bioactive molecules (e.g., antibodies, DNA and other receptors). In addition, NMs can interface biological recognition events with electronic signal transduction while being used as labels [4].

Due to their high specificity, speed, portability, and low cost, NM-based electrochemical biosensors offer exciting opportunities for numerous applications in biomedical fields [5].

Given the importance of nanoparticles, between various NMs, in the following part some general considerations about their use in biosensors will be given.

1.2. Use of nanoparticles in electrochemical biosensors

The application of nanoparticles (NPs) in biosensors strongly relates to their properties that derive to a certain extent from their synthesis and later modifications (chemical and biological) [6].NP characterization and quantification play a crucial role in the final biosensing applications [7]. The size and the composition of a NP seems to be advantageous over the corresponding bulk structure, because a target binding event (i.e. DNA hybridization or immunoreaction [8–10]) involving NPs have a significant effect in optical (change of the light absorption or emission) or electrochemical properties (oxidation or reduction current onto a transducing platform), offering novel options for bioanalysis.

Given their special properties, a special attention is given to gold nanoparticles (AuNP) that are mostly studied in this PhD thesis. In addition, Prussian blue nanoparticles (PBNPs), given their size and electrochemical properties, are also used and will be discussed in the following sections.

1.2.1. Gold nanoparticles.

Gold nanoparticles (AuNPs) are the most stable metal nanoparticles. They have size-related electronic, magnetic and optical properties with interest for applications in catalysis and biology as well as other fields [11,12].

Among the conventional methods of synthesis of AuNPs by reduction of gold(III) derivatives, the most popular one for a long time has been that using citrate reduction of $HAuCl_4$ in water with trisodium citrate, which was introduced by Turkevich in 1951 [13]. AuNPs shapes can be tuned through specifically devised synthetic procedures and later chemical and biological modifications of their surfaces.

Different methodologies for AuNP detection such as optical (through UV-Vis or lateral flow devices) or electrical/ electrochemical methods have been applied through various sensing technologies.

One of the most important applications of AuNPs has been its use as labels in various biosensing technologies. Recently the use of AuNPs as electroactive labels for the detection of analytes of clinical interest such as proteins in human serum [14] and cancer cells [15–17] have been reported. A special role in the biosensing performance plays the size of AuNPs. For example the electrochemical properties of AuNP suspensions, as studied recently by our group, are found to be strongly dependent on the size and the hydrodynamic properties of the solvent, while working in a bioassay systems [18].

1.2.2. Prussian blue nanoparticles.

Prussian blue nanoparticles (PBNPs) is a colloidal form of a mixed-valence transition metal hexacyanoferrate with the general formula of $Fe^{III}_4[Fe^{II}(CN)_6]_3 \cdot nH_2O$ that exhibit interesting electro photochemical, biochemical and magnetic properties. PBNPS have been used as Magnetic Resonance Imaging (MRI) contrast agent [19], in cell imaging and drug delivery [20] thanks also to their easy surface modification and size control [21]. These properties make PBNPs modified electrodes potentially applicable for sensors or electrochromic display devices [22].

PBNPS can be prepared by different ways such as from solutions of Fe^{2+} ions and $[Fe(CN)_6]^{3-}$ ions, from Fe^{3+} ions and a solution containing $[Fe(CN)_6]^{4-}$ ions or from of Fe^{3+} and $[Fe(CN)_6]^{3-}$ ions [23,24]. Two structural variations of PB are known: soluble ($KFeIII[FeII(CN)_6]$) and insoluble ($FeIII^4$ $[FeII(CN)_6]^3$). Prussian blue is able to exhibit a reversible transparent-blue-green multiple color change corresponding to the following redox states: Prussian white (PW, $K_2FeII[FeII(CN)_6]$), and Berlin green ($BG, \{KFeIII[FeII(CN)_6]\}^{1/3}\{FeIII[FeIII(CN)_6]\}^{2/3}$) [25].

The main application of PB relies in the development of electrochemical sensors using PB solutions deposited on the electrode surface by a layer-by-layer approach. The reduced form of PB, PW, is able to catalyze the electrochemical reduction of hydrogen peroxide at low potentials. The use of these nanoparticles is reported to improve the analytical performance related to hydrogen peroxide detection and could be used as i.e. glucose sensor [26,27].

1.3.Nanochannels

1.3.1. Sensing using nanochannels: from the Coulter counter to the stochastic sensing

The fundament of sensing using nanochannels [28] is based on the concept of the Coulter counter [29,30] a device that consists of two electrolyte-filled chambers separated by one or few more microchannels. When a microscopic particle enters through the microchannel, a change in the electrical conductance is recorded as electric current or voltage pulse, which can be correlated to size, mobility, surface charge, and concentration of the microparticle. The Coulter counter was designed to measure particles in the micrometric scale, but for biosensing purposes, devices able to detect molecules in the nanometric scale (i.e. proteins, ssDNA) are

needed and for this reason the research in this field was focused in the last years on the development of channels of nanometric size [31–33], inspired by the natural ion channels. The pioneer approach to build these biomimetic nanochannels consisted in the insertion of the α-hemolysin bacterial protein pore (Figure 1-1A) in artificial lipid bilayers. The as-prepared biological single nanochannels work in a similar way as the Coulter counter, being able to detect nanosized molecules.

The resistive-pulse process, called stochastic sensing, entails mounting the membrane containing the nanochannel between two electrolyte solutions, applying a transmembrane potential difference, and measuring the resultant ion current flowing across the electrolyte-filled nanochannel (Figure 1-1B) [34]. The selectivity of the system is given by specific receptors that can be inserted inside the nanochannel by using genetic engineering techniques.

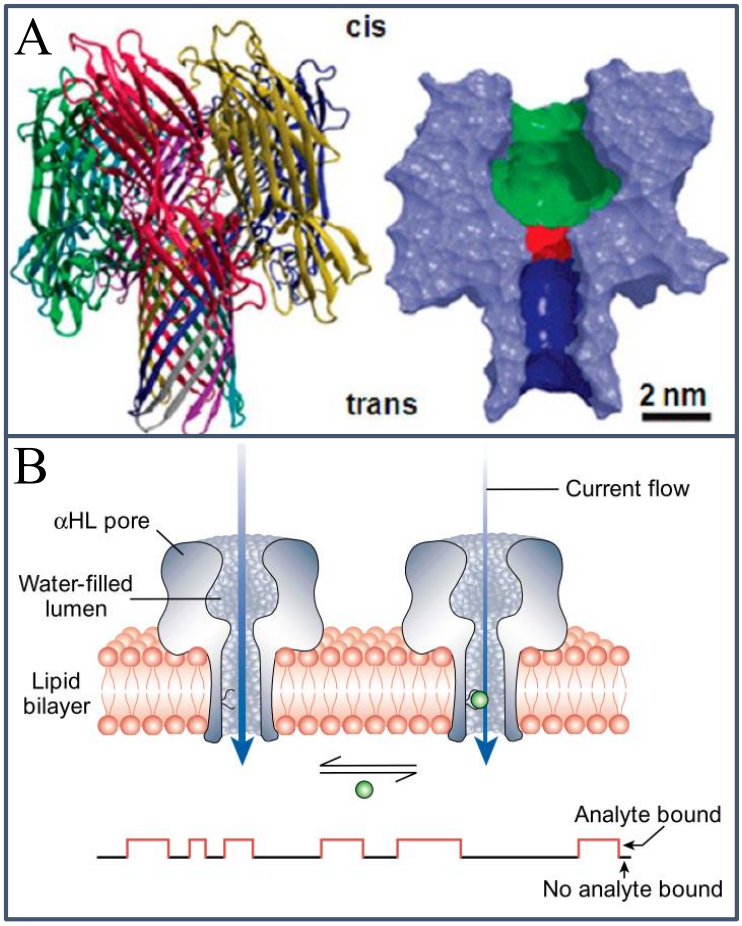

Figure 1-1. (A) Detailed structure of the heptameric α-hemolysin channel. The cross-sectional view on the right displays the inner cavity (green), inner constriction (red), and β-barrel (blue).[35] *(B) Stochastic Sensing: schematic representation of the*

sensing using an engineered α-hemolysin protein nanochannel inserted in a lipid bilayer membrane. The change in conductance between the two sides of the membrane in the absence (left) and presence (right) of an analyte in the sample allows its detection and quantification.[34]

Stochastic sensing using biological ion channels has been widely applied for the detection of different analytes, such as DNA [36], proteins [37] and others [38]. Of special relevance are the exciting perspectives related to the potential ability of the α-hemolysin nanochannel for DNA sequencing. DNA single strands could be electrophoretically driven through the α-hemolysin channel [39] and pass in an elongated conformation generating a "fingerprint"-like blocking of the ionic current, which would be specific for each strand. The transit time and extent of the current could reveal information about the length of the nucleic acid and its base composition [40–42].

However, in spite of the advantages of the biological ion channels in terms of sensitivity, selectivity, and ability for the analysis of a variety of analytes, limitations related to their low stability, time consuming analysis and the need of genetic engineering techniques for the insertion of specific receptors have directed the research in this field to the preparation and application of more robust systems based on solid-state nanochannels. This opened the way to a broad research area, where not only single nanochannels but also nanochannel arrays can be prepared. These nanochannel arrays bring novel sensing possibilities, both optical [43–46] and electrochemical, totally different from those based on the stochastic sensing.

Next section will be focused on some representative methods of preparation of solid-state nanochannel arrays and their application in electrochemical biosensing.

1.3.2. Solid-state nanochannel arrays preparation

Different methods for the preparation of solid-state nanochannels like anodization [47], ion sputtering [48], quantum lithography [49], nanosphere lithography [50], microchannel compression

[51], electron-beam lithography [52], block polymer self-assembly [53], microcontact printing [54], micromolding [55], water-assisted self-assembly [56], nanoimprint lithography [57], and high ordered mesoporous thin films formation [58,59] have been reported.

In this thesis, special emphasis will be given to the main methods used for the preparation of arrays of these solid-state nanochannels such as highly ordered mesoporous thin film formation by nanoparticle assembling, micro-/nanomolding techniques and metallic substrates anodization.

a) Highly ordered mesoporous thin film formation by nanoparticle assembling

Monodisperse polymer nanospheres have been used to fabricate monolayer nanopore arrays. The surface of polymer particles can be modified by proteins or biopolymers via physical adsorption [60]. These monolayers have a high specific surface area and an ordered arrangement of pores. These structures have already been applied in catalysis, separations, sensors [61], bioscience, photonics and optoelectronic devices. Polymer nanospheres modified with functional surface groups provide strong chemical bonds for immunoreagents. Carboxylic groups with the capacity to form amide bonds with the amino groups of bioligands are the most used. These monolayers have been deposited onto transparent conductive oxides (TCO) and used for photovoltaic applications (for example nanostructured solar cells). *Guerín* et al., [62] reported the use of polystyrene microsphere to modify the surface of the transparent fluorine doped tin oxide (FTO) with interest for solar cells. These monolayers could be used as templates for the fabrication of nanocavities by the inverse opal technique [63] for different applications as the fabrication of large-scale ZnO ordered pore arrays for gas sensors [64]. An example of the process steps for the fabrication of these monolayers are described in Figure 1-2, where the fabrication of a monolayer of microparticles on indium tin oxide (ITO) glass substrate as well as the cavities formation is illustrated. A substrate of ITO was treated with

UV light to obtain hydrophilic surfaces, and put into a Petri dish adding deionized water; a PS colloid solution was dropped onto the surface of the dispersion substrate, after a surfactant was dropped into the Petri dish. After that, the support substrate was removed from the petri dish and treated on a hot plate to fix the array on the surface of the substrate. To obtain the nanocavities a mixed solution was added onto the surface of the arrays by spin coating technique. Then, the PS nanosphere array template was removed using a solvent and ultrasonication [65].

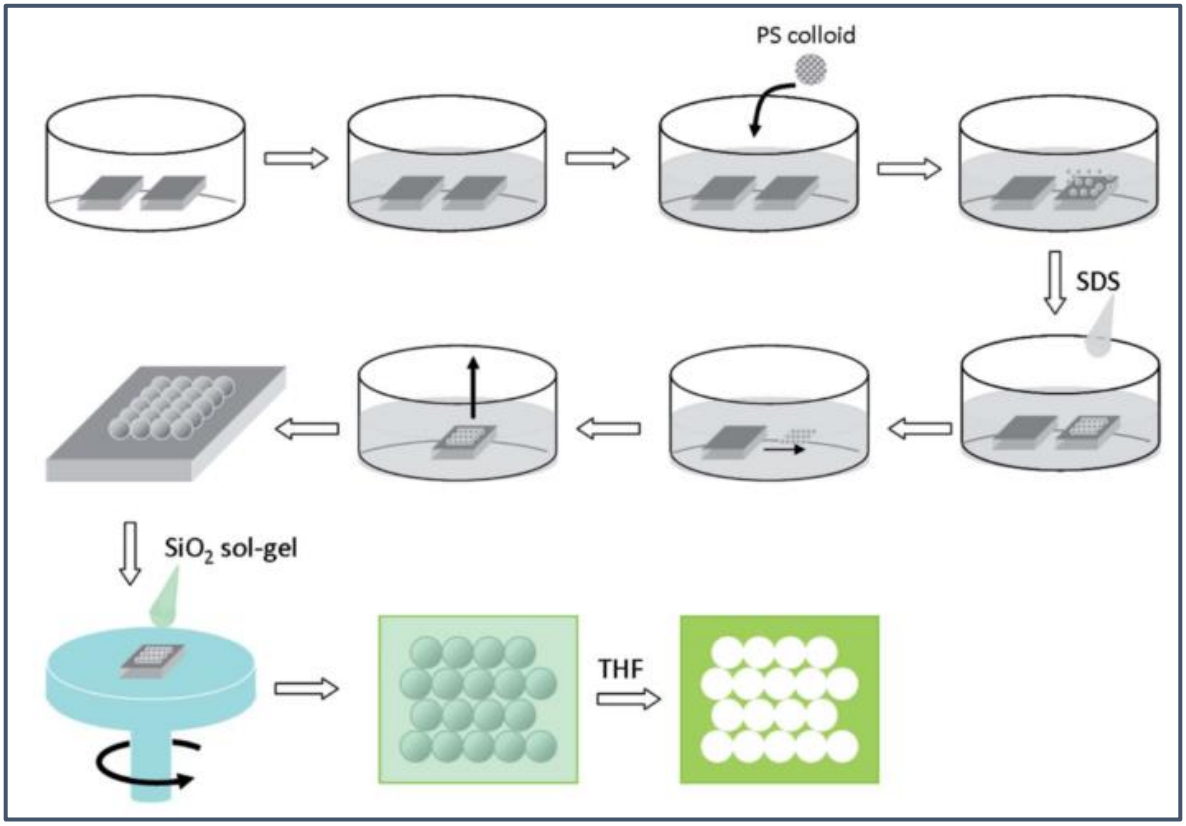

Figure 1-2. Highly ordered mesoporous thin film formation by nanoparticle assembling. Detailed preparation procedure for an inversed opal mask of SiO_2 on a substrate [65].

The holes formed between the nanospheres can be used as nanochannels and FTO serving then as a working electrode.

b) Micro-/Nanomolding techniques: nanoimprint lithography

Nanoimprint lithography (NIL) was developed in 1995 as a low-cost and high throughput alternative for researchers who need high-resolution patterning [66]. NIL depend on direct mechanical deformation of the resist and can therefore achieve resolutions beyond the limitations set by light diffraction or beam scattering that are encountered in conventional lithographic techniques [67]. NIL provides the ability to pattern materials into small structures with interest for various applications ranging from the production of integrated circuits, information storage devices, sensors, actuators, biochips, microfluidic devices, and micro-optical components [68,69].

Figure 1-3 describes the basic process steps to print a large-area of nanostructures.

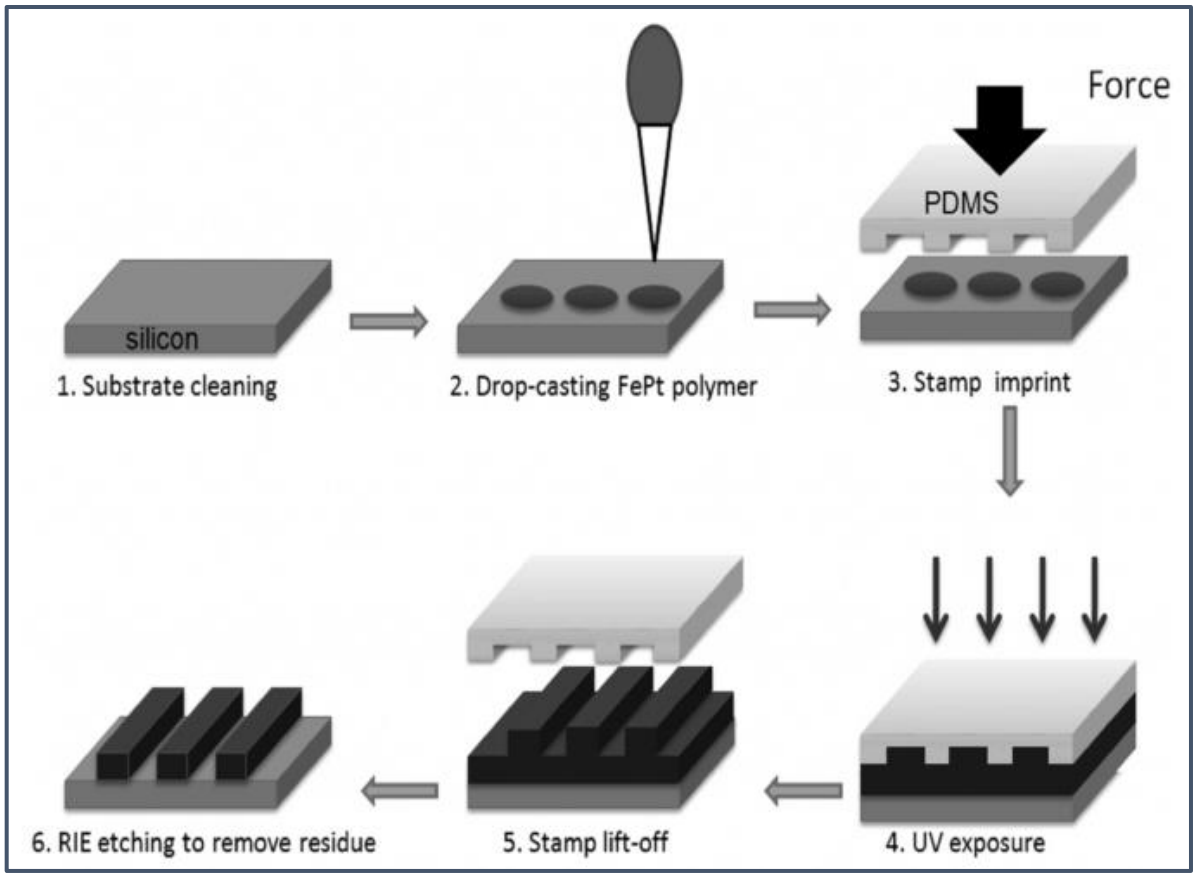

Figure 1-3 Micro-/Nanomolding techniques: Nanoimprint lithography. Schematic illustration of the fabrication of large-area nanostructures by nanoimprint lithography. ; 1, a silicon substrate is cleaned with acetone and deionized water together with sonication. 2, a polymer is drop-casted onto the silicon substrate with a dropper. 3, the PDMS stamp is pressed onto the sample with a uniform force. 4, the whole sample and the stamp is irradiated with UV light to induce cross-linking. 5, the stamp is then lifted off. 6, the residue is removed by reactive-ion etching (RIE). [70]

Depending on the application, the requirements for a successful lithographic process can vary substantially. The minimum feature size of a test pattern is usually the most obvious issue one must consider when selecting a proper lithographic technique.

c) Metallic substrates anodization: anodic aluminum oxide (AAO) nanoporous membranes preparation

Anodic aluminum oxide (AAO) is a rigid and dense porous material and is chemically and thermally stable. The principal characteristics of AAO are the perfectly ordered and size controlled nanopores [71]. The fabrication process is based on facile and inexpensive electrochemical anodization, wide accessibility, the capability of top-bottom fabrication with nanoscale precision and access to high aspect ratio structures. Figure 1-4 shows the two-step anodization process under hard conditions [72]. The structure of AAO can be described as a close-packed hexagonal array of parallel cylindrical nanopore perpendicular to the surface on top of the underlying Al substrates [73].

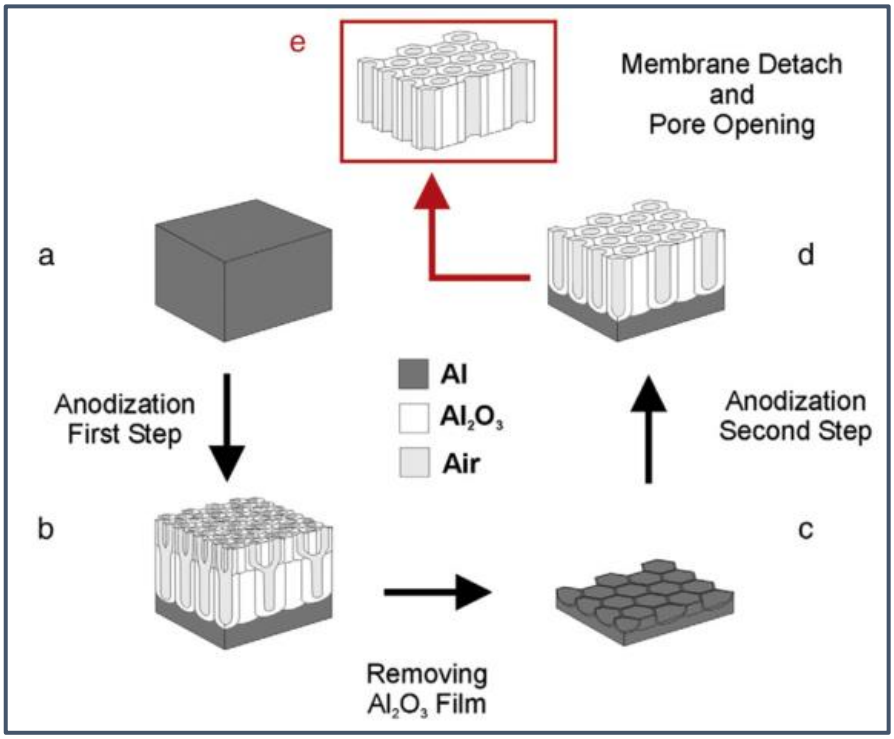

Figure 1-4 Metallic substrates anodization: Anodic aluminum oxide (AAO) nanoporous membranes preparation. The two-step anodization process under hard conditions. (a) Annealed and electropolished aluminium substrate. (b) nanoporous anodic alumina with a protective layer on the top and ordered pores on the bottom. (c) Patterned Al substrate after removing the oxide film. (d) nanoporous anodic alumina membrane with straight and closed pores. (e) nanoporous anodic alumina membrane with straight and open pores after performing the membrane detach and the pore opening at the same time [72]

The rich content of hydroxyl groups on the alumina membrane surface allow them to be easily modified via modification with organic molecules with the desired functionality [74].

1.3.3. Solid-state nanochannel arrays functionalization

Binding ligands are commonly used to modify the inner nanochannel walls to provide recognition sites for analytes; these ligands play a crucial role in achieving the desired sensing performance [75]. One of the common surface modification techniques is by wet chemical approach as: silanes, organic acids, and layer-by-layer deposition. Subsequent modifications of the thus introduced functionality with biomolecules or nanoparticles can be carried out. The chemical modification mainly refers to the chemical reactions between the inner wall of the nanochannel and functional molecules in a solution to create new covalent bonds. One method is based on the formation of functional groups as -COOH inside the nanochannels able to react with molecules to form covalent bonds (for example, -C(O)-NH-). Another

method for chemical modification of nanochannels is based on functional thiol molecules to form Au–S covalent bonds after the gold electrodes deposition onto the inner surface of the nanochannel. It is obvious that by reducing the diameter of the orifice to the nm range, the size of the detectable species can be extended down to the molecular level.

Layer-by-layer (LBL) assembly is a very versatile method for incorporating functional groups into nanochannels. This method avoids the need for complex chemical steps in the process [76].

Nanoporous membranes modified with various functional groups can be functionalized with antibodies or ssDNA for later biosensing applications, as shown in Figure 1-5.

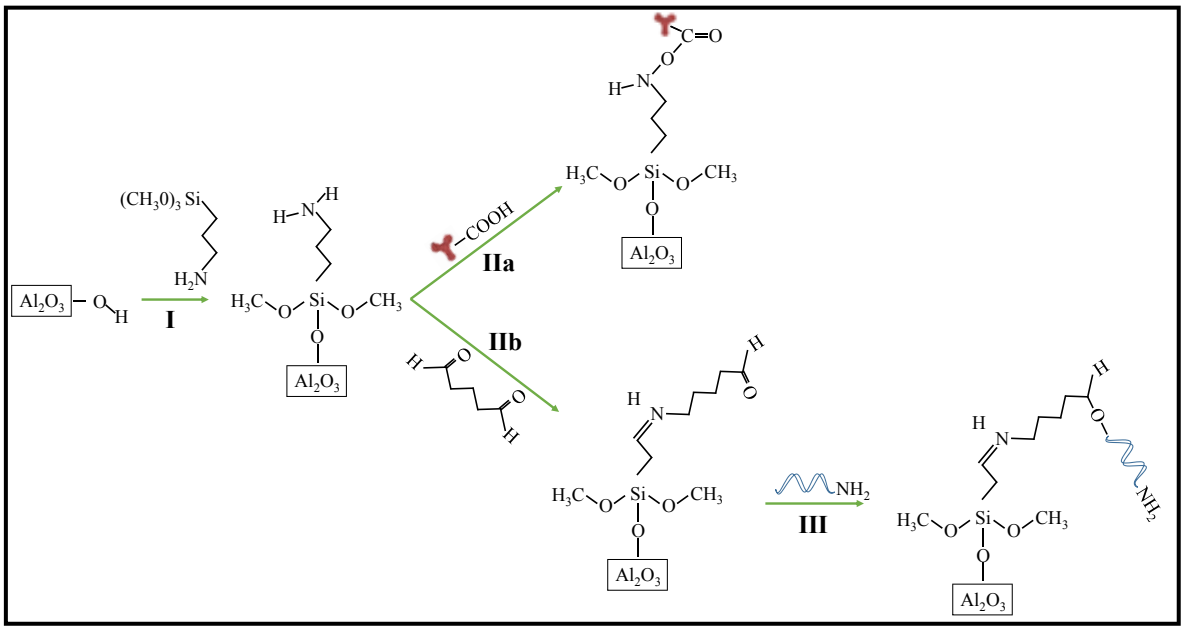

Figure 1 -5. Solid-state nanochannels functionalization. Scheme of the biofunctionalization procedure for antibodies immobilization in AAO nanoporous membranes: generation of amino groups by silanization process (I) followed by covalent binding of antibodies using EDC/sulfo-NHS cross-linker (IIa). In the case of ssDNA, carboxyl groups by reaction with glutaraldehyde (IIb) are generated after the silanization, followed by the immobilization of the amino-modified probe ssDNA by the peptide bond (III) [77–79].

The efficient antibody immobilization inside nanochannels can be checked by using antibodies labelled with a fluorescent tag (i.e. FITC), observing in the confocal microscope

the presence of fluorescence not only on the external surface of the membranes but also in the inner walls (Figure 1-6).

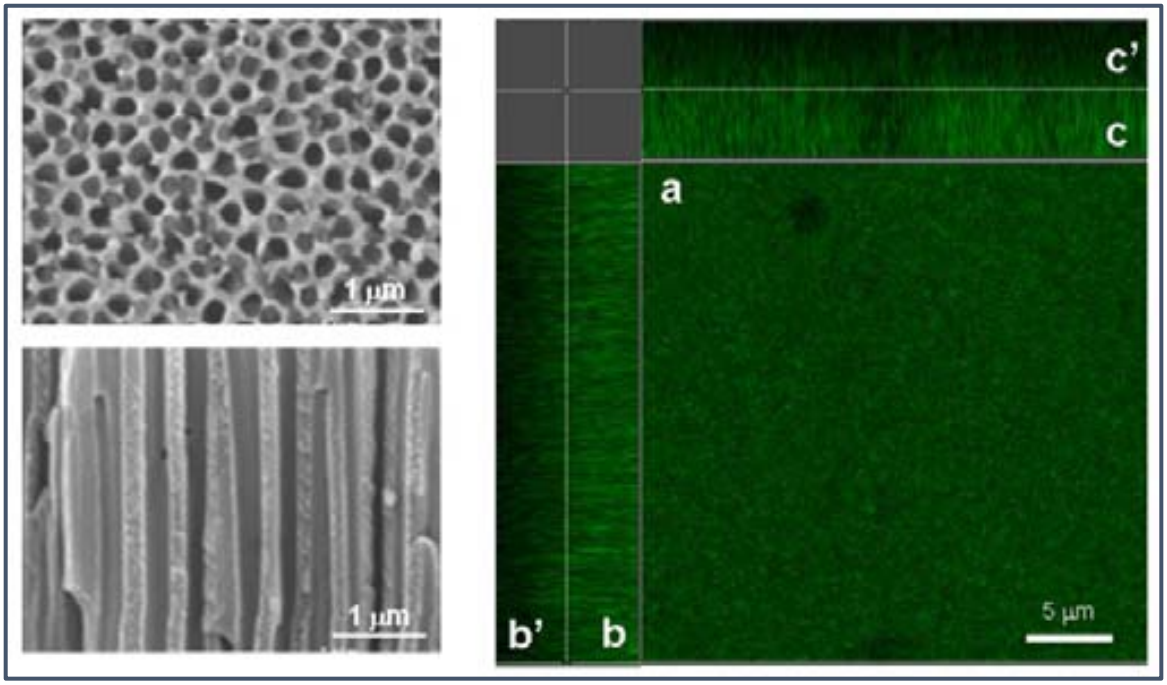

Figure 1-6. (Left) SEM images of a plan (top) and cross-sectional view (bottom) of the 200 nm pore AAO nanoporous membranes. (Right) Confocal image of a 200 nm pore AAO filter membrane with antibody-FITC immobilized. Plan view (a) and planes until 5 µm in depth from the top surface (b,c) and from the bottom surface (b',c') [78].

1.3.4. Electrochemical biosensing systems based on solid-state nanochannel arrays

1.3.4.1. Detection principle

The most recent and representative approaches are focused on the use of arrays of solid-state nanochannels as modifiers of conventional electrotransducer surfaces, measuring the changes of the electrochemical response of an electroactive species in solution due to the presence of the analyte inside the channels. AAO membranes prepared by anodization have a high pore density ($1x10^9/cm^2$) and small pore diameters, which results in a substrate with high surface

area that can be easily functionalized (as stated before) being very advantageous for biosensing. These characteristics, together with their commercial availability, have made them one of the preferred nanoporous substrates for biosensing applications. The sensing principle for the detection of proteins and DNA is explained in Figure 1-7. In the case of proteins, the formation of the immunocomplex inside the nanochannels produces a partial blockage in the diffusion of electroactive species through the nanoporous membranes to the electrochemical transducer surface (working electrode) leading to a decrease of the electrochemical signal related to $[Fe(CN)_6]^{4-}$ oxidation to $[Fe(CN)_6]^{3-}$. Differential pulse voltammetry (DPV) oxidation peak is selected as analytical signal. The blockage of the pores due to the formation of DNA hybridization complexes is also detected following the same principle. Furthermore, nanoporous membranes can act as filters of i.e. cells present in real samples (as illustrated in the figure), allowing to minimize matrix effects [79].

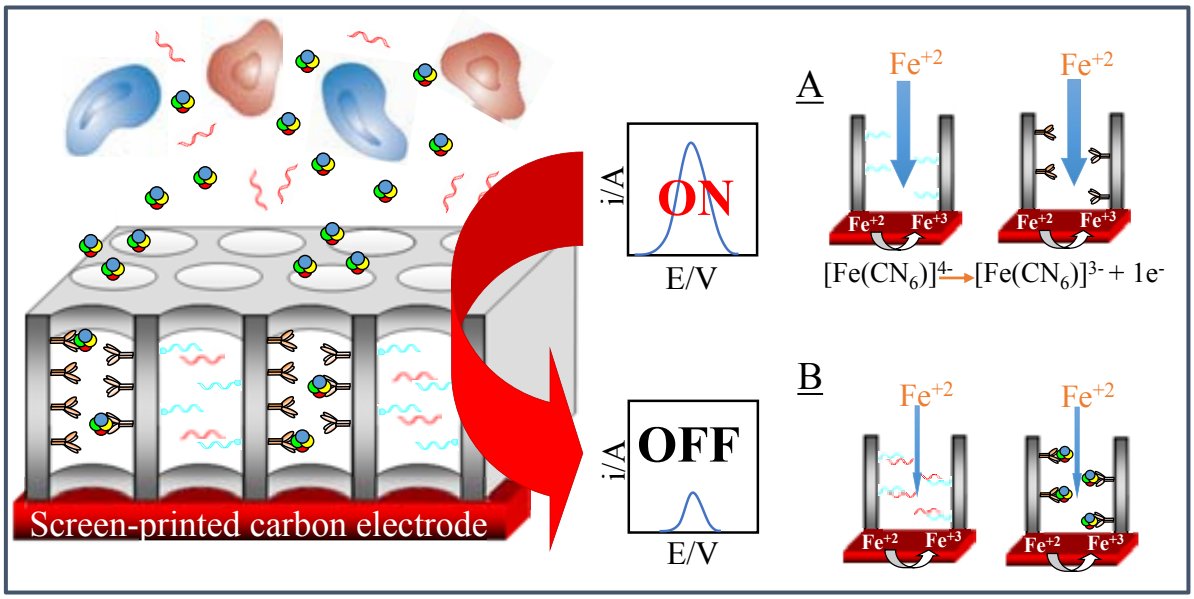

Figure 1-7. Principle of electrochemical biosensing using AAO nanoporous membranes. Left: cells in the sample remain outside the pores while the proteins (or ssDNA) enter inside are recognized by specific antibodies (or complementary ssDNA). Right: sensing principle in the absence (A) and presence (B) of the specific biomolecule in the sample [78].

This system is consistent with the relation between the pore size of the nanopore membrane used (typically 200 nm) and the length of both antibody and antigen , that is, 14.5 nm × 8.5 nm × 4 nm in the case of human immunoglobulin H(IgG) and also with the size of a i.e. 21-mer ssDNA (approximately diameter of 1.84 nm and length of 0.38 nm).

1.3.4.2. Application for protein biomarkers detection

The above explained sensing principle has been applied for the detection of protein biomarkers in whole human blood samples, without any sample preparation, taking advantage of the dual ability of the membranes to act not only as sensing platforms but also as filter of complex components such as red and blood cells. That is the case of the detection of CA15-3 breast cancer marker spiked in whole human blood [78]. The sensitivity of the system is here improved thanks to the use of gold nanoparticle (AuNPs) tags in sandwich assay approaches. The presence of such AuNPs inside the channels increase in a high extent the blockage of the diffusion of the electroactive species achieving in this way lower detection limits. Moreover, the catalytic activity of the AuNPs toward the silver deposition is approached for the selective formation of silver crystals around the AuNPs, increasing in this way the AuNP size and consequently the blockage of the channels and the limit of detection of proteins.

Figure 1-8 top, shows a schematic representation about how the differential pulse voltammograms decrease due to the blockage effect occurring inside the nanochannels, and its effect on the limit of detection of human IgG (chosen as model protein), starting with the label-free assay, antibody labeled with AuNPs 20 nm, 80 nm AuNPs and finally 80 nm AuNPs after silver deposition.

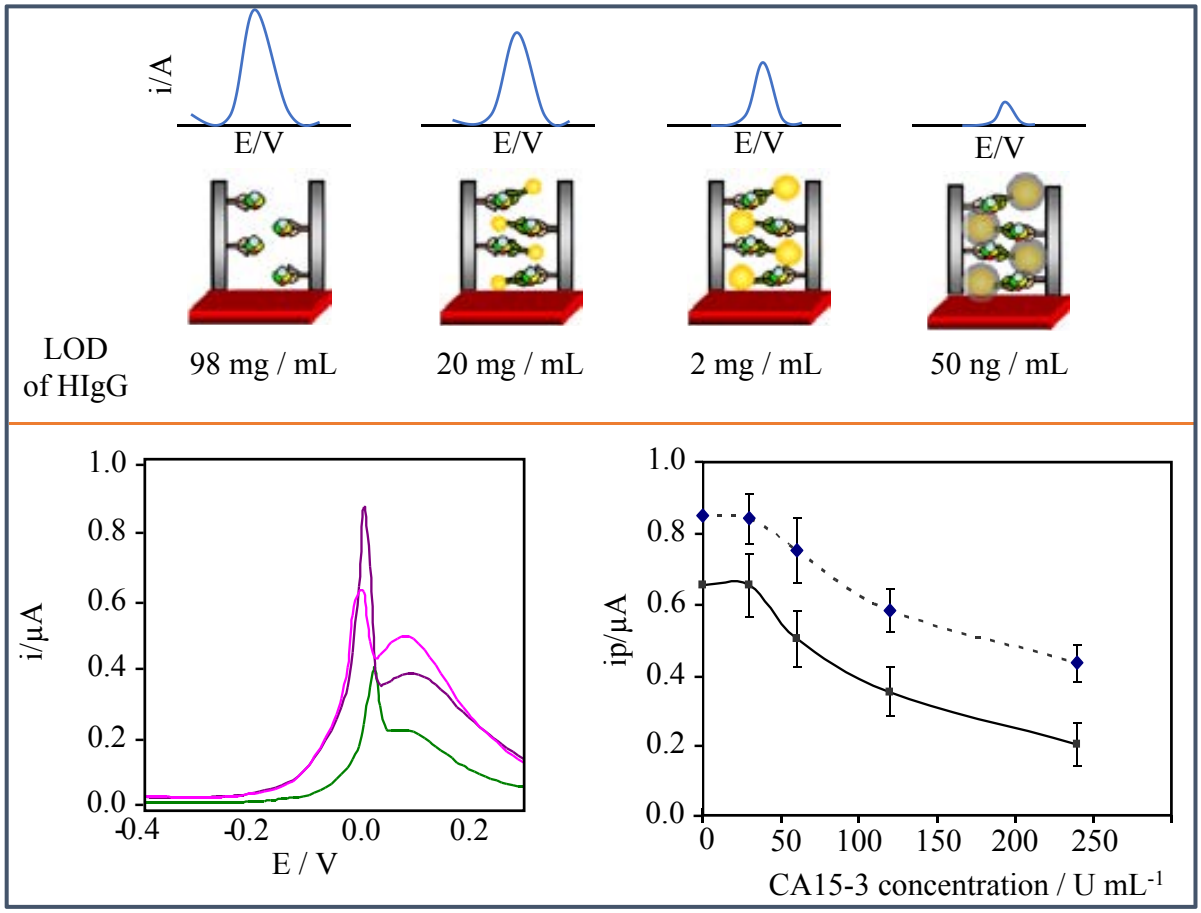

Figure 1-8 Top: Schematic representation of the differential pulse voltammograms response obtained depending on the blockage degree inside the nanochannels. Bottom left; DPV results for blood samples containing different concentrations of added CA15-3: 60, 120 and 240 U mL^{-1} (from top to bottom). DPV parameters Pre-concentration potential: –550 mV; preconcentration time: 30 s; step potential: 10 mV; modulation amplitude: 50 mV; scan rate: 33.5 mV s^{-1}. Bottom right; Comparison of the effect of the concentration of CA15-3 on the voltammetric peak current obtained in PBS buffer (dotted line) and in the blood sample (solid line).[78]

With this methodology a new system for detection of CA15-3 cancer marker spiked in whole blood was developed capable to detect 52 U mL^{-1} of CA15-3 with very low matrix effects, as shown in Figure 1-8 (bottom). In addition, the developed device presents the advantage of the quantitative analysis that can be performed with the low-cost electrochemical analyzers using a simple and low-cost detection technology. Another interesting application developed by our group is the rapid determination of the thrombin spiked in whole blood [80], taking advantage of both aptamer-based recognition and the use of a nanoporous membrane. The protocol involves sandwich format (aptamer/thrombin/antibody-AuNP) and silver amplification in the inner walls of an AAO membrane. The effect of the electrostatic interactions between

thrombin and the aptamer modified inner walls of the nanochannel including the steric effects were also investigated here. The resulted biosensing system allows detecting thrombin spiked in whole blood at very low levels, which are within the range of clinical interest for the diagnostic of coagulation abnormalities as well as pulmonary metastasis.

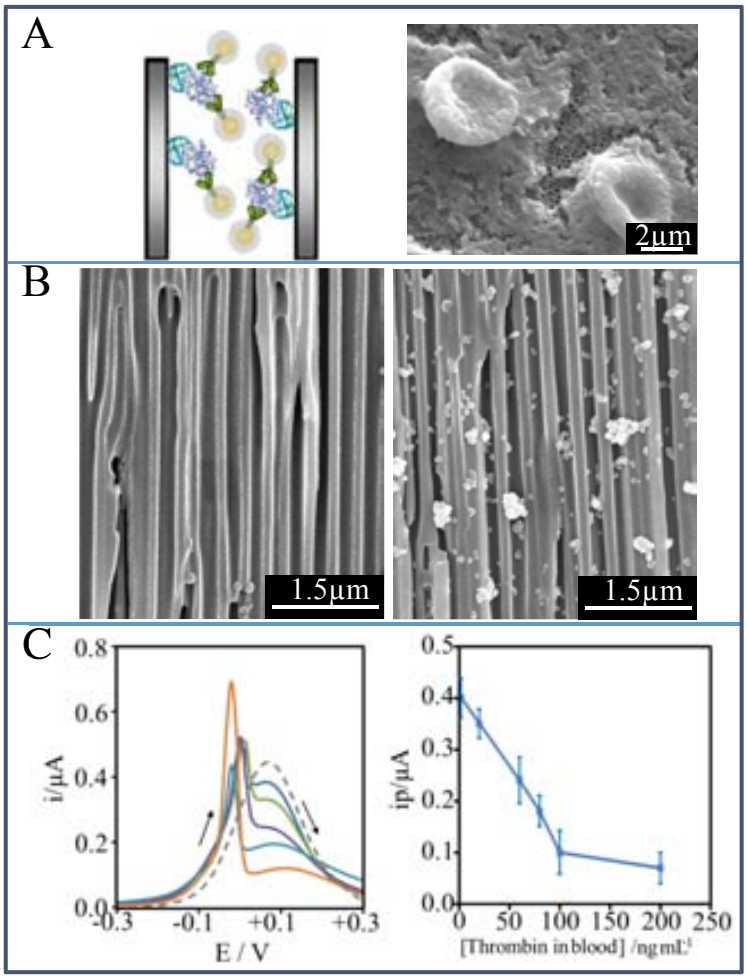

Figure 1-9. (A) Left; schematic representation (not in scale) of a sandwich assay with AuNP labeled antibodies and silver deposition. (A) Right; SEM top view images AAO filter membrane of 200 nm pore size on which a 30 µL drop of blood was deposited. White and red blood cells as well as the nanochannels are observed. (Note that these images are representative of what happens, although the morphology of the cells is altered due to the sample treatment necessary for the SEM analysis). (B) SEM (cross-sectional view) images of AAO filter membranes of 200 nm pore size modified with the aptamer and (left) to react with a blood sample containing 100 ng mL^{-1} of spiked thrombin (Right) and a blood sample without spiked thrombin (Left). The sandwich assay is then completed with anti-thrombin/AuNPs followed by silver enhancement (white silver crystals are observed). (C) Right; DPVs registered 1mM $K_3[Fe(CN)_6]$/ 0.1M $NaNO_3$ following the optimized experimental procedure for blood samples containing spiked thrombin at concentrations of (up to down): 0 (dashed line), 2, 20, 60, 80 and 100 $ngmL^{-1}$. DPV parameters: pre-concentration potential: -0.3 V; pre-concentration time: 30 s; step potential: 10 mV; modulation amplitude: 50 mV; scan rate: 33.5 mV s^{-1}. (C) Left; Effect of the concentration of thrombin spiked in blood on the voltammetric peak current of oxidation of $[Fe(CN)_6]^{4-}$ to $[Fe(CN)_6]^{3-}$ (approx. +0.1 V) chosen as analytical signal [80].

Figure 1-9A left, is a schematic representation of the blockage occuring inside the nanochannels after a sandwich assay and silver deposition onto AuNP tags. In Figure 1-9A

right, the filtering ability of the AAO membranes in the analysis of whole human blood is illustrated by the SEM image showing white and red blood cells that remain out of the nanochannels. This image also shows that the solution containing the blood cells doesn´t block the entire pores so thrombin biomarker can pass through the nanochannels to be in contact with the working electrode surface. Figure 1-9B shows SEM images, cross-sectional view, of AAO filter membranes of 200 nm nanochannels size modified with the aptamer and left to react with a blood sample containing 100 ng mL^{-1} of spiked thrombin (right) and a blood sample without spiked thrombin (left). The sandwich assay is then completed with anti-thrombin/AuNPs followed by silver enhancement (silver crystals are observed; B right). The DPV signals and the quantitative analysis for different quantities of spiked thrombin are shown in Figure 1-9C, which allow to obtain a detection limit of 1.8 ng of thrombin per mLof human blood [80].

1.3.4.3. DNA detection

Following the sensing principle described in section 1.3.4.1, a novel methodology for the detection of ssDNA using nanoporous alumina filter membranes was also developed by our group. The blockage of the pores due to the hybridization is detected by measuring the decrease in the differential pulse voltammetric response of the $[Fe(CN)_6]^{4-/3-}$ redox indicator and using screen printed carbon electrodes. AuNPs tags are used again in order to increase the sensitivity of the assay. (Figure 1-10).

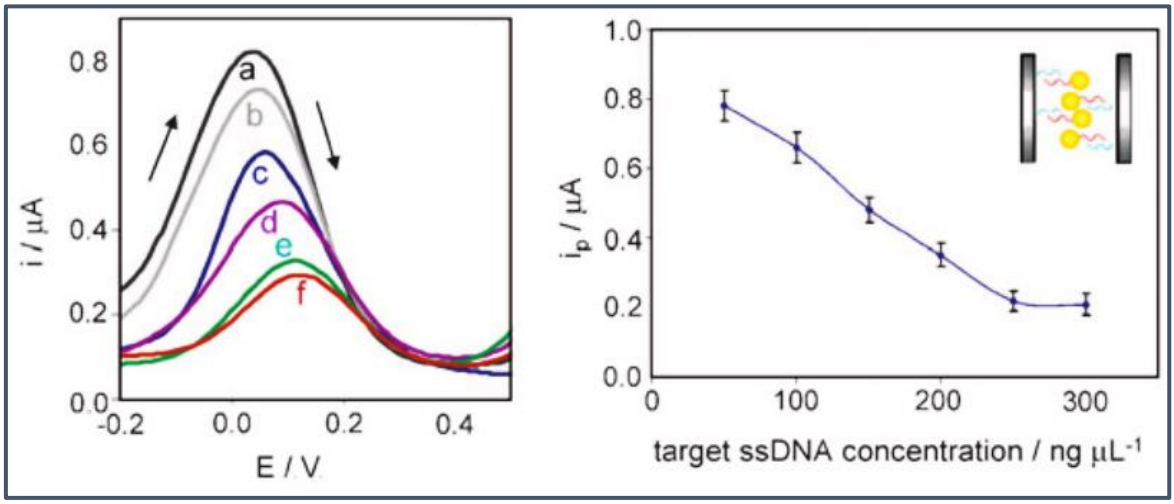

Figure 1-10. Left; differential pulse voltammograms obtained for solutions with different concentrations of target ssDNA labeled with 20 nm AuNPs: (a) 50, (b) 100, (c) 150, (d) 200, (e) 250 and (f) 300 ng mL^{-1}. Pre-concentration potential: -0.55 V; pre-concentration time: 30 s; step potential: 10 mV; modulation amplitude: 50 mV; scan rate: 33.5 mV s^{-1}. Right: effect of the concentration of the target ssDNA labeled with 20 nm AuNPs on the analytical signal.

The effect of the concentration of target ssDNA labeled with AuNPs on the DPV peak current used as analytical signal was evaluated (Figure 1-10 left), obtaining a linear correlation in the range 50–250 ng mL^{-1}. The limit of detection (calculated as the concentration of target ssDNA corresponding to three times the standard deviation of the estimate) was 42 ng mL^{-1} (Figure 1-10 right).

1.4. Conclusions and future perspectives

Since the first in-vitro use of biological channels the appearance of novel technologies able to fabricate synthetic/solid nanochannels has significantly improve the biosensing systems based on such platforms. Nanopores in both synthetic and biological membranes are used as resistive-pulse sensors for molecular and macro-molecular analyte detection. The nanoporous membranes have been shown not only to act as platform for the protein and DNA recognition but also as filter of the micrometric components.

The most reported nanochannel platform is the anodic alumina oxide membrane due to the homogeneity and precision in the distribution in the pore diameter. AAO membranes can be manufactured with high feasibility and easily reach the specific requirements of the detection systems. As demonstrated in several reports by reducing the pore diameter it is possible to reduce the biosensing detection limits. Further enhancements also can be achieved by amplification by using bigger size nanoparticles including enlargement by catalytic reactions (ex. Ag deposition onto AuNPs). The combinations of nanochannel sensing capability with the known advantages of nanoparticles in immunosensing bring new benefits in the diagnostics of proteins.

The integration of nanochannel/nanoporous membrane with electrochemical transducer (ex. screen-printed electrode) seems to be one of the most important challenge in the development of robust sensing devices that may bring electrochemical/nanochannel-based biosensing technology to the market.

1.5. References

(1) Ronkainen, N. J.; Halsall, H. B.; Heineman, W. R. Electrochemical Biosensors. Chem. Soc. Rev. 2010, 39, 1747–1763.

(2) Turner, A. P. F. Biosensor: Sense and Sensibility. Chem. Soc. Rev. 2013, 42, 3175–3648.

(3) Valentini, F.; Palleschi, G. Nanomaterials and Analytical Chemistry. Anal. Lett. 2008, 41, 479–520.

(4) Merkoci, A.; Aldabert, M.; Marón, S.; Alegret, S. New Materials for Electrochemical Sensing V: Nanoparticles for DNA Labeling. Trends Anal. Chem. 2005, 24, 341–349.

(5) Windmiller, J. R.; Wang, J. Wearable Electrochemical Sensors and Biosensors: A Review. Electroanalysis 2013, 25, 29–46.

(6) Pérez-López, B.; Merkoçi, A. Nanoparticles for the Development of Improved (bio)sensing Systems. Anal. Bioanal. Chem. 2011, 399, 1577–1590.

(7) De la Escosura-Muñiz, A.; Ambrosi, A.; Merkoçi, A. Electrochemical Analysis with Nanoparticle-Based Biosystems. Trends Anal. Chem. 2008, 27, 568–584.

(8) Merkoçi, A. Nanoparticles-Based Strategies for DNA, Protein and Cell Sensors. Biosens. Bioelectron. 2010, 26, 1164–1177.

(9) De la Escosura-Muñiz, A.; Parolo, C.; Merkoçi, A. Immunosensing Using Nanoparticles. Mater. Today 2010, 13, 24–34.

(10) De la Escosura-Muñiz, A.; Merkoçi, A.; Merkoci, A. Electrochemical Detection of Proteins Using Nanoparticles: Applications to Diagnostics. Expert Opin. Med. Diagn. 2010, 4, 21–37.

(11) Jans, H.; Huo, Q. Gold Nanoparticle-Enabled Biological and Chemical Detection and Analysis. Chem. Soc. Rev. 2012, 41, 2849–2866.

(12) Daniel, M.-C.; Astruc, D. Gold Nanoparticles: Assembly, Supramolecular Chemistry, Quantum-Size-Related Properties, and Applications toward Biology, Catalysis, and Nanotechnology. Chem. Rev. 2004, 104, 293–346.

(13) Turkevich, J.; Cooper Stevenson, P.; Hillier, J. A Study of the Nucleation and Growth Processes in the Synthesis of Colloidal Gold. Discuss. Faraday Soc. 1951, 11, 55–75.

(14) De la Escosura-Muñiz, A.; Maltez-da Costa, M.; Sánchez-Espinel, C.; Díaz-Freitas, B.; Fernández-Suarez, J.; González-Fernández, Á.; Merkoçi, A. Gold Nanoparticle-Based Electrochemical Magnetoimmunosensor for Rapid Detection of Anti-Hepatitis B Virus Antibodies in Human Serum. Biosens. Bioelectron. 2010, 26, 1710–1714.

(15) De la Escosura-Muñiz, A.; Sánchez-Espinel, C.; Díaz-Freitas, B.; González-Fernández, A.; Maltez-da Costa, M.; Merkoçi, A. Rapid Identification and Quantification of Tumor Cells Using an Electrocatalytic Method Based on Gold Nanoparticles. Anal. Chem. 2009, 81, 10268–10274.

(16) Maltez-da Costa, M.; de la Escosura-Muñiz, A.; Nogués, C.; Barrios, L.; Ibáñez, E.; Merkoçi, A. Detection of Circulating Cancer Cells Using Electrocatalytic Gold Nanoparticles. Small 2012, 8, 360536–12.

(17) Maltez-da Costa, M.; de la Escosura-Muñiz, A.; Nogués, C.; Barrios, L.; Ibáñez, E.; Merkoçi, A. Simple Monitoring of Cancer Cells Using Nanoparticles. Nano Lett. 2012, 12, 4164–4171.

(18) De la Escosura-Muñiz, A.; Parolo, C.; Maran, F.; Mekoçi, A. Size-Dependent Direct Electrochemical Detection of Gold Nanoparticles: Application in Magnetoimmunoassays. Nanoscale 2011, 3, 3350–3356.

(19) Shokouhimehr, M.; Soehnlen, E. S.; Khitrin, A.; Basu, S.; Huang, S. D. Biocompatible Prussian Blue Nanoparticles: Preparation, Stability, Cytotoxicity, and Potential Use as an MRI Contrast Agent. Inorg. Chem. Commun. 2010, 13, 58–61.

(20) Shokouhimehr, M.; Soehnlen, E. S.; Hao, J.; Griswold, M.; Flask, C.; Fan, X.; Basilion, J. P.; Basu, S.; Huang, S. D. Dual Purpose Prussian Blue Nanoparticles for Cellular Imaging and Drug Delivery: A New Generation of T1-Weighted MRI Contrast and Small Molecule Delivery Agents. J. Mater. Chem. 2010, 20, 5251.

(21) Fiorito, P. a; Gonçales, V. R.; Ponzio, E. a; de Torresi, S. I. C. Synthesis, Characterization and Immobilization of Prussian Blue Nanoparticles. A Potential Tool for Biosensing Devices. Chem. Commun. 2005, 366–368.

(22) Hornok, V.; Dékány, I. Synthesis and Stabilization of Prussian Blue Nanoparticles and Application for Sensors. Colloid Interface Sci. 2007, 309, 176–182.

(23) Uemura, T.; Ohba, M.; Kitagawa, S. Size and Surface Effects of Prussian Blue Nanoparticles Protected by Organic Polymers. Inorg. Chem. 2004, 43, 7339–7345.

(24) Zhang, Q.; Zhang, L.; Li, J. Fabrication and Electrochemical Study of Monodisperse and Size Controlled Prussian Blue Nanoparticles Protected by Biocompatible Polymer. Electrochim. Acta 2008, 53, 3050–3055.

(25) Miao, Y.; Chen, J.; Wu, X. Electrochemical Characterization of Prussian Blue Nanoparticles. Colloid J. 2007, 69, 334–337.

(26) Han, L.; Tricard, S.; Fang, J.; Zhao, J.; Shen, W. Prussian Blue @ Platinum Nanoparticles/graphite Felt Nanocomposite Electrodes: Application as Hydrogen Peroxide Sensor. Biosens. Bioelectron. 2013, 43, 120–124.

(27) Li, J.; Wei, X.; Yuan, Y. Synthesis of Magnetic Nanoparticles Composed by Prussian Blue and Glucose Oxidase for Preparing Highly Sensitive and Selective Glucose Biosensor. Sensors Actuators B Chem. 2009, 139, 400–406.

(28) De la Escosura-Muñiz, A.; Merkoci, A. Nanochannels Preparation and Application in Biosensing. ACS Nano 2012, 6, 7556–7583.

(29) Coulter, W. H. Means for Counting Particles Suspended in a Fluid. 2,656,508, 1953.

(30) Coulter, W. H.; Coulter, J. High Speed Automatic Blood Cell Counter and Cell Size Analyzer. Proc. Natl. Electron. Conf . 1956, 12, 1034–1040.

(31) Bezrukov, S.; Vodyanoy, I.; Parsegian, A. Counting Polymers Moving through a Single Ion Channel. Nature 1994, 370, 279–281.

(32) Vercoutere, W.; Winter-Hilt, S.; DeGuzman, V.; Deamer, D.; Ridio, S.; Rodgers, J.; Olse, H.; Marziali, A.; Akeson, M. Discrimination among Individual Watson-Crick Base Pairs at the Termini of Single DNA Hairpin Molecules. Nucleic Acids Res. 2003, 31, 1311–1318.

(33) Albrecht, T.; Edel, J. B.; Winterhalter, M. New Developments in Nanopore Research-from Fundamentals to Applications. J. Phys.Condens. Matter. 2010, 22, 450301 (1pp).

(34) Bayley, H.; Cremer, P. S. Stochastic Sensors Inspired by Biology. Nature 2001, 413, 226–230.

(35) Howorka, S.; Siwy, Z. Nanopore Analytics: Sensing of Single Molecules. Chem. Soc. Rev. 2009, 38, 2360–2384.

(36) Purnell, R. F.; Schmidt, J. J. Discrimination of Single Base Substitutions in a DNA Strand Immobilized in a Biological Nanopore. ACS Nano 2009, 3, 2533–2538.

(37) Rotem, D.; Jayasinghe, L.; Salichou, M.; Bayley, H. Protein Detection by Nanopores Equipped with Aptamers. J. Am. Chem. Soc. 2012, 134, 2781–2787.

(38) Oukhaled, G.; Mathé, J.; Biance, A.-L.; Bacri, L.; Betton, J.-M.; Lairez, D.; Pelta, J.; Auvray, L. Unfolding of Proteins and Long Transient Conformations Detected by Single Nanopore Recording. Phys. Rev. Lett. 2007, 98, 158101–158104.

(39) Kasianowicz, J.; Brandin, E.; Branton, D.; Deamer, D. Characterization of Individual Polynucleotide Molecules Using a Membrane Channel. Proc. Natl. Acad. Sci. U.S.A. 1996, 93, 13770–13773.

(40) Kasianowicz, J. J.; Robertson, J. W. F.; Chan, E. R.; Reiner, J. E.; Stanford, V. M. Nanoscopic Porous Sensors. Annu. Rev. Anal. Chem. 2008, 1, 737–766.

(41) Venkatesan, B. M.; Bashir, R. Nanopore Sensors for Nucleic Acid Analysis. Nat. Nanotechnol. 2011, 6, 615–624.

(42) Branton, D.; Deamer, D. W.; Marziali, A.; Bayley, H.; Benner, S. a; Butler, T.; Di Ventra, M.; Garaj, S.; Hibbs, A.; Huang, X.; et al. The Potential and Challenges of Nanopore Sequencing. Nat. Biotechnol. 2008, 26, 1146–1153.

(43) Santos, A.; Kumeria, T.; Losic, D. Optically Optimized Photoluminescent and Interferometric Biosensors Based on Nanoporous Anodic Alumina: A Comparison. Anal. Chem. 2013, 85, 7904–7911.

(44) Santos, A.; Macías, G.; Ferré-Borrull, J.; Pallarès, J.; Marsal, L. F. Photoluminescent Enzymatic Sensor Based on Nanoporous Anodic Alumina. ACS Applied. Mater. Interfaces 2012, 4, 3584–3588.

(45) Kumeria, T.; Santos, A.; Losic, D. Ultrasensitive Nanoporous Interferometric Sensor for Label-Free Detection of gold(III) Ions. ACS Appl. Mater. Interfaces 2013, 5, 11783–11790.

(46) Arroyo, J. O.; Andrecka, J.; Spillane, K. M.; Billington, N.; Takagi, Y.; Sellers, J. R.; Kukura, P.; Ortega Arroyo, J. Label-Free, All-Optical Detection, Imaging, and Tracking of a Single Protein. Nano Lett. 2014, 14, 2065–2070.

(47) Wang, K.; Liu, G.; Hoivik, N.; Johannessen, E.; Jakobsen, H.; Jalobsen, H. Electrochemical Engineering of Hollow Nanoarchitectures: Pulse/step Anodization (Si, Al, Ti) and Their Applications. Chem. Soc. Rev. 2014, 43, 1476–1500.

(48) Tian, Y.; Hou, X.; Jiang, L. Biomimetic Ionic Rectifier Systems: Asymmetric Modification of Single Nanochannels by Ion Sputtering Technology. J. Electroanal. Chem. 2011, 656, 231–236.

(49) Chou, S. Y.; Li, W.-D.; Liang, X. Quantized Patterning Using Nanoimprinted Blanks. Nanotechnology 2009, 20, 155303.

(50) Klein, M. J. K.; Montagne, F.; Blondiaux, N.; Vazquez-Mena, O.; Heinzelmann, H.; Pugin, R.; Brugger, J.; Savu, V. SiN Membranes with Submicrometer Hole Arrays Patterned by Wafer-Scale Nanosphere Lithography. J. Vac. Sci. Technol. B 2011, 29, 0210121–0210125.

(51) Li, J.-M.; Liu, C.; Ke, X.; Duan, Y.; Fan, Y.; Li, M.; Zhang, K.; Xu, Z.; Wang, L. Fabrication of 1D Nanochannels on Thermoplastic Substrates Using Microchannel Compression. Microsyst. Technol. 2013, 19, 1845–1850.

(52) Devlin, N. R.; Brown, D. K.; Kohl, P. A. Patterning Decomposable Polynorbornene with Electron Beam Lithography to Create Nanochannels. J. Vac. Sci. Technol. B 2009, 27, 2508–2511.

(53) Cheng, J. Y.; Ross, C. a.; Smith, H. I.; Thomas, E. L. Templated Self-Assembly of Block Copolymers: Top-Down Helps Bottom-Up. Adv. Mater. 2006, 18, 2505–2521.

(54) Quist, A. P.; Pavlovic, E.; Oscarsson, S. Recent Advances in Microcontact Printing. Anal. Bioanal. Chem. 2005, 381, 591–600.

(55) Wang, P.; Paik, S.; Chen, S.; Rajaraman, S.; Kim, S.; Allen, M. G. Fabrication and Characterization of Polymer Hollow Microneedle Array Using UV Lithography Into Micromolds. J. Microelectromechanical Syst. 2013, 22, 1041–1053.

(56) Zhang, W.; Meng, Z.; Zhai, J.; Heng, L. Ion Current Behaviors of Mesoporous Zeolite-Polymer Composite Nanochannels Prepared by Water-Assisted Self-Assembly. Chem. Commun. (Camb). 2014, 50, 3552–3555.

(57) Li, X.; You, H.; Jiang, H.; Lin, R.; Kong, D.; Jiang, R.; Zhu, L.; Gao, J.; Tang, M.; Wang, X.; et al. Fabrication of Size Controllable SU-8 Nanochannels Using Nanoimprint Lithography and Low-Pressure Thermal Bonding Methods. Micro Nano Lett. 2014, 9, 105–108.

(58) Yamaguchi, A.; Teramae, N. Fabrication and Analytical Applications of Hybrid Mesoporous Membranes. Anal. Sci. 2008, 24, 25–30.

(59) Cao, B.; Cai, W.; Sun, F.; Li, Y.; Lei, Y.; Zhang, L. Fabrication of Large-Scale Zinc Oxide Ordered Pore Arrays with Controllable Morphology. Chem. Commun. 2004, 1604–4605.

(60) Menshikova, A. Y.; Evseeva, T. G.; Skurkis, Y. O.; Tennikova, T. B.; Ivanchev, S. S. Monodisperse Carboxylated Polystyrene Particles: Synthesis, Electrokinetic and Adsorptive Properties. Polymer (Guildf). 2005, 46, 1417–1425.

(61) Walcarius, A. Electrocatalysis, Sensors and Biosensors in Analytical Chemistry Based on Ordered Mesoporous and Macroporous Carbon-Modified Electrodes. Trends Anal. Chem. 2012, 38, 79–97.

(62) Guérin, V.-M.; Elias, J.; Nguyen, T. T.; Philippe, L.; Pauporté, T. Ordered Networks of ZnO-Nanowire Hierarchical Urchin-like Structures for Improved Dye-Sensitized Solar Cells. Phys. Chem. C hem. Phys 2012, 14, 12948–12955.

(63) Teh, L. K.; Yeo, K. H.; Wong, C. C. Isotropic Photonic Pseudogap in Electrodeposited ZnO Inverse Opal. Appl. Phys. Lett. 2006, 89, 051105.

(64) Scott, R. W. J.; Yang, S. M.; Chabanis, G.; Coombs, N.; Williams, D. E.; Ozin, G. a. Tin Dioxide Opals and Inverted Opals: Near-Ideal Microstructures for Gas Sensors. Adv. Mater. 2001, 13, 1468–1472.

(65) Chen, L.-Y.; Yang, K.-H.; Chen, H.-C.; Liu, Y.-C.; Chen, C.-H.; Chen, Q.-Y. Innovative Fabrication of a Au Nanoparticle-Decorated SiO2 Mask and Its Activity on Surface-Enhanced Raman Scattering. Analyst 2014, 139, 1929–1937.

(66) Bender, M.; Fuchs, a.; Plachetka, U.; Kurz, H. Status and Prospects of UV-Nanoimprint Technology. Microelectron. Eng. 2006, 83, 827–830.

(67) Lan, H.; Ding, Y. Nanoimprint Lithography. In Lithography; Wang, M., Ed.; In Tech: Croatia, 2010; pp. 458–494.

(68) Shen, Y.; Yao, L.; Li, Z.; Kou, J.; Cui, Y.; Bian, J.; Yuan, C.; Ge, H.; Li, W.-D.; Wu, W.; et al. Double Transfer UV-Curing Nanoimprint Lithography. Nanotechnology 2013, 24, 465304.

(69) Simao, C.; Khunsin, W.; Kehagias, N.; Salaun, M.; Zelsmann, M.; Morris, M. A.; Sotomayor Torres, C. M. Order Quantification of Hexagonal Periodic Arrays Fabricated by in Situ Solvent-Assisted Nanoimprint Lithography of Block Copolymers. Nanotechnology 2014, 25, 175703.

(70) Dong, Q.; Li, G.; Ho, C.-L.; Faisal, M.; Leung, C.-W.; Pong, P. W.-T.; Liu, K.; Tang, B.-Z.; Manners, I.; Wong, W.-Y. A Polyferroplatinyne Precursor for the Rapid Fabrication of L1o -FePt-Type Bit Patterned Media by Nanoimprint Lithography. Adv. Mater. 2012, 24, 1034–1040.

(71) Kasi, A. K.; Kasi, J. K.; Afzulpurkar, N.; Hasan, M. M.; Mahaisavariya, B. Bending and Branching of Anodic Aluminum Oxide Nanochannels and Their Applications. J. Vac. Sci. Technol. B 2012, 30, 031805 1–6.

(72) Santos, a.; Formentín, P.; Ferré-Borrull, J.; Pallarès, J.; Marsal, L. F. Nanoporous Anodic Alumina Obtained without Protective Oxide Layer by Hard Anodization. Mater. Lett. 2012, 67, 296–299.

(73) Santos, A.; Kumeria, T.; Losic, D. Nanoporous Anodic Aluminum Oxide for Chemical Sensing and Biosensors. TrAC Trends Anal. Chem. 2013, 44, 25–38.

(74) Koh, G.; Agarwal, S.; Cheow, P.-S.; Toh, C.-S. Development of a Membrane-Based Electrochemical Immunosensor. Electrochim. Acta 2007, 53, 803–810.

(75) Debrassi, A.; Ribbera, A.; Vos, W. M. De; Wennekes, T.; Zuilhof, H.; de Vos, W. M. Stability of (bio)functionalized Porous Aluminum Oxide. Langmuir 2014, 30, 1311–1320.

(76) Wen, L.; Sun, Z.; Han, C.; Imene, B.; Tian, D.; Li, H.; Jiang, L. Fabrication of Layer-by-Layer Assembled Biomimetic Nanochannels for Highly Sensitive Acetylcholine Sensing. Chem. a Eur. J. 2013, 19, 7686–7690.

(77) De la Escosura-Muñiz, A.; Merkoçi, A. Label-Free Voltammetric Immunosensor Using a Nanoporous Membrane Based Platform. Electrochem. commun. 2010, 12, 859–863.

(78) De la Escosura-Muñiz, A.; Merkoçi, A. A Nanochannel/nanoparticle-Based Filtering and Sensing Platform for Direct Detection of a Cancer Biomarker in Blood. Small 2011, 7, 675–682.

(79) De la Escosura-Muñiz, A.; Mekoçi, A. Nanoparticle Based Enhancement of Electrochemical DNA Hybridization Signal Using Nanoporous Electrodes. Chem. Commun. 2010, 46, 9007–9009.

(80) De la Escosura-Muñiz, A.; Chunglok, W.; Surareungchai, W.; Merkoçi, A. Nanochannels for Diagnostic of Thrombin-Related Diseases in Human Blood. Biosens. Bioelectron. 2013, 40, 24–31.

Chapter 2.

Objectives

General objectives

The main objective of this thesis is the design, fabrication and study of the analytical performance of novel electrochemical biosensing systems based on the advantageous properties of nanostructured materials such as nanoparticles and nanochannels including the evaluation of their potential application in the detection of various biomolecules with interest in clinical analysis and food control.

More in details the objectives are:

1. **Design and evaluation of novel gold nanoparticles (AuNP)-based theranostic system for bacteria sensing and use as inhibitor with interest in animal health protection**. Evaluation of the capability of AuNPs to act as both electrocatalytic tags (sensing application) for fimbriae bacteria recognition and quantification and as carriers of peptides to be used as inhibitors of bacterial adhesion in animals.

2. **Study of highly integrated nanochannel-based platforms with interest for biosensing applications.** Design and development of novel methodologies for the direct nanochannel arrays fabrication onto electrotransducer surfaces based on nanoimprint lithography and nanoparticle assembling.

3. **Development of alternative electroactive indicators with interest for nanochannel-based platforms**. Synthesis and characterization of Prussian blue nanoparticles (BPNPs) for their application as advantageous red-ox indicator in nanochannel array-based label-free immunosensing systems.

4. **Application of the above mentioned nanoparticle/nanochannel-based sensing systems for the detection of cancer biomarkers**. Evaluation of the analytical performance of the developed platforms in standard solutions and real samples / biological fluids.

Chapter 3.

Modification of gold nanoparticles for future theranostic applications

Related publication

Casein modified gold nanoparticles for future theranostic applications.

*Marisol Espinoza-Castañeda[1], Alfredo de la Escosura-Muñiz[1], Gemma González-Ortiz[2], Susana M. Martín-Orúe[2], José Francisco Pérez[2], Arben Merkoçi [1,3]**

[1] Nanobioelectronics & Biosensors Group, Institut Català de Nanotecnologia, Universidad Autónoma de Barcelona, Bellaterra, Barcelona, Spain
[2] Nutrition, Management and Welfare Research Group, Animal and Food Science Department, Universitat Autònoma de Barcelona, Barcelona, Spain
[3] ICREA, Barcelona, Spain

Biosensors and Bioelectronics 40 (2013) 271–276

Chapter 3. Modification of gold nanoparticles for future theranostic applications

3.1. Introduction

Nanomaterials (NMs) play an important role in current sensing and biosensing technologies. These materials are showing improvement of the performance of biosensing systems in general (i.e. proteins [1], cells [2], heavy metals [3] and that of electrochemical sensing devices particularly. In addition to the biosensing applications [4–6], the use of nanoparticles (NPs) as carriers of biomolecules and their application in biomedical and nutritional technologies, between others, is an emerging research field in the last years. It is well known that NPs exhibit physical properties that are truly different from both small molecules and bulk material [7]. The special properties of NPs are due to their high ratio between surface area/total volume and the high surface energy, allowing a strong biomolecules adsorption. These biomolecules can be used in order to carry the nanoparticles to the target organ and/or the biomolecules by themselves to exert therapeutic effects [8]. Gold nanoparticles (AuNPs) are specially suitable for such applications, due to their low toxicity [9] and good biocompatibility with peptides, proteins, DNAs, etc. [10]. These nanomaterials can be synthesized reproducibly, modified with seemingly limitless chemical functional groups, and in certain cases, characterized with atomic-level precision [11].

Thanks to the combination of all these properties, AuNPs have been extensively proposed for applications in several fields such as the environmental and the food/agriculture one [12–14] being especially relevant their application for biomedical and therapeutic purposes [15]. Functional nanomaterials show different modalities for treatment of common diseases such as cancers, abnormal blood vessel growth, infectious diseases and tissues.

Among potential target diseases for functional nanomaterials are the enteric diseases, in both humans and animals. While infants diarrhoea is a major cause of mortality in developing countries, enteric diseases is also a leading cause of mortality in piglets and a major cause of economic losses in the pig industry [16]. Enterotoxigenic Escherichia coli (ETEC) K88 is the main bacterial cause of diarrhea in piglets around weaning and the adhesion of ETEC to the intestinal mucosa is a prerequisite step for its colonization. Specifically, Escherichia coli (*E. coli*) F4, K88 serotype expresses fimbrial adhesions which specifically identifies affinities to glycoproteins, sialoglycoproteins or glycosphingolipids in the membrane of host cells [17,18]. Recently, different authors have suggested that the dietary inclusion of some receptor analogues, on the basis of their glycoside composition, would be a practical strategy to reduce the number of some intestinal pathogens that bind to the animal cells via carbohydrate-specific adhesions [19,20].

The casein glycomacropeptide (CGMP), a glycoprotein originating during cheese manufacture, has shown promising effects on the interaction with the microbiota through the activity of carbohydrate moieties present in the molecule (sialic acid content of around 4.2% [21]). Some authors have reported that CGMP binds the cholera toxin of Vibrio cholera [22] and inhibits the adhesion of pathogenic *E. coli* to the mucosal surface or its growth in vitro [23] and in vivo (Schematic representation of the steps involved in the experimental procedure. Peptide/AuNPs conjugates are formed (A), incubated with both fimbriae (K88) (B) and non-fimbriae (NF) (B') *E. coli* and finally detected/discriminated in screen-printed carbon electrodes through the AuNPs electrocatalyzed hydrogen evolution reaction (C, C'). TEM images correspond to K88 (D) and NF (D') *E. coli* after their incubation with the CGP/AuNPs conjugate. The inset image is a zoom that shows AuNPs (small black points) on the surface of the K88 bacteria [24]. In line with its antimicrobial effects, the CGMP has also cariogenic properties and has been proposed to be used in tooth paste [25]. In addition CGMP may also interfere with the host cells, and has been shown to affect both innate and adaptive immunity,

modulating the immune/inflammatory response by the activation of macrophages, down-regulation of IL-6 and up-regulation of IL-10 [26].

In the present study, we have worked on the design of AuNPs, as both carriers/electrocatalytic labels, with the properties of k-casein derived peptides to bind specific bacteria fimbriae adhesions. These peptides modified nanoparticles are used for the evaluation of the interaction between the peptides and the K88 fimbriae bacteria (K88) and found with interest for future potential applications not only for biosensing purposes but also for therapeutic applications. Such a theranostic platform can also be extended to other biotechnological applications including food, health and pharmaceutical fields.

3.2. Experimental section

3.2.1. Apparatus and electrodes

Zeta potential of the AuNPs and peptide/AuNPs conjugates was determined with a Malvern Zetasizer Nano-ZS (Malvern Instruments Ltd., UK) according to the manufacturer's recommendations.

Optical characterizations of the AuNPs and peptide/AuNPs conjugates were performed using a Transmission Electron Microscope (TEM) Jeol JEM-2011 (Jeol Ltd, Japan) and a Gemini SpectraMax M2e Multi-Mode Microplate Reader (Molecular Devices, CA, U.S.A.).

The electrochemical transducers used were homemade screen-printed carbon electrodes (SPCEs), consisting of three electrodes: working electrode, reference electrode and counter electrode in a single strip fabricated with a semi-automatic screen-printing machine DEK248 (DEK International, Switzerland). The reagents used for this process were: Autostat HT5

polyester sheet (McDermid Autotype, UK) and Electrodag 423SS carbon ink, Electrodag 6037SS silver/silver chloride ink and Minico 7000 Blue insulating ink (Acheson Industries, The Netherlands).

An ultrasonic bath (JP Selecta, Spain) was used for the bacteria/peptide/AuNP conjugate pre-treatment before the electrochemical measurements.

The electrochemical measurements were taken using a CompactStat potentiostat (Ivium Technologies, The Netherlands) connected to a PC. All the measurements were carried out at room temperature with a working volume of 50 μL, which was enough to cover the three electrodes contained in the SPCEs connected to the potentiostat by a homemade edge connector module.

3.2.2. Reagents and solutions

Caseinoglycopeptide (CGP) was purchased from Sigma-Aldrich (Spain) and dissolved in 0.01 M PBS, pH 6.8. Lacprodan (CGMP-10) was purchased from Arla Foods Ingredients (Denmark) and its solutions were prepared in 0.01 M PBS, pH 7.4.

Hydrogen tetrachloroaurate (III) trihydrate ($HAuCl_4 \cdot 3H_2O$, 99.9%) and trisodium citrate ($Na_3C_6H_5O_7 \cdot 2H_2O$) reagents used for the gold nanoparticles preparation were also purchased from Sigma-Aldrich (Spain). KH_2PO_4 and K_2HPO_4 reagents used for the preparation of the phosphate buffer solutions (PBS) were acquired from Fluka (Spain).

An *E. coli* K88 fimbriae bacteria (K88) isolated from a colibacillosis outbreak in Spain (Blanco et al., 1997), serotype (O149:K91:H10 [K-88]/LT-I/STb) was provided by the *E. coli* Reference Laboratory, Veterinary Faculty of Santiago de Compostela (Spain). A non-fimbriated *E. coli* (F4 -, F6 -, F18 -, LT1 -, ST1 -, ST2 +, Stx2e -) (NF) isolated from the faeces of a post-weaning piglet was donated by the Department of Animal Health and Anatomy from the Universitat Autònoma de Barcelona (Spain). *E. coli* K88 was cultured in

unshaken Luria Broth (Sigma, St Louis) at 37 ºC while the *E. coli* NF was cultured shaking the media. Cultures were serially passage every 48 h, at least three times. All chemicals were used as received and all aqueous solutions were prepared in Milli-Q water.

3.3.Methods

3.3.1. Fabrication of screen-printed carbon electrodes (SPCEs)

The electrochemical transducers were homemade screen-printed carbon electrodes (SPCEs), consisting of three electrodes: working electrode (WE) reference electrode (RE) and counter electrode (CE) in a single strip. The full size of the sensor strip was 29 mm x 6.7 mm, and the WE diameter was 3 mm. The fabrication of the SPCEs was carried out in three steps. First, a graphite layer was printed onto the polyester sheet, using the screen-printing machine with the stencil (where it is the electron pattern). After curing for 45 minutes at 95 ºC, an Ag/AgCl layer was printed and cured for 30 minutes at 95 ºC. Finally, the insulating ink was printed and cured at 95 ºC for 30 minutes. Figure 3-1 shows images of the 45-sensor sheet obtained following the detailed experimental procedure (A) and a detail of a single sensor (B).

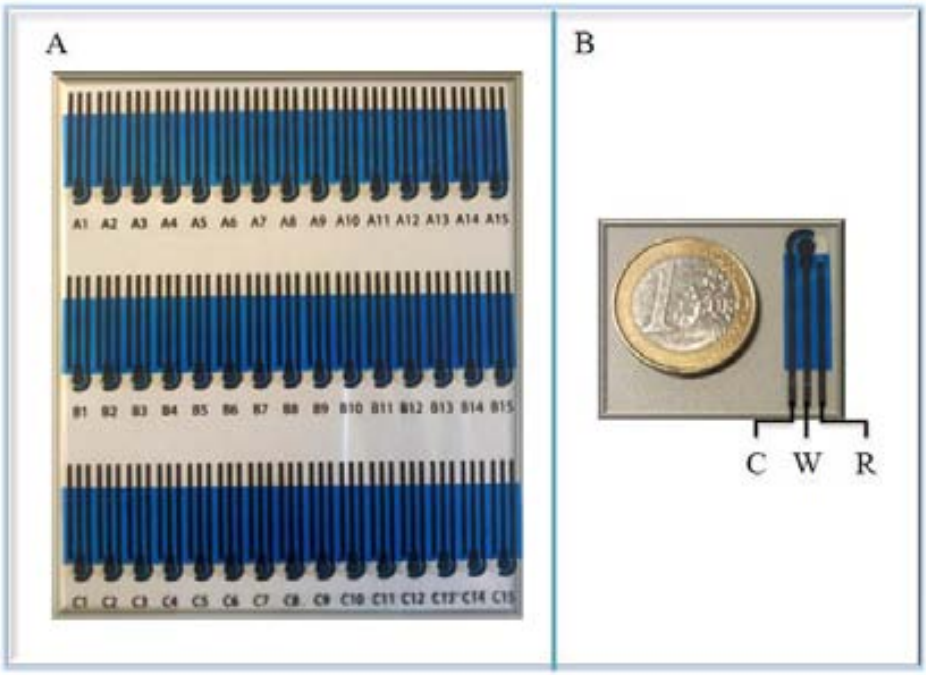

Figure 3-1(A) A 45-sensor sheet obtained following the experimental procedure detailed, and (B) detail of a SPCE, showing the area with the three electrodes: reference silver electrode (R), carbon working electrode (W) and carbon counter electrode (C).

3.3.2. Preparation of gold nanoparticles and modification with peptides

20 nm gold nanoparticles (AuNPs) were synthesized by reducing tetrachloroauric acid with trisodium citrate, a method pioneered by Turkevich [27]. A total of 200 mL of 0.01% $HAuCl_4$ solution were boiled with vigorous stirring. 5 mL of a 1% trisodium citrate solution were added quickly to the boiling solution. When the solution turned deep red, indicating the formation of gold nanoparticles, it was left stirring and cooling down. In this way, a dispersed solution of 20 nm AuNPs was obtained.

The conjugation of AuNPs with CGP was performed adapting the procedure reported by Liu et al. [28] where it is described that the critical micelle concentration of casein is around 1.0 mg/mL in 0.01 M PBS pH 6.8. Considering this, different mixtures of CGP in the above mentioned buffer and AuNPs solution (from the obtained stock solution of around 3 nM concentration) were prepared at different ratios. Concretely, three different concentrations of CGP (1, 0.1 and 0.01 mg/mL) and three different CGP/AuNPs concentration ratios (1:1, 1:3

and 3:1) were assayed. The incubations of the CGP/AuNPs solutions were performed in a final volume of 500 µL at 20 °C for 30 minutes with gentle mixing. Finally, in order to remove the excess of CGP, the conjugate was centrifuged 1X at 14,000 rpm (25 ºC) and re-suspended in 500 µL of 0.01 M PBS pH 6.8.

In the case of the CGMP-10 peptide, a similar procedure was followed but using 0.01 M PBS, pH 7.4 as buffer and only a fixed condition: a 0.01 mg/mL concentration of peptide and a CGMP-10/AuNP concentration ratio of 3:1.

3.3.3. TEM analysis with negative staining

3 µL of uranyl acetate were added to 3 µL of the peptide/AuNPs conjugates previously placed on the carbon grill. After 1 minute, the excess of acetate was removed with filter paper and dried at room temperature. For comparison purposes, this pre-treatment was also applied for the AuNPs without peptides modification.

3.3.4. Zeta Potential Measurements

1 mL suspension of AuNPs (the same as for the peptide /AuNP conjugates) was transferred into a 1 mL polystyrene cuvette (DTS1061, Malvern Instruments Ltd). The data were collected and analyzed with the Dispersion Technology software 4.20 (Malvern) producing diagrams for the zeta potential as a distribution versus total counts.

3.3.5. UV-Vis spectroscopic measurements

300 µL suspension of AuNPs (the same as for the peptide /AuNP conjugates) were introduced in a well of a microplate and the optical density in the range between 400-600 nm was read with a microplate reader and analyzed using the SoftMax Pro 5.2 program.

3.3.6. *E. coli* bacteria culture

Both *E. coli* bacterial cells, K88 and NF, from an overnight culture were harvested by centrifuging 15 mL broth volume (5 min, 1700 g). All the supernatants were removed and 0.01 M PBS buffer, at the convenient pH, was added to the cell pellets to achieve an optical density of the bacterial suspensions of 1.30, 1.15 and 1 (650 nm) that corresponds with log 10, log 9 and log 8 CFU/mL, respectively.

3.3.7. Incubation of the peptide/AuNPs conjugates with *E. coli* bacteria

The incubation was carried out by mixing 500 µL of the peptide/AuNP conjugate with 500 µL of *E. coli* (both K88 and NF) at log 8, log 9 and log 10 CFU/mL during 30 min at 37 ºC under gentle stirring. After that, the solution was centrifuged at 1700 g (20 ºC, 5') the supernatant was removed and the pellet re-suspended in 50 µL of 0.01 M PBS buffer (at the pH convenient for each peptide, as detailed previously). All the assays were performed in triplicate.

3.3.8. Electrocatalytic detection

50 µL of the bacteria/peptide/AuNP conjugate (different concentrations of bacteria, as detailed in the previous section) were mixed with 50 µL of 2 M HCl and treated in an ultrasonic bath for 5 min. 50 µL of this solution were placed onto the surface of the electrochemical transducer and kept there for 2 min. After that, quantitative analyses were carried out taking advantage of the chronoamperometric mode [29,30]. Chronoamperograms were obtained by subsequently holding the working electrode at a potential of +1.35 V for 1 min and then applying a negative potential of -1.00 V for 100 seconds, recording the cathodic current generated. The absolute value of the current registered at 100 seconds was chosen as analytical signal.

The background was recorded for 50 µL of 1 M HCl. A new electrode was employed for each measurement.

3.4. Results and discussion

3.4.1. Optimization/characterization of peptide/AuNPs conjugates

The mechanism of the peptide immobilization onto the surface of the AuNPs consists in a physical adsorption [28,31]. The pH plays here an important role since changes in its value give rise to a variation in the charge of the formed cells which consequently affects their adsorptive properties [28,32]. For this reason, the two peptides (CGP and CGMP-10) assayed in this work were dissolved in 0.01 M PBS buffers at different pHs (6.8 and 7.4 respectively).

The critical micelle concentration (defined as the solute concentration at which micelles first appear in solution [33]) of casein is also a crucial parameter to be considered since the micelles can either encapsulate the AuNPs or form agglomerates. For this reason, the concentrations of peptides assayed were below this value, as described at methods section.

Following the experimental procedure detailed at methods section, stable suspensions of both CGP/AuNPs and CGMP-10/AuNPs conjugates were obtained. In order to check the AuNPs surface modification after the conjugation, these suspensions were evaluated following different characterization techniques.

They were first characterized by TEM analysis using a negative staining pre-treatment. Negative staining is an established method, often used in diagnostic microscopy, for contrasting a thin specimen with an optically opaque fluid. Typical stainers are ammonium molybdate, uranyl acetate, uranyl formate, phosphotungstic acid, osmium tetroxide, osmium ferricyanide or auroglucothionate because they scatter electrons well and easily adsorb onto biological matter. Due to these properties, this method is used to view viruses, bacteria, bacterial flagella, biological membrane structures and proteins or protein aggregates, which

all have a low electron-scattering power. For this reason, this sample pre-treatment was chosen in order to observe the presence of the peptides around the AuNPs in the prepared conjugates.

As detailed in methods section, first of all different CGP peptide concentrations and different CGP/AuNPs conjugation ratios were assayed. A summary of the TEM images obtained under these different conditions and the proposed conjugate configurations are shown in Figure 3-2, finding that the optimum conditions corresponded to a CGP concentration of 0.01 mg/mL and a CGP:AuNPs concentration ratio of 3:1. Under these conditions, the agglomeration induced by micelles as well as the encapsulation of the AuNPs inside the micelles are avoided (both phenomena are observed for higher peptide concentrations).

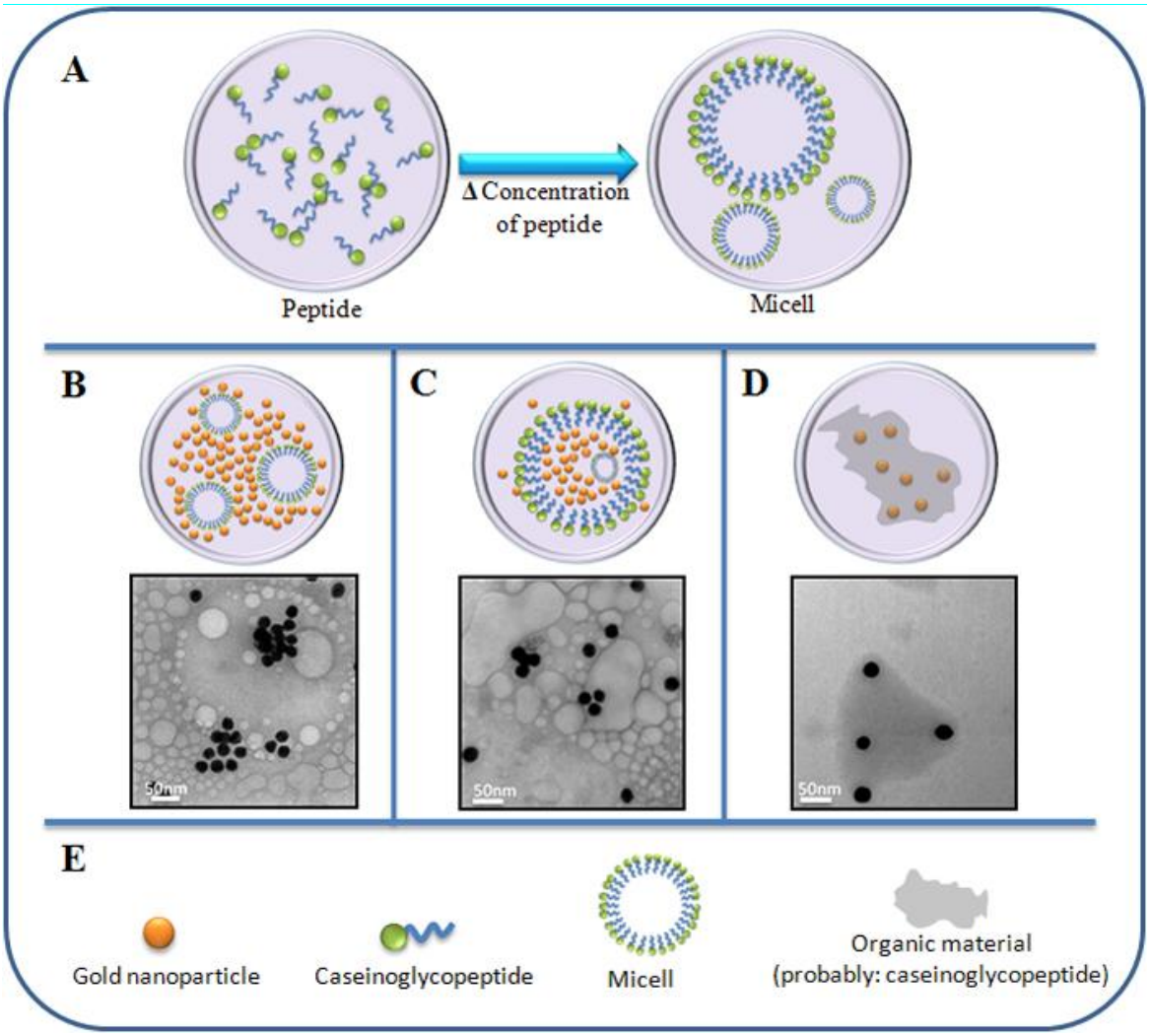

Figure 3-2. Schematic representation of the proposed CGP/AuNPs configurations and the corresponding TEM images (obtained after negative staining pre-treatment). (A) Scheme of the self-assembly of micelles due to high concentrations of CGP in solution (1 mg/mL). At this high concentration in solution, the AuNPs can be either agglomerated by the presence of the micelles (B) or encapsulated inside the micelles (D). However, for lower CGP concentrations (0.01 mg/mL) the AuNPs are well dispersed and the organic material (the "dark shadow") seems to cover the AuNPs. (E) Definitions of the images symbol.

Under these optimum conditions, a good AuNPs dispersion along with a "dark shadow" around them is noticed, as can be observed in Figure 3-3A, left; this shadow is not observed for the unmodified AuNPs (Figure 3-3A, right). The conjugates prepared with both peptides under the above mentioned optimized conditions were also evaluated by UV-Vis spectroscopy. As observed in Figure 3-3B, a shift in the wavelength of the maximum of absorbance from 520 nm (AuNPs) to 525 nm (CGP/AuNPs) and to 523 nm (CGMP-

10/AuNPs) is noticed. These shifts evidence that the surface of the AuNPs has been modified, suggesting again the conjugate formation.

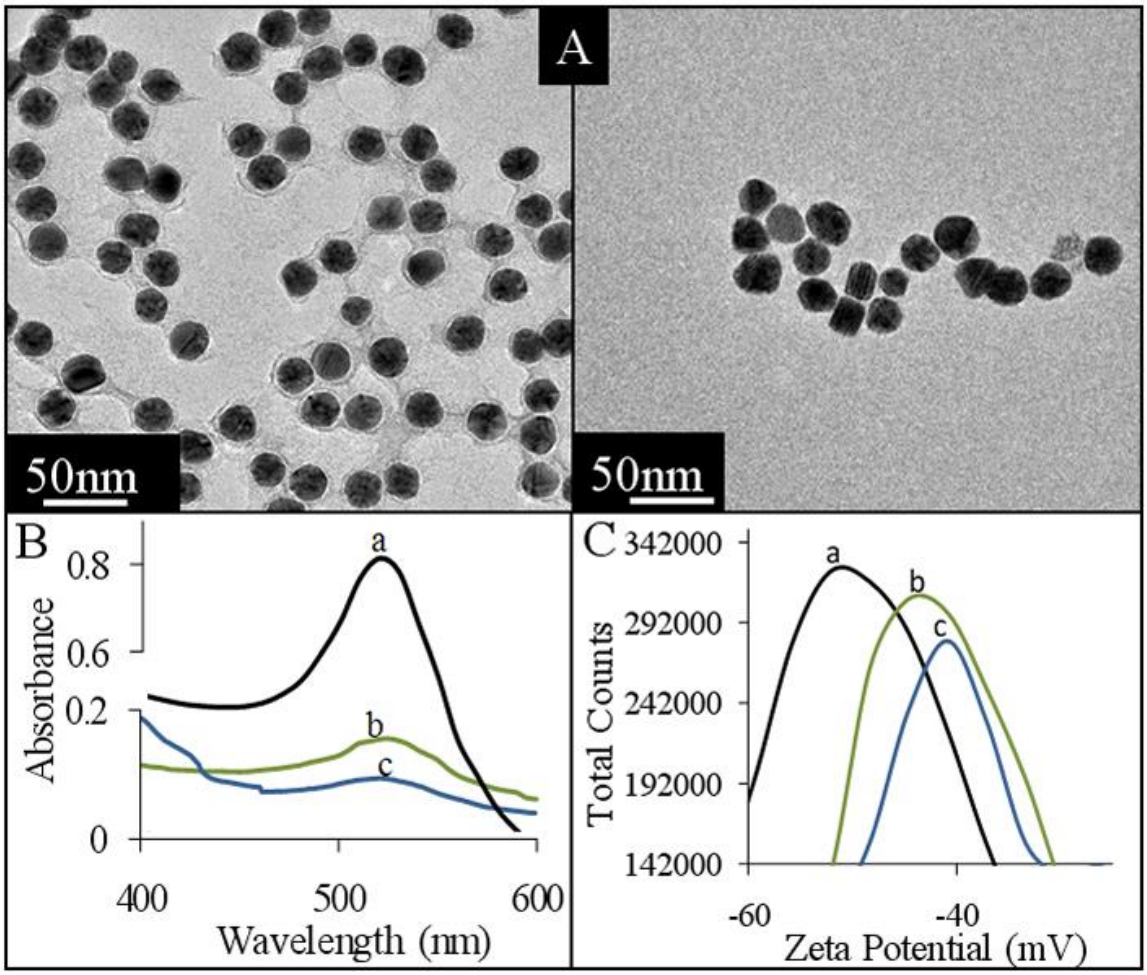

Figure 3-3. (A) TEM image (after negative staining pre-treatment) obtained for a CGP/AuNPs suspension prepared following the experimental procedure detailed at methods section (left) and an unmodified AuNPs suspension (right). (B) UV-Vis spectra obtained for: a. AuNPs, b. CGP/AuNPs and c. CGMP-10/AuNPs. (C) Diagram for the zeta potential as a distribution versus total counts for: a. AuNPs, b. CGP/AuNPs and c. CGMP/AuNPs.

Finally, zeta potential technique was also used for the characterization of the optimized conjugate. This technique has been recently reported as an efficient tool which allows the monitoring and analysis of chemical modifications on the surface of nanoparticles, with minimal sample preparation [34]. The easily measurable zeta potential has been used to obtain information concerning the particle surface charge, chemical modifications and also stability of colloid suspensions. A high zeta potential (positive or negative) confers stability since the solution or dispersion resists aggregation. When the absolute value of the zeta potential is

low, attraction exceeds repulsion and the dispersion breaks and flocculates. Due to all that, it has been defined that nanoparticle suspensions begin to be stable for absolute zeta potential values higher than 10 mV. As can be observed in Figure 3-3C, the surface charge of the AuNPs reaches a maximum at -52.2 mV, indicating a very good stability of the obtained suspension. When the AuNPs are coated by CGP (CGP/AuNPs) or by CGMP-10 (CGMP-10/AuNPs) a change in the surface charge is noticed through the shift in the value to -44.7 mV and -40.9 mV respectively, indicating again the conjugate formation.

3.4.2. Electrocatalytic evaluation of the peptide/AuNP interaction with fimbriated bacteria

Once the peptide/AuNPs conjugates were formed, their interaction with a fimbriated *E. coli* (K88) was evaluated. As explained before, it is known that some peptides such as k-casein derived ones (this is the case of CGP and CGMP-10) are potential inhibitors of bacterial adhesion to intestinal mucous, being this of potential application in nutritional treatments in order to avoid serious digestive affections, mainly thanks to their ability to bind cholera and *E. coli* enterotoxins. It is proposed that such interaction takes place via the specific adhesion factors (fimbriae) of the bacteria (responsible of the colonization of the small intestine) [35], so a NF was used as control to check the selectivity of the assay.

The interaction of both CGP/AuNPs and CGMP-10/AuNPs conjugates with both kinds of bacteria was studied under the experimental conditions detailed at methods (see also a scheme of this procedure in Figure 3-4A, B, B').

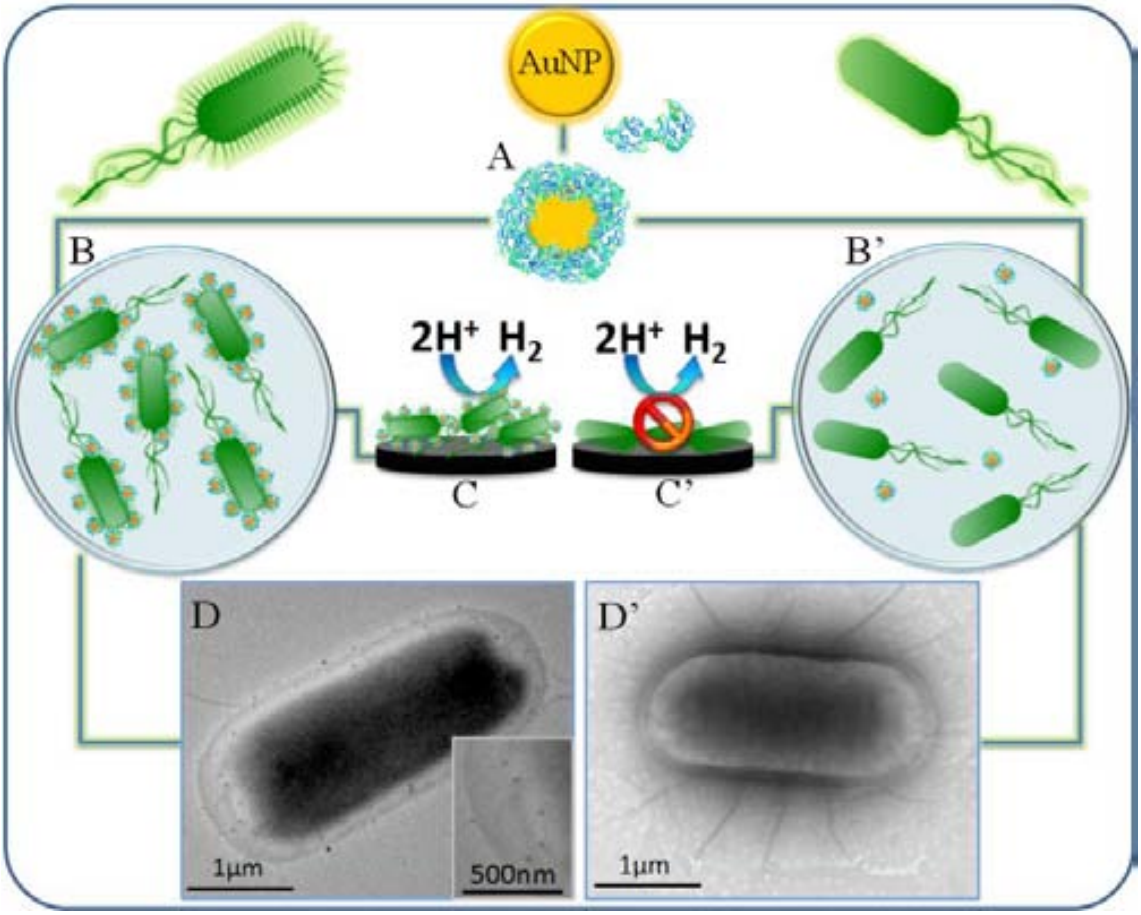

Figure 3-4. Schematic representation of the steps involved in the experimental procedure. Peptide/AuNPs conjugates are formed (A), incubated with both fimbriae (K88) (B) and non-fimbriae (NF) (B') E. coli and finally detected/discriminated in screen-printed carbon electrodes through the AuNPs electrocatalyzed hydrogen evolution reaction (C, C'). TEM images correspond to K88 (D) and NF (D') E. coli after their incubation with the CGP/AuNPs conjugate. The inset image is a zoom that shows AuNPs (small black points) on the surface of the K88 bacteria.

The final electrochemical identification is performed thanks to the electrocatalytic effect of the AuNPs on the electrocatalytic hydrogen evolution reaction on screen-printed carbon electrodes [29] (Figure 3-4 C,C'). The presence of the AuNPs on the electrode surface catalyzes the reduction of hydrogen ions (present in the acidic electrolyte) to hydrogen. This hydrogen evolution generates a cathodic current that can be chronoamperometrically monitored, being the absolute value of the current registered at 100 seconds (previously optimized) the analytical signal which is proportional to the quantity of AuNPs and, consequently, to the quantity of bacteria. This electrochemically evaluated interaction takes also advantages of the ability of the AuNPs to act as carriers of a high number of peptides which in turns can

increase their attachment with K88, ensuring an amplified signal useful for both identification and quantification of bacteria.

First of all, the CGP/AuNP was assayed, not observing any catalytic current for both bacteria (data not shown), suggesting that there was not any affinity of this peptide for the bacteria.

However, when the CGMP-10/AuNPs conjugate was assayed, a significant catalytic current was registered, being its value considerably higher for the assay performed with the K88 bacteria in comparison with the obtained for the NF one. As it observed in Figure 3-5, the value of this analytical signal is bacteria concentration-dependent in the range of log 10 - log 8 CFU/mL, allowing to discriminate in all cases both kinds of bacteria.

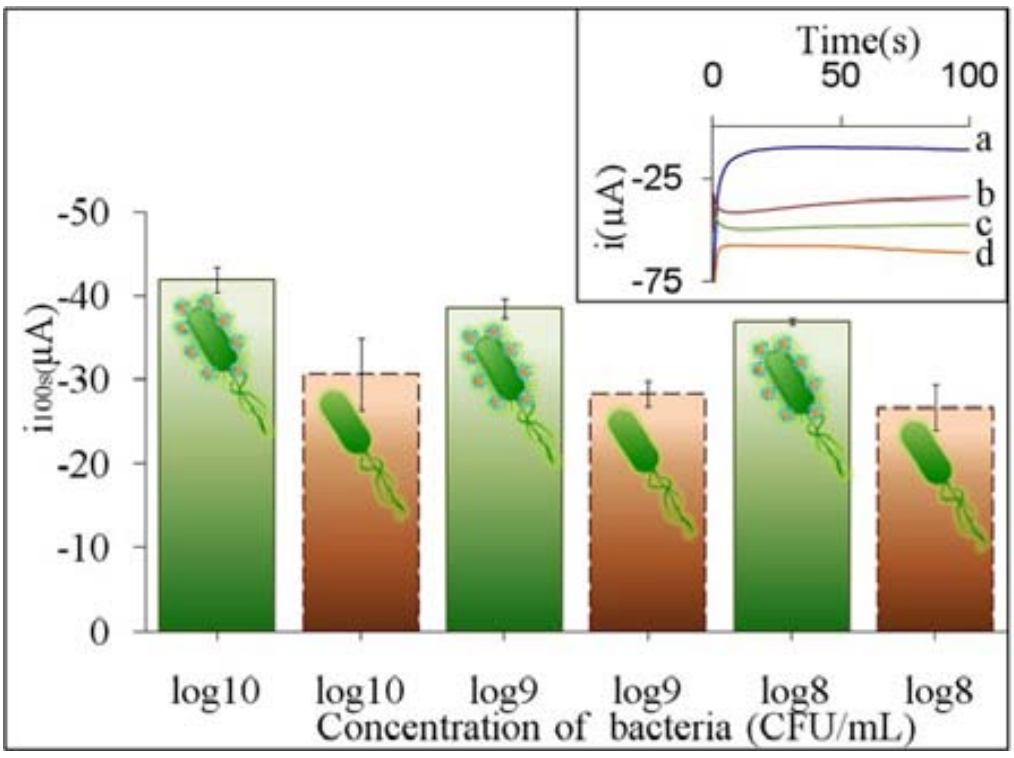

Figure 3-5. Summary of the analytical signals (value of the chronoamperometric current at 100 seconds) obtained for different concentrations of K88 (columns with solid line) and NF (columns with dotted line) bacteria after their incubation with the CGMP-10/AuNPs conjugate, following the experimental procedure detailed at methods section. The inset graph corresponds to the chronoamperograms obtained during the electrocatalytic hydrogen evolution at -1V in 1 M HCl for a log 10 CFU/mL concentration of K88 (c) and NF (b) after incubation with CGMP-10. For comparison purposes, the background (1 M HCl, a) and the register obtained for AuNPs in 1 M HCl (d) are also shown.

The observed non-specific signals coming from the NF bacteria remain approximately constant for all the assayed concentrations. This behavior seems to indicate that these non-

specific signals can be probably due to remaining of peptide/AuNPs not efficiently removed after their incubation with the bacteria (related to low efficiency of the centrifugation/purification step). Anyway even under such experimental conditions a clear discrimination between the two kinds of bacteria can be observed.

The electrochemical results were also corroborated by TEM analysis. Figure 3-4 are shown TEM images of the K88 (D) and the NF (D') bacteria after the incubation with the CGMP-10/AuNP conjugate. It can be clearly observed the presence of AuNPs (small black points) attached to the K88 bacteria while by contrary, there aren't nanoparticles observed in the case of the NF bacteria, evidencing the high affinity of the CGMP-10 peptide for the fimbriae. Such an interaction is probably related to the strain-depend behavior. CGMP-10 contains 3 glycosylation sites with a heterogeneous array of glycans, based on a core of Galβ1→3GalNAc [36,37]. These glycans carrying terminal N-acetylneuraminic acid residues (commonly referred to as sialic acids) are known to act as receptors for several pathogens, including enterotoxigenic and enteroaggregative *E. coli* strains, allowing thus the interaction with the fimbriae *E. coli.*

3.5.Conclusions

A simple electrochemical theranostic platform based on the use of gold nanoparticles with interest for the study of the effect of k-casein derived peptides as inhibitors of bacterial adhesion is developed. The peptide modified gold nanoparticles are firstly characterized by TEM, UV-Vis, and Z-potential so as to ensure stable, size-homogenous and well dispersed nanoinhibitors. The prepared peptide modified nanoparticles are used for the evaluation of the interaction between the peptides and the K88 fimbriae bacteria (K88). The hydrogen

evolution reaction (occurred onto screen-printed carbon electrodes) induced by gold nanoparticles used also as carriers of inhibitors is followed by a simple chronoamperometric measurement at an applied fixed potential. The efficiency of the developed theranostic system is also evaluated using another class of bacteria (NF) that do not present fimbriae onto its surface. The obtained results show that gold nanoparticles can be easily loaded with k-casein derived, drive toward fimbria bacteria and electrochemically detected distinguishing the fimbriae (K88) from non-fimbriae (NF) bacteria.

The developed proof of concept system, given its simplicity and fast development possibility, could be with interest for several other biotechnological applications including food, health and pharmaceutical fields.

3.6. References

(1) De la Escosura-Muñiz, A.; Merkoçi, A. Electrochemical Detection of Proteins Using Nanoparticles: Applications to Diagnostics. Expert Opin. Med. Diagn. 2010, 4, 21–37.

(2) Perfézou, M.; Turner, A.; Merkoçi, A. Cancer Detection Using Nanoparticle-Based Sensors. Chem. Soc. Rev. 2011, 41, 2606–2622.

(3) Aragay, G.; Pons, J.; Merkoçi, A. Enhanced Electrochemical Detection of Heavy Metals at Heated Graphite Nanoparticle-Based Screen-Printed Electrodes. J. Mater. Chem. 2011, 21, 4326.

(4) De la Escosura-Muñiz, A.; Ambrosi, A.; Merkoçi, A. Electrochemical Analysis with Nanoparticle-Based Biosystems. Anal. Chem. 2008, 27, 568–584.

(5) Merkoçi, A. Nanoparticles-Based Strategies for DNA, Protein and Cell Sensors. Biosens. Bioelectron. 2010, 26, 1164–77.

(6) Pérez-López, B.; Merkoçi, A. Nanoparticles for the Development of Improved (bio)sensing Systems. Anal. Bioanal. Chem. 2011, 399, 1577–1590.

(7) Dreaden, E. C.; Alkilany, A. M.; Huang, X.; Murphy, C. J.; El-Sayed, M. A. The Golden Age: Gold Nanoparticles for Biomedicine. Chem. Soc. Rev. 2012, 41, 2740–2779.

(8) Mohanraj, V. J.; Chen, Y. Nanoparticles – A Review. Trop. J. Pharm. Res. 2006, 5, 561–573.

(9) Xue, X.; Wang, F.; Liu, X. Emerging Functional Nanomaterials for Therapeutics. J. Mater. Chem. 2011, 21, 13107–13127.

(10) Xu, Z. P.; Zeng, Q. H.; Lu, G. Q.; Yu, A. B. Inorganic Nanoparticles as Carriers for Efficient Cellular Delivery. Chem. Eng. Sci. 2006, 61, 1027–1040.

(11) Giljohann, D. a; Seferos, D. S.; Daniel, W. L.; Massich, M. D.; Patel, P. C.; Mirkin, C. a. Gold Nanoparticles for Biology and Medicine. Angew. Chem., Int. Ed. 2010, 49, 3280–3294.

(12) Huang, L.; Guo, Y.; Peng, Z.; Porter, A. L. Characterising a Technology Development at the Stage of Early Emerging Applications : Nanomaterial- Enhanced Biosensors. Technol. Anal. Strateg. 2011, 23, 527–544.

(13) Dykman, L.; Khlebtsov, N. Gold Nanoparticles in Biomedical Applications: Recent Advances and Perspectives. Chem. Soc. Rev. 2012, 41, 2256–2282.

(14) Jans, H.; Huo, Q. Gold Nanoparticle-Enabled Biological and Chemical Detection and Analysis. Chem. Soc. Rev. 2012, 41, 2849–2866.

(15) Merkoçi, A. Nanoparticles-Based Strategies for DNA, Protein and Cell Sensors. Biosens. Bioelectron. 2010, 26, 1164–77.

(16) Madec, F.; Bridoux, N.; Bounaix, S.; Cariolet, R.; Duval-Iflah, Y.; Hampson, D. J.; Jestin, A. Experimental Models of Porcine Post-Weaning Colibacillosis and Their Relationship to Post-Weaning Diarrhoea and Digestive Disorders as Encountered in the Field. Vet. Microbiol. 2000, 72, 295–310.

(17) Sharon, N.; Gallagher, J. Selected Topics from the Advancing Forefront of Glycoprotein and Glycolipid Research. Curr. Opin. Struct. Biol. 2009, 19, 495–497.

(18) Shoaf-Sweeney, K. D.; Hutkins, R. W. Adherence, Anti-Adherence, and Oligosaccharides Preventing Pathogens from Sticking to the Host. Adv. Food Nutr. Res. 2009, 55, 101–161.

(19) Lane, J. a; Mehra, R. K.; Carrington, S. D.; Hickey, R. M. The Food Glycome: A Source of Protection against Pathogen Colonization in the Gastrointestinal Tract. Int. J. Food Microbiol. 2010, 142, 1–13.

(20) Tiralonngo, G.; Moran, A. P. Bacterial Lectin-like Interactions in Cell Recognition and Adhesion. In Microbial Glycobiology: Structures, Relevance and Applications; Moran, A. P.; Holst, O.; Brennan, Pa.; von Itzstein, M., Eds.; Academic Press: United Kingdom, 2009; pp. 551–656.

(21) Nakano, T.; Inoue, I.; Koyama, I.; Kanazawa, K.; Nakamura, K.-I.; Narisawa, S.; Tanaka, K.; Akita, M.; Masuyama, T.; Seo, M.; Hokari, S.; Katayama, S.; Alpers, D. H.; Millán, J. L.; Komoda, T. Disruption of the Murine Intestinal Alkaline Phosphatase Gene Akp3 Impairs Lipid Transcytosis and Induces Visceral Fat Accumulation and Hepatic Steatosis. Am. J. Physiol. Gastrointest. Liver Physiol. 2007, 292, G1439–G1449.

(22) Kawasaki, Y.; Isoda, H.; Tanimoto, M.; Dosako, S.; Idota, T.; Ahiko, K. Inhibition by Lactoferrin and Kappa-Casein Glycomacropeptide of Binding of Cholera Toxin to Its Receptor. Biosci. Biotech. Biochem. 1992, 56, 195–198.

(23) Malkoski, M.; Dashper, S. G.; O'Brien-Simpson, N. .; Talbo, G. H.; Macris, M.; Cross, K. J.; Reynolds, E. C. Kappacin , a Novel Antibacterial Peptide from Bovine Milk Kappacin , a Novel Antibacterial Peptide from Bovine Milk. Antimicrob. Agents Chemother. 2001, 45, 2309–2315.

(24) Hermes, R. G.; Molist, F.; Pérez, J. F.; de Segura, A. G.; Ywazaki, M.; MArtín-Orue, S. . 2010 Joint Annual Meeting of the American Society of Animal Science. In Casein glycomacropeptide (CGMP) in the diet of early weaned piglets reduces the Escherichia coli attachment to the intestinal mucosa and increases lactobacillar numbers in digesta; Denver, Colorado., 2010; Vol. 88, pp. 88–90.

(25) Aimutis, W. R. Bioactive Properties of Milk Proteins with Particular Focus on Anticariogenesis. J. Nutr 2004, 134, 989S–995S.

(26) De Medina, F. S.; Daddaoua, A.; Requena, P.; Capitán-Cañadas, F.; Zarzuelo, A.; Dolores Suárez, M.; Martínez-Augustin, O. New Insights into the Immunological Effects of Food Bioactive Peptides in Animal Models of Intestinal Inflammation. P. Nutr, Soc. 2010, 69, 454–462.

(27) Turkevich, J.; Cooper Stevenson, P.; Hillier, J. A Study of the Nucleation and Growth Processes in the Synthesis of Colloidal Gold. Discuss. Faraday Soc. 1951, 11, 55–75.

(28) Liu, Y.; Guo, R. The Interaction between Casein Micelles and Gold Nanoparticles. J. Colloid Interface Sci. 2009, 332, 265–269.

(29) De la Escosura-Muñiz, A.; Sánchez-Espinel, C.; Díaz-Freitas, B.; González-Fernández, A.; Maltez-da Costa, M.; Merkoçi, A. Rapid Identification and Quantification of Tumor Cells Using an Electrocatalytic Method Based on Gold Nanoparticles. Anal. Chem. 2009, 81, 10268–74.

(30) De la Escosura-Muñiz, A.; Mekoçi, A. Nanoparticle Based Enhancement of Electrochemical DNA Hybridization Signal Using Nanoporous Electrodes. Chem. Commun. 2010, 46, 9007–9.

(31) Walstra, P. Casein Sub-Micelles : Do They Exist ? Int. Dairy J. 1999, 9, 189–192.

(32) Jiang, X.; Jiang, J.; Jin, Y.; Wang, E.; Dong, S. Effect of Colloidal Gold Size on the Conformational Changes of Adsorbed Cytochrome c: Probing by Circular Dichroism, UV-Visible, and Infrared Spectroscopy. Biomacromolecules 2005, 6, 46–53.

(33) Reis, S.; Moutinho, C. G.; Matos, C.; de Castro, B.; Gameiro, P.; Lima, J. L. F. C. Noninvasive Methods to Determine the Critical Micelle Concentration of Some Bile Acid Salts. Anal. Biochem. 2004, 334, 117–26.

(34) Thielbeer, F.; Donaldson, K.; Bradley, M. Zeta Potential Mediated Reaction Monitoring on Nano and Microparticles. Bioconjugate Chem. 2011, 22, 144–150.

(35) Sun, R.; Anderson, T. J.; Erickson, A. K.; Nelson, E. A.; Francis, D. H. Inhibition of Adhesion of Escherichia Coli K88ac Fimbria to Its Receptor , Intestinal Mucin-Type Glycoproteins , by a Monoclonal Antibody Directed against a Variable Domain of the Fimbria Inhibition of Adhesion of Escherichia Coli K88ac Fimbria to Its Rec. Infect. Immun. 2000, 68, 3509–3515.

(36) Rhoades, J. R.; Gibson, G. R.; Formentin, K.; Beer, M.; Greenberg, N.; Rastall, R. a. Caseinoglycomacropeptide Inhibits Adhesion of Pathogenic Escherichia Coli Strains to Human Cells in Culture. J. Dairy Sci. 2005, 88, 3455–3459.

(37) Brody, E. P. Biological Activities of Bovine Glycomacropeptide. Br. J. Nutr. 2000, 84, S39–S46.

Chapter 4.

Design and fabrication of a new electrode based on ITO/PET and serigraphy imprinted as integrated system

Related publication

Assembled Nanoparticles-based Nanochannels onto a Plastic Flexible Substrate for Label-Free Immunosensing

*Marisol Espinoza-Castañeda†, Alfredo de la Escosura-Muñiz†, Madoka Hasegawa‡, Laetitia Philippe ‡, Arben Merkoçi†,§**

† Nanobioelectronics & Biosensors Group. ICN2 - Institut Català de Nanociencia i Nanotecnologia, Campus UAB, 08193 Bellaterra (Barcelona), Spain.

‡EMPA, Swiss Federal Laboratories for Materials Science and Technology, Feuerwerkerstrasse 39, 3602 Thun. Switzerland

§ICREA - Institució Catalana de Recerca i Estudis Avançats, 08010 Barcelona, Spain.

Submitted

Chapter 4. Design and fabrication of a new electrode based on ITO/PET and serigraphy imprinted as integrated system

4.1.Introduction

Nanochannels have been proposed in the last decade as very interesting and advantageous platforms for biosensing applications [1]. The great interest in nanoporous materials has started from the electrochemical stochastic sensing approaches which mimic the processes that occur in natural ion channels [2]. The typical experimental setup consists of measuring the changes in electrical conductance between both sides of the membrane where a single nanochannel is inserted, inspired by the Coulter counter concept [3], which has been applied for the detection of mainly DNA[4–7] and also of proteins and other analytes [8–10].

In spite of the advantages of biological ion channels in terms of sensitivity, selectivity, and ability for the analysis of a variety of analytes, their inherent limitations related to the difficulty of keeping a natural environment in an artificial device made necessary the development of novel strategies for the fabrication of solid-state nanochannels based on synthetic materials. In most cases, silicon nitride/oxide membranes have been used as substrate material to generate single solid-state nanochannels using electron-beam lithography and ion beam sculpting [11].

Alternative technologies have been reported in the last years for the preparation of not only single ones but also arrays of solid-state nanochannels, which opened the way to sensing systems totally different from the stochastic based approaches. Here, anodic aluminum oxide (AAO) nanoporous membranes prepared by anodization of aluminum metal substrates [12] have been the most used materials, due to their advantageous properties and mass production opportunities. These membranes possess optical properties which have been approached in

biosensing systems based on interferometric [13,14] detection, but is in the electrochemical analysis field where their potentiality has been mostly exploited. Our group has reported the most representative and versatile electrochemical sensing strategies using AAO nanoporous membranes, based on the monitoring of the diffusion of electroactive molecules (typically $[Fe(CN)_6]^{4-}$) through the AAO membrane, attached onto a SPCE and its differential pulse voltammetry signal change upon biomolecule recognition which allowed to detect proteins [15] and DNA [16].

Furthermore, these nanoporous membranes have been shown as excellent platforms for the analysis of real samples of, for example, human blood, due to their filtering properties, allowing minimization of matrix effects [17,18]. However, the practical application of this sensing system is limited due to two main factors: i) the membrane and the electrotransducer have to be assembled prior the detection(not integrated system); and ii) the large thickness of Al_2O_3 membranes (60 μm approx.) made necessary the use of nanoparticle tags for the enhancement of nanochannel blockage. For these reasons, nanochannels with nanosized thickness integrated on the electrotransducer surface are highly required to overcome such limitations.

In this context, a very interesting alternative recently proposed for the preparation of nanochannels on solid substrates consists on the formation of highly ordered mesoporous thin film coatings, which has a great potential application in electrochemical analysis [19]. Strategies such as the use of self-assembled nanoparticle templates [20], self-assembled surfactant templates [21] and hard templating/nanocasting approaches [22] have been recently reported in order to get ordered nanochannel array films on electrodes. Of special relevance are the approaches based on the self-assembling of polystyrene nanospheres to build nanostructured surfaces on transparent conductive oxide (TCO) substrates [23,24].

Based on these principles, we report here for the first time a disposable label-free immunosensing device based on screen-printed ITO/PET electrodes modified with nanochannels created by dip-coating deposition of a homogeneous monolayer of polystyrene nanospheres. The presented approach brings new opportunities in terms of robustness and mass production toward various applications for protein, DNA, and cell sensing.

4.2. Experimental section

4.2.1. Apparatus and electrodes

Optical characterizations were performed using a Scanning Electron Microscope (FEI Quanta 650 FEG ESEM), and a CLSM Leica TCS-SP5 AOBS spectral fluorescence microscope (Leica Microsystems Heidelberg GmbH; Mannheim, Germany) using a Plan-Apochromatic 63× objective (NA 1.4, oil). All the SEM images were obtained using secondary electrons detector at high voltage (20 kV).

The electrochemical transducers used were home-made screen-printed ITO/PET electrodes (SPIEs). A semiautomatic screen-printing machine DEK248 (DEK international, Switzerland) was used for the printing of the carbon and silver/silver chloride counter and reference electrodes respectively as well as an insulating layer. The materials and reagents used for this process were: Autostat HT5 polyester sheet (McDermid Autotype, UK), Electrodag 423SS carbon ink, Electrodag 6037SS silver/silver chloride ink, and Minico 7000 Blue insulating ink (Acheson Industries, The Netherlands). These inks were printed onto a transparent adhesive plastic Aironfix (1 mm of thickness). The electrochemical measurements were carried out using an Autolab 20 (Eco-chemie, The Netherlands).

4.2.2. Reagents and solutions

Anti-human IgG (I1886; polyclonal antibody developed in goat), anti-human IgG-FITC (Sigma F3512 produced in goat) were purchased from Sigma-Aldrich (Spain). Working aliquots of both antibodies were prepared in 0.01 M PBS buffer pH 7.4, containing 5 mM 3-aminopropyltrimethoxysilane (APS), and [N-(3-dimethylamino) propyl-N-ethylcarbodimide (EDC), sulfo N-hydroxysuccinimide (sulfo-NHS). IgG from Human serum (I2511) was purchased from Sigma-Aldrich (Spain) and its aliquots were prepared in 0.01 M PBS buffer pH 7.4. Carboxylated Polystyrene nanospheres of 500 nm and 200 nm in diameter were purchased from microParticles GmbH, Research- and Development Laboratory (Berlin). Ethanol was purchase from Sigma-Aldrich (Switzerland). Sodium dodecyl sulfate (SDS) was purchase from Fluka, Indium tin oxide coated PET (surface resistivity 60 Ω/sq) was purchased from Sigma-Aldrich (Spain). All chemicals were of analytical grade and their aqueous solutions were prepared in Milli-Q water.

4.3. Methods

4.3.1. Preparation of screen-printed ITO electrodes (SPIEs)

Carbon counter and silver/silver chloride reference electrodes as well as insulating ink were screen-printed on an Ironfix layers (20 x 20 cm). After that, holes of 3 mm in diameter were done on the ironfix just between the counter and reference electrodes so as to define the place of the working electrode. In addition, holes were also done in the area of connection of the electrodes so as to allow the further connection of the working electrode to the potentiostat. Finally, the electrodes were cut by each line containing 15 electrodes and adhered onto the ITO/PET surface.

4.3.2. Modification of SPIE with polystyrene (PS) nanospheres (PS) monolayer

The PS modification was performed on the SPIE by dip-coating technique [23]. Prior to the coating process, the SPIE was cleaned in the oxygen plasma (100 W) for 30 s, rinsed in deionized water, and dried under nitrogen flow. The PS microsphere suspension (5 w/v % aqueous suspension) was diluted with an equal volume of ethanol and dispersed on the surface of deionized water in a petri dish. By adding a few drops of 10 wt% aqueous solution of sodium dodecyl sulfate, PS microspheres form a close-packed self-assembled monolayer at the air/water interface. The electrode was gently immersed into the water with the tilt angle around 45°. The PS monolayer was transferred on the electrode surface by slowly removing the electrode from the water by maintaining the angle at 45°.

4.3.3. Optical and electrochemical characterizations of SPIEs modified with PS monolayer

SEM analysis for the evaluation of the homogeneity of the PS monolayers as well as for measuring the size of the created nanochannels was performed. For this analysis, a platinum layer of 4 nm was previously sputtered on the samples so as to get a conductive layer.

SPIEs were electrochemically characterized by measuring the standard red-ox signals of the $[Fe(CN)_6]^{3-}/[Fe(CN)_6]^{4-}$ red-ox pair using cyclic voltammetry (CV) and differential pulse voltammetry (DPV). For this purpose the red-ox mediator, formed by 50 µL of 1 mM $K_3[Fe(CN)_6]$ in 0.1 M $NaNO_3$ were placed on the electrode surface and the voltammogram was recorded.

4.3.4. Antibody immobilization and immunoassay

8µL of 1 mg/mL solution of anti-human IgG antibody in PBS buffer containing 5 mM EDC/sulfo-NHS were deposited onto the working electrode surface (where the carboxylated PS monolayer was previously created) and incubated overnight at 4 ºC. Following this procedure, the antibodies were immobilized through the covalent coupling of peptide/proteins to the nanospheres. After washing in PBS buffer, 8 µL of human IgG antigen (HIgG) at different concentrations were deposited onto the working electrode surface and incubated during 2 h at room temperature. All the concentrations assayed were prepared by triplicate, and a control test using a PBS buffer without the antigen was done.

Antibody immobilization on the surface of the PS was evaluated by confocal microscopy. For this purpose, anti-human IgG labeled with a fluorescent tag (FITC) was incubated on the monolayer of PS following the same experimental procedure ImageJ software (version 1.47 V) was used to determine the arbitrary units of fluorescence.

4.3.5. Electrochemical detection of HIgG

After washing in PBS buffer, 50 µL of 1 mM $K_3[Fe(CN)_6]$ in 0.1 M $NaNO_3$ were added. An electrochemical pre-concentration step applying a potential of –550 mV during 30 s was carried out to ensure that all the Fe^{3+} ions were transformed to Fe^{2+}. Immediately after, DPV was performed by scanning from – 400 mV to + 400 mV (step potential 10 mV, modulation amplitude 50 mV, non-stirred solution). The analytical signal corresponds to the peak of DPV current generated during the process of oxidation of $[Fe(CN)_6]^{4-}$ to $[Fe(CN)_6]^{3-}$. The peak potential value shifts from 100 mV to 300 mV approx., depending on the degree of the blockage of the electrode.

4.4. Results and discussion

4.4.1. Electrochemical performance of SPIEs

Cheap, disposable, single-use screen-printed ITO electrodes (SPIEs) were prepared following the experimental procedure detailed at methods section. Figure 4-1A shows a schematic representation of the different materials and layers forming the final electrode, together with pictures of a sheet of transducers and a detail of a single one.

The SPIE electrodes were characterized first by cyclic voltammetry (CV), scanning from - 400 mV to + 400 mV in $K_3[Fe(CN)_6]$ /0.1 M $NaNO_3$. As can be observed in Figure 4-1B (top), a well-defined pair of red-ox peaks was recorded at + 140 mV and - 48 mV, corresponding to oxidation and reduction processes of the $[Fe(CN)_6]^{3-}$/$[Fe(CN)_6]^{4-}$systems respectively. This behavior is similar to the one obtained for well-established screen-printed electrodes such as the carbon-based ones [18]. This result demonstrates the good performance of this hybrid screen-printed ITO electrode.

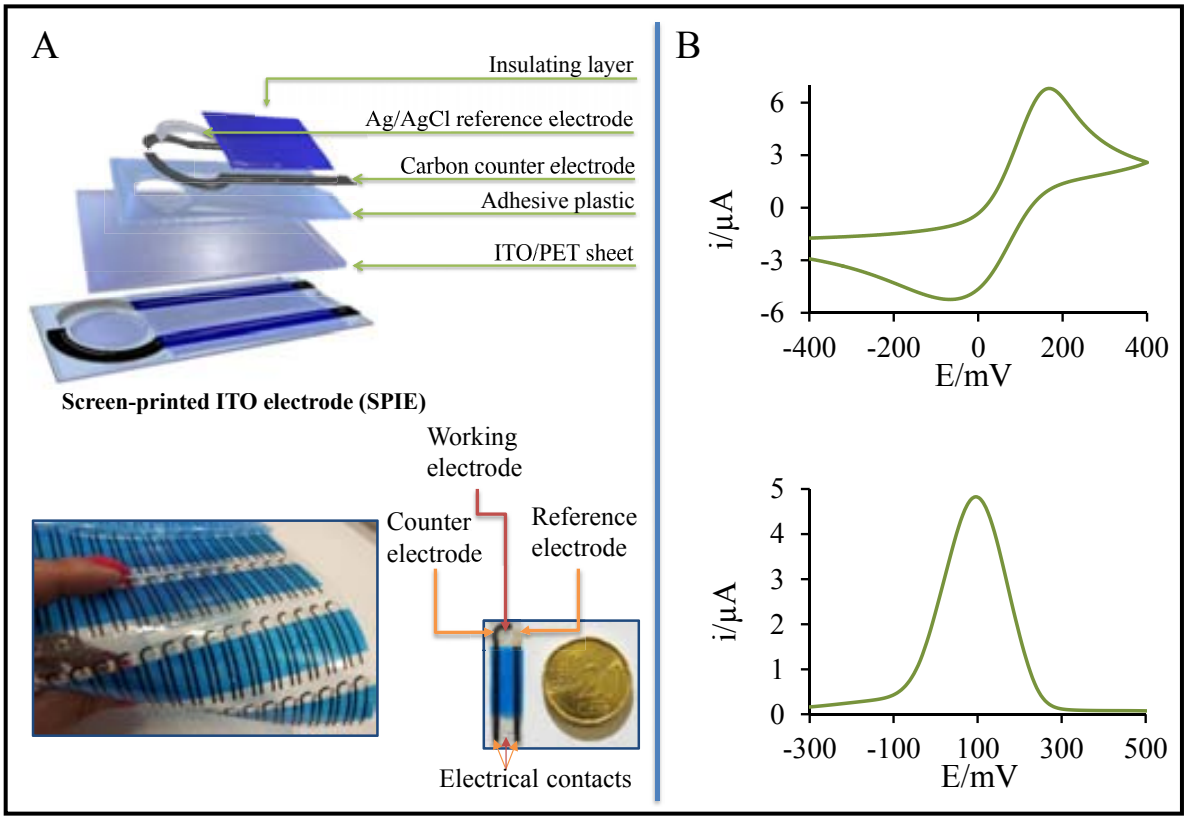

Figure 4-1. (A) Schematic representation of the different materials and layers which form the SPIE, together with pictures of a sheet of transducers and of a single one; (B) Top, cyclic voltammogram (CV) performed from – 400 mV to + 400 mV in 1 mM $K_3[Fe(CN)_6]$/0.1 M $NaNO_3$. Pre-concentration step at –550 mV during 30 s, scan rate: 50 mV/s. Bottom, differential pulse voltammogram (DPV) performed from – 300 mV to + 500 mV in 1 mM $K_3[Fe(CN)_6]$ /0.1 M $NaNO_3$.

Differential pulse voltammetry (DPV) was also used given its higher sensitivity and better reproducibility in comparison to cyclic voltammetry measurements[15]. The DPV obtained in the range from -300 mV to + 500 mV (Figure 4-1B, bottom) exhibits a well-defined current peak at approximately + 100 mV, which also corroborates the excellent performance of SPIEs.

4.4.2. Evaluation of the PS modified SPIEs

The morphology and homogeneity of the PS monolayer deposited onto the SPIE working electrode, prepared as detailed in the methods section, was evaluated by SEM analysis. Micrographs in Figure 4-2 show a homogeneous monolayer of PS nanoparticles formed on

the electrode for both 200 nm (A) and 500 nm (B) sized ones. Furthermore, the inter-particles spaces were measured, evidencing that nanochannels of around 65 nm in diameter (500 nm in length) and of 24 nm in diameter (200 nm in length) were generated, respectively. These sizes perfectly fit the requirements of a nanochannel-based electrochemical immunosensing system, as will be detailed in the following section.

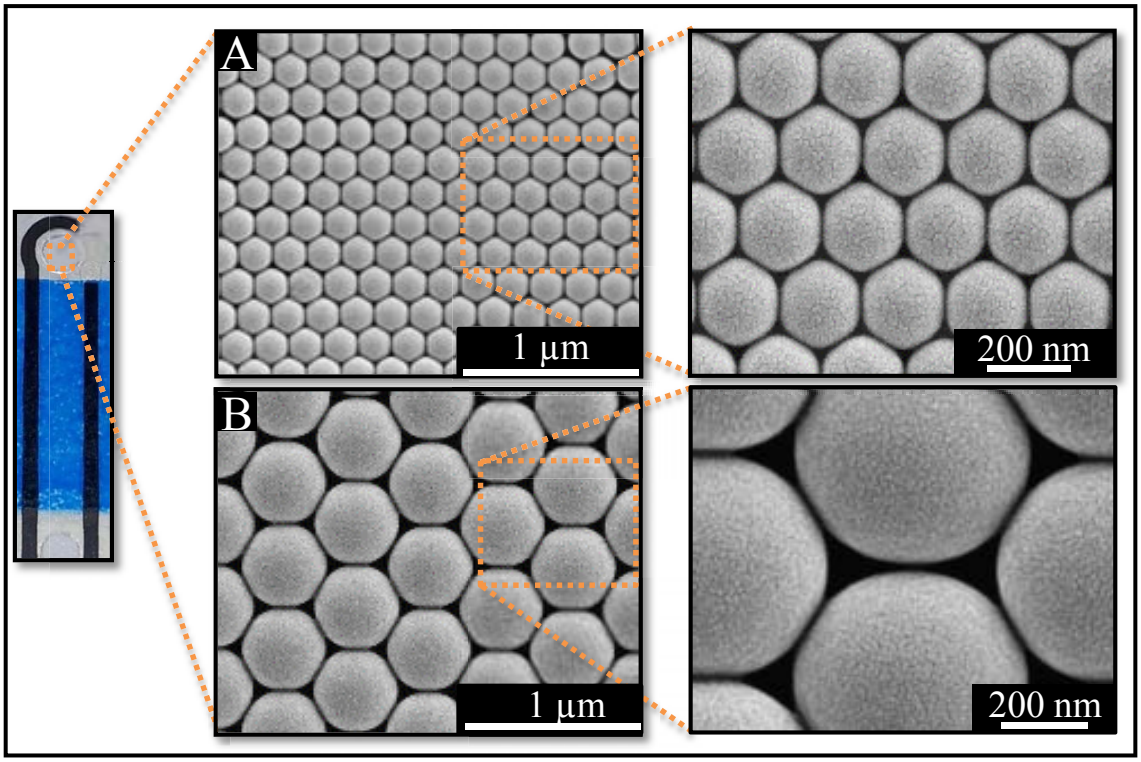

Figure 4-2. SEM images of the monolayer of 200 nm (A) and 500 nm (B) PS on the working electrode of the SPIE.

4.4.3. Evaluation of antibody immobilization on PS monolayers formed on SPIEs

Furthermore, the efficient immobilization of antibodies on the PS surface was checked by evaluating antibodies modified with a fluorescence marker (anti-human IgG–FITC) Antibody immobilization on the surface of the PS was evaluated by confocal microscopy. For this purpose, anti-human IgG labeled with a fluorescent tag (FITC) was incubated on the monolayer of PS following the experimental procedure detailed in the main text.

In Figure 4-3, a confocal microscopy image using the xyz mode, which allows to scan the xy plane a long the z axis, is shown. Fluorescence dots corresponding to the PS a re c learly observed (maximum of florescence of around 19.2 ± 7.6 (A) and 33.2 ± 9.4 (B) arbitrary units of fluorescence for the 200 nm and 500 nm PS respectively being 0-255 the range of arbitrary units of fluorescence), demonstrating the efficient covering of the PS by antibodies.

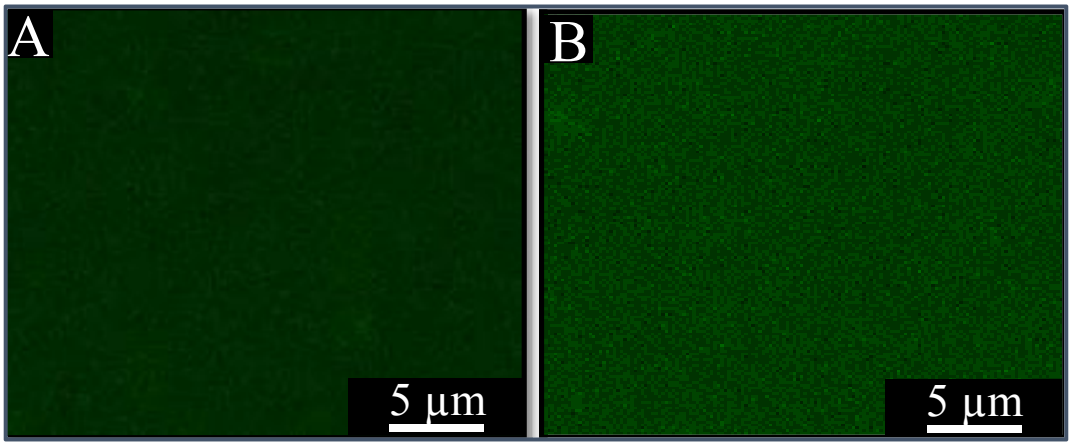

Figure 4-3. Confocal micrographs (xyz mode) of the 200 nm (A) and 500 nm (B) PS monolayers on SPIEs after immobilizing anti-HIgG-FITC antibodies.

4.4.4. Biosensing application: label-free detection of human IgG

SPIEs modified with PS were evaluated as biosensing platforms for the detection of proteins. The de tection princ iple is based on th e moni toring o f $[Fe(CN)_6]^{4-}$ diffusion throug h the formed nanochannels toward the electrode a nd it s differential pulse voltammetric (D PV) signal change upon immunocomplex formation . Human IgG was chosen as model protein for the evaluation of the sensing system.

Figure 4-4A shows a schematic representation of this sensing principle. Since the size of both antibody and antigen (human immunoglobulin G, HIgG) is 14.5 nm × 8.5 nm × 4 nm [25], the formation of the im munocomplex insi de the generated na nochannels partially blo cks the diffusion of the electroactive spe cies along the nanochannel resulting in a de crease in the voltammetric sig nal of $[Fe(CN)_6]^{4-}$ oxidation to $[Fe(CN)_6]^{3-}$. This decrease in the a nalytical

signal is proportional to the quantity of antigen, as shown in the DPVs of Figure 4-4B, corresponding to SPIEs modified with 500 nm PS. A logarithmic relationship between the value of the analytical signal and the HIgG concentration in the range between 1 - 300 µg/mL (Figure 4-4C gray line), with a correlation coefficient of 0.9812, according to the following equation: ip (µA) = -0.202 ln [HIgG] (µg/mL) + 1.4347 was obtained. The reproducibility of the method shows a RSD of 4.3 % (n= 3) for a HIgG concentration of 1 µg/mL. A limit of detection (LOD) of 2 µg/mL of HIgG calculated as the analyte concentration giving a signal equal to the blank signal + 3SD is estimated.

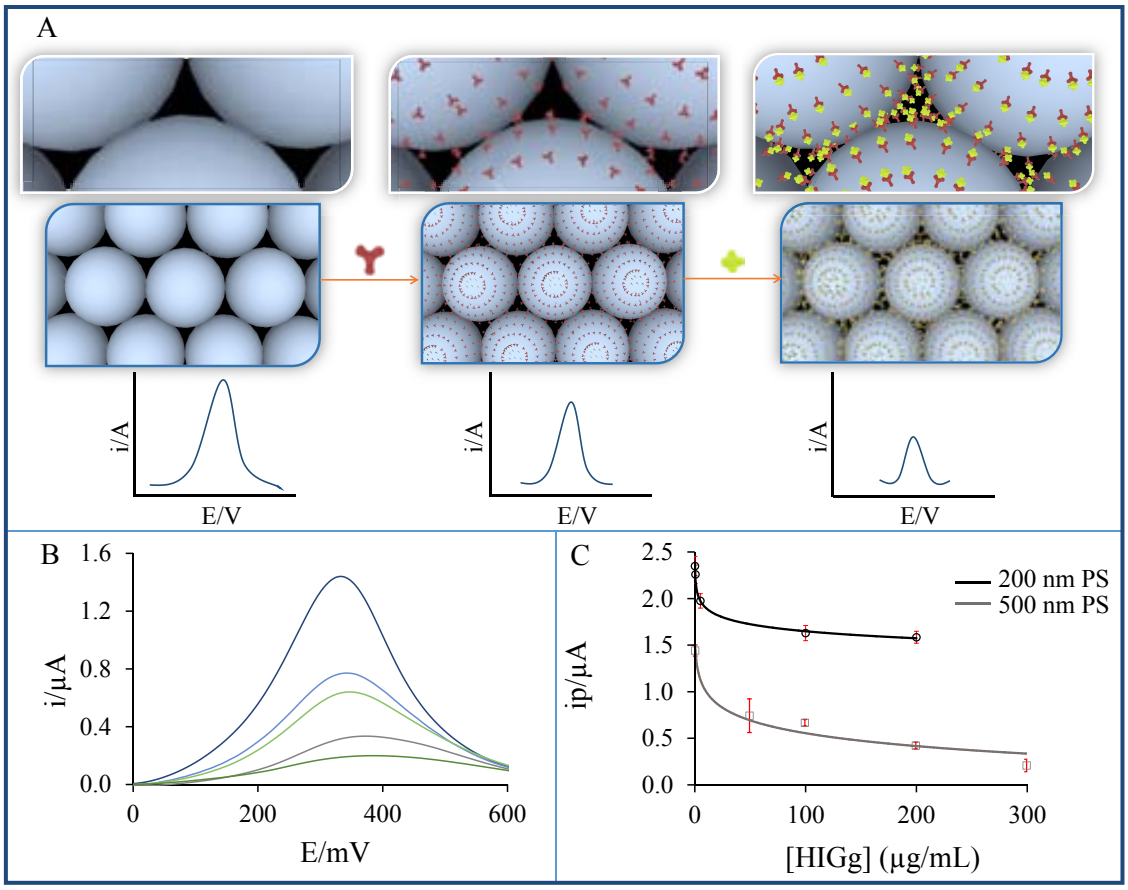

Figure 4-4. (A) Schematic representation (not in scale) of the sensing principle. (B) DPV obtained in 1 mM $K_3[Fe(CN)_6]$ /0.1 M $NaNO_3$ for different concentrations of human IgG, from top to bottom: 1, 50, 100, 200 and 300 µg/mL (SPIEs modified with 500 nm PS monolayer). Pre-concentration potential: –550 mV; pre-concentration time: 30 s; step potential: 10 mV; modulation amplitude: 50 mV; (C) Relationship between the analytical signal and the concentration of HIgG for SPIEs modified with 200 nm PS monolayer (black line) and 500 nm PS monolayer (gray line).

It was also observed that the blocking effect exerted by the immunocomplex formation was stronger when smaller was the nanochannel diameter, as expected. As summarized in Figure 4-4C (black line), in the case of the 200 nm sized PS, the range of logarithmic response was found between 0.125 - 200 μg/mL, with a correlation coefficient of 0.9975, according to the following equation: ip (μA) = -0.109 ln [HIgG] (μg/mL) + 2.1501. In this case the reproducibility of the method showed a RSD of 3.9 % (n= 3) for a HIgG concentration of 5 μg/mL. The higher sensitivity of the biosensing system prepared with the 200 nm sized PS is evidenced. A limit of detection of 580 ng/mL of HIgG was estimated The better performance of the immunosensor prepared with the 200 nm sized PS, in terms of sensitivity, detection range and linear response make this system optimum for further biosensing applications. Furthermore, the reproducibility of the biosensing system is also excellent, evidencing that possible defects in the PS monolayer are not relevant from the biosensing point of view.

Negative controls were performed by evaluating a non-specific antigen (goat IgG) for both 200 nm and 500 nm sized PS, not observing any significant decrease in the analytical signal (data not shown).

The performance of the system is much better than the previously obtained in label-free approaches using commercial anodic aluminum oxide (AAO) membranes (detection limits of 100-200 μg/mL depending on the pore size assayed) and screen-printed carbon electrodes [15]. These results are in agreement with the expected, since the shorter channel lengths created with the nanospheres (200-500 nm) compared with those of the commercial membranes (60 μm) allow a better blocking with lower quantities of antigen. In addition to the better sensitivity, this novel approach presents a simpler and more integrated sensing system. After the PS monolayer creation and antibody immobilization, SPIEs can be offered as really disposable biosensing devices for a one-step sensing procedure, enormously reducing the time of analysis.

4.5. Conclusion

A novel nanochannels-based biosensing platform on cheap, disposable and single-use screen-printed ITO electrodes (SPIEs) has been developed. Homogeneous monolayers of assembled polystyrene nanospheres (PS) have been successfully deposited on the working surface of the SPIEs by dip coating, creating well-ordered nanochannels in the inter-particle spaces. Antibodies are efficiently immobilized on the carboxy-modified PS through covalent binding, allowing the capturing of specific antigens and further quantification by voltammetric evaluation of the nanochannels blockage due to the immunocomplex formation. The limit of detection obtained with such a label-free approach is lower when smaller is the PS diameter, and consequently the nanochannels size, reaching values as low as 580 ng/mL for human IgG, chosen as model protein.

This novel system overcomes many of the limitations of previously reported approaches based on commercial anodic aluminum oxide (AAO) membranes in terms of integration and sensitivity, representing a really disposable biosensing device for a one-step sensing procedure. Moreover, this approach brings new opportunities in terms of robustness and mass production toward various applications for protein, DNA, and cell sensing.

4.6. References

(1) De la Escosura-Muñiz, A.; Merkoci, A. Nanochannels Preparation and Application in Biosensing. ACS Nano 2012, 6, 7556–7583.

(2) Bayley, H.; Cremer, P. S. Stochastic Sensors Inspired by Biology. Nature 2001, 413, 226–230.

(3) Coulter, W. H.; Coulter, J. High Speed Automatic Blood Cell Counter and Cell Size Analyzer. Proc. Natl. Electron. Conf . 1956, 12, 1034–1040.

(4) Howorka, S.; Cheley, S.; Bayley, H. Sequence-Specific Detection of Individual DNA Strands Using Engineered Nanopores. Nat. Biotechnol. 2001, 19, 636–639.

(5) Stoddart, D.; Heron, A. J.; Mikhailova, E.; Maglia, G.; Bayley, H. Single-Nucleotide Discrimination in Immobilized DNA Oligonucleotides with a Biological Nanopore. Proc. Natl. Acad. Sci. U.S.A. 2009, 106, 7702–7707.

(6) Purnell, R. F.; Schmidt, J. J. Discrimination of Single Base Substitutions in a DNA Strand Immobilized in a Biological Nanopore. ACS Nano 2009, 3, 2533–2538.

(7) Wang, Y.; Zheng, D.; Tan, Q.; Wang, M. X.; Gu, L.-Q. Nanopore-Based Detection of Circulating microRNAs in Lung Cancer Patients. Nat. Nanotechnol. 2011, 6, 668–674.

(8) Rotem, D.; Jayasinghe, L.; Salichou, M.; Bayley, H. Protein Detection by Nanopores Equipped with Aptamers. J. Am. Chem. Soc. 2012, 134, 2781–2787.

(9) Hurt, N.; Wang, H.; Akeson, M.; Lieberman, K. R. Specific Nucleotide Binding and Rebinding to Individual DNA Polymerase Complexes Captured on a Nanopore. J. Am. Chem. Soc. 2009, 131, 3772–3378.

(10) Stefureac, R.; Waldner, L.; Howard, P.; Lee, J. S. Nanopore Analysis of a Small 86-Residue Protein. Small 2008, 4, 59–63.

(11) Menard, L. D.; Ramsey, J. M. Fabrication of Sub-5 Nm Nanochannels in Insulating Substrates Using Focused Ion Beam Milling. Nano Lett. 2011, 11, 512–517.

(12) Foong, T. R. B.; Sellinger, A.; Hu, X. Origin of the Bottlenecks in Preparing Anodized Aluminum Oxide (AAO) Templates on ITO Glass. ACS Nano 2008, 2, 2250–2256.

(13) Alvarez, S. D.; Li, C.; Chiang, C. E.; Schuller, I. K.; Sailor, M. J. A Label-Free Porous Alumina Interferometric Immunosensor. ACS Nano 2009, 3, 3301–3307.

(14) Santos, A.; Balderrama, V. S.; Alba, M.; Formentín, P.; Ferré-Borrull, J.; Pallarès, J.; Marsal, L. F. Nanoporous Anodic Alumina Barcodes: Toward Smart Optical Biosensors. Adv. Mater. 2012, 24, 1050–1054.

(15) De la Escosura-Muñiz, A.; Merkoçi, A. Label-Free Voltammetric Immunosensor Using a Nanoporous Membrane Based Platform. Electrochem. Commun. 2010, 12, 859–863.

(16) De la Escosura-Muñiz, A.; Mekoçi, A. Nanoparticle Based Enhancement of Electrochemical DNA Hybridization Signal Using Nanoporous Electrodes. Chem. Commun. 2010, 46, 9007–9009.

(17) De la Escosura-Muñiz, A.; Chunglok, W.; Surareungchai, W.; Merkoçi, A. Nanochannels for Diagnostic of Thrombin-Related Diseases in Human Blood. Biosens. Bioelectron. 2013, 40, 24–31.

(18) De la Escosura-Muñiz, A.; Merkoçi, A. A Nanochannel/nanoparticle-Based Filtering and Sensing Platform for Direct Detection of a Cancer Biomarker in Blood. Small. 2011, 7, 675–682.

(19) Walcarius, A.; Kuhn, A. Ordered Porous Thin Films in Electrochemical Analysis. Trends Anal. Chem. 2008, 27, 593–603.

(20) Walcarius, a; Sibottier, E.; Etienne, M.; Ghanbaja, J. Electrochemically Assisted Self-Assembly of Mesoporous Silica Thin Films. Nat. Mater. 2007, 6, 602–8.

(21) Wan, Y.; Zhao, D. On the Controllable Soft-Templating Approach to Mesoporous Silicates. Chem. Rev. 2007, 107, 2821–6280.

(22) Chang, H.; Joo, S. H.; Pak, C. Synthesis and Characterization of Mesoporous Carbon for Fuel Cell Applications. J. Mater. Chem. 2007, 17, 3078.

(23) Guérin, V.-M.; Elias, J.; Nguyen, T. T.; Philippe, L.; Pauporté, T. Ordered Networks of ZnO-Nanowire Hierarchical Urchin-like Structures for Improved Dye-Sensitized Solar Cells. Phys. Chem. Chem. Phys 2012, 14, 12948–12955.

(24) Elias, J.; Lévy-Clément, C.; Bechelany, M.; Michler, J.; Wang, G.-Y.; Wang, Z.; Philippe, L. Hollow Urchin-like ZnO Thin Films by Electrochemical Deposition. Adv. Mater. 2010, 22, 1607–1612.

(25) Amit, a G.; Mariuzza, R. a; Phillips, S. E.; Poljak, R. J. Three-Dimensional Structure of an Antigen-Antibody Complex at 2.8 A Resolution. Science 1986, 233, 747–53.

Chapter 5.

Nanochannel array device operating through Prussian blue nanoparticles for sensitive label free immunodetection of a cancer biomarker

Related publication

Nanochannel array device operating through Prussian blue nanoparticles for sensitive label free immunodetection of a cancer biomarker

*Marisol Espinoza-Castañeda[1], Alfredo de la Escosura-Muñiz[1], Alejandro Chamorro[1,2], Carmen de Torres[2], Arben Merkoçi[1,3]**

[1] Nanobioelectronics & Biosensors Group. ICN2 - Institut Català de Nanociencia i Nanotecnologia, Campus UAB, 08193 Bellaterra (Barcelona), Spain.

[2] Hospital Sant Joan de Déu, Paseo Sant Joan de Déu, 2, 08950 Esplugues de Llobregat, Barcelona, Spain.

[3] ICREA - Institució Catalana de Recerca i Estudis Avançats, 08010 Barcelona, Spain

Submitted

Chapter 5. Nanochannel array device operating through Prussian blue nanoparticles for sensitive label free immunodetection of a cancer biomarker

5.1. Introduction

The Coulter counter established in the 50s' of last [1,2] opened the way to a simple microscale sensing that was then adapted to the nanoscale thanks to the intense research in the building of both biological and solid-state single ion channels [3–5] giving rise to the so-called stochastic sensing [6]. As a single nanochannel can detect only a single molecule at a time, strategies for manufacturing arrays of nanochannels were developed in the last decade's [7]. However, the difficulty of simultaneous measurement of the ionic current in a high number of channels opened the way to optical and electrochemical sensing approaches, different from the one based on the stochastic sensing [8]. Our group has recently developed protein [9,10] and DNA [11] electrochemical detection technologies based on solid-state nanochannel arrays with interest for rapid and cost-effective diagnostics. The detection principle is based on the monitoring of $[Fe(CN)_6]^{4-}$ indicator ions diffusion through anodized aluminum oxide (AAO) membranes attached onto a screen-printed carbon electrotransducer by differential pulse voltammetry signal change after biomolecule recognition. However, the use of this indicator ions based nanochannel technology as label-free immunosensing suffers of lack of sensitivity, probably due to the small size of the $[Fe(CN)_6]^{4-}$ ions. These drawbacks have constrained up to date the current technology to be applied for high quantities of protein so as to ensure efficient blocking in addition of making necessary sandwich based strategies that use nanoparticles (ex. AuNP) or even related enhancement strategies (ex. silver enhancement). However, sandwich immunoassays have inherent drawbacks in terms of time of analysis and antibodies consumption beside the rather low efficiency while being applied for small proteins analysis. For this reason, alternative red-ox indicators with sizes bigger than that of $[Fe(CN)_6]^{4-}$ ions would be potentially useful for the improvement of the label-free approach.

In this context, Prussian blue nanoparticles (PBNPs) appear as ideal candidates for this purpose. The Prussian blue (PB) is a mixed valence compound widely used as an electron transfer mediator for analytical applications [12–14]. Prussian blue has been described in two forms: the soluble PB with formula $KFe^{III}[Fe^{II}(CN)_6]$ and the insoluble PB with the formula $Fe^{III}_4[Fe^{II}(CN)_6]_3 \cdot 6H_20$, [15,16]. Colloidal structures of PB, so-called Prussian blue nanoparticles (PBNPs) can be prepared following different strategies such as reverse micelle, miniemulsion periphery polymerization [17,18], and properties offering novel size-dependent properties.

We here describe a novel and improved strategy to work with electrochemical nanochannel array system based on PBNPs (4 nm sized) as flow through red-ox indicator that achieves high sensitive label-free immunodetection. This approach is used for the detection of parathyroid hormone-related protein (PTHrP). PTHrP was first discovered as the factor responsible for tumor-induced hypercalcemia [19]. Over the following years, it became apparent that this peptide had major roles in cancer and also in non-neoplastic tissues [20]. In fetal and adult normal tissues, it acts locally, but in cancer it is produced by tumor cells and circulates in the bloodstream to the bone [21,22]. Measuring the levels of circulating PTHrP was initially reported to be a useful marker to monitor the state of malignant-associated hypercalcemia and the effectiveness of treatment in cancer patients [23]. Later, another study also indicated that serum PTHrP as determined at the time of first presentation was a useful indicator of not only hypercalcemia but also bone metastases and survival in lung carcinoma patients [24]. So, measurement of PTHrP is indeed of clinical relevance.

Several methods were developed since its first identification [21,25]. The most commonly used are immunoradiometric and immunochemiluminometric assays. Both of them are sandwich immunoassay based approaches, using two affinity-purified antibodies. These methods are able to detect circulating PTHrP with high sensitivity. However, they are not available in many basic research laboratories using cell and molecular biology approaches to analyze the role of PTHrP in cancer and non-neoplastic

models. Thus, the aim of our work was to develop a novel simple and efficient technology for PTHrP measurement that could eventually be implemented in point of care applications.

5.2. Experimental section

5.2.1. Apparatus and electrodes

Anodized alumina oxide filter membranes (Whatman anodisc AAO filters, 13 mm diameter; 60 μm thickness; containing 20 nm pores with higher pore density) were purchased from Scharlab (Spain). Optical measurements of ELISA assays were performed using a Gemini SpectraMax M2e Multi-Mode Microplate Reader (Molecular Devices, CA, U.S.A.). The electrochemical transducers used were homemade screen printed carbon electrodes (SPCEs), consisting of three electrodes: working electrode, reference electrode and counter electrode in a single strip fabricated with a semi-automatic screen-printing machine DEK248 (DEK International, Switzerland). The reagents used for this process were: Autostat HT5 polyester sheet (McDermid Autotype, UK) and Electrodag 423SS carbon ink, Electrodag 6037SS silver/silver chloride ink and Minico 7000 blue insulating ink (Acheson Industries, The Netherlands), (see details previously described in C**hapter 3**).

A home-made methacrylate electrochemical cell set-up was used for electrochemical measurements that were performed with an Autolab 20 (Eco-chemie, The Netherlands) connected to a PC. All the measurements were carried out at room temperature with a working volume of 200 μL, which was enough to cover the three electrodes contained in the SPCEs connected to the potentiostat by a homemade edge connector module.

Optical characterizations of PBNPs were performed using a Transmission Electron Microscope (TEM) Jeol JEM-2011 (Jeol Ltd, Japan) and a Gemini SpectraMax M2e Multi-Mode Microplate Reader (Molecular Devices, CA, USA).

Zeta potential of the PBNPs was determined with a Malvern Zetasizer Nano-ZS (Malvern Instruments Ltd., UK) according to the manufacturer's recommendations.

5.2.2. Reagents and solutions

Anti-human IgG (I1886; polyclonal antibody developed in goat), 3,3′,5,5′-Tetramethylbenzidine (TMB) Liquid Substrate System for ELISA and Bovine Serum Albumin (BSA) were purchased from Sigma-Aldrich (Spain). Anti-PTHrP (PC09; 34-53; polyclonal antibody developed in rabbit) was purchased from Calbiochem (Spain). Anti-PTHrP (Ab40642) rabbit polyclonal was purchased from Abcam. Anti-PTHrP (SC H137) rabbit polyclonal was purchased from Santa Cruz.

Aliquots of both antibodies were prepared in 0.01 M PBS buffer pH 7.4, containing 5 mM EDC/sulfo-NHS. IgG from Human serum (I2511), IgG from goat serum (I5256) and Parathyroid Hormone-Related Peptide (PTHrP) (SRP4651; human recombinant, expressed in *E.coli*) were purchased from Sigma-Aldrich (Spain). Aliquots of both antigens were prepared in 0.01 M PBS buffer pH 7.4. $FeCl_2 \cdot 4H_2O$ and $K_3[Fe(CN)]_6$) were purchased from Panreac Química SA (Spain). Polyvinylpyrrolidone (PVP) (average MW 40 KDa), 3-aminopropyltrimethoxysilane (APS), [N -(3-dimethylamino) propyl)]-N-ethylcarbodimide (EDC), sulfo N-hydroxysuccinimide (sulfo-NHS), phosphate buffer solutions tablets (PBS) were purchased from Sigma-Aldrich (Spain). All chemicals were of analytical grade and used as received. All aqueous solutions were prepared in Milli-Q water.

5.3. Methods

5.3.1. Preparation and characterization of Prussian blue nanoparticles protected by polyvinylpyrrolidone

8 mL of an aqueous solution of PVP/$FeCl_2 \cdot 4H_2O$ (concentration ratio 20:1) containing 10 mM $FeCl_2 \cdot 4H_2O$ was first prepared. After that, 2 mL of a 10 mM $K_3[Fe(CN)]_6$ aqueous solution was added at 500 µL/min using a syringe pump and left reacting for 2h at room temperature with vigorous stirring. 2.5 mL of acetone for each mL of the reaction mixture were added. This procedure was repeated several times and the obtained PBNPs were dried at room temperature giving a blue powder that was dissolved by using a 1 M HCl solution. A 10 µg PBNPs/mL solution was used for the electrochemical measurements.

5.3.2. UV-Vis Measurements

For the UV-Vis spectrophotometric characterization, 300 µL of 2.5 µg/mL PBNPs suspension was placed in a well of a microplate reader and the optical density in the range between 500-800 nm was measured and analyzed using the SoftMax Pro 5.2 program.

5.3.3. Transmission Electron Microscopy

For the TEM characterization, 5 µL of 20 µg/mL PBNPs suspension was placed on a carbon grill. After 5 min, the excess was removed with filter paper and the carbon grill dried at room temperature before the analysis.

5.3.4. Zeta Potential Measurements

For the Zeta potential measurements, 1 mL of 2.5 µg/mL PBNPs suspension was transferred into a 1 mL polystyrene cuvette of the measuring instrument (DTS1061, Malvern Instruments Ltd). The data were collected and analyzed with the Dispersion Technology software 4.20 (Malvern) producing diagrams for the zeta potential as a distribution versus total counts.

5.3.5. Indirect ELISA assay

The micro-well plates were incubated with 50 µL, 20 µg/mL PTHrP incubated over night at 4 °C, washed with 200 µL PBS pH 7.4 and blocked with BSA 1%, 2 hours at room temperature. After that, the micro-well was washed with PBS and samples with antibodies 0.1 mg/mL were added and incubated 2 hours at room temperature. After washing with PBS, 100 µL antibody labeled with HRP were added, incubated 2 hours and washed. Finally 200 µL of TMB was added observing the evolution of a blue color in the solution. 1 N H_2SO_4 stopping solution was added at 15 minutes after the addition of TMB and the resulted solution was measured in UV-Vis spectra at 450 nm of wavelength.

5.3.6. Nanoporous membranes functionalization, antibody immobilization and immunoassay

The AAO filter membranes were boiled in Milli-Q water for 1 h. After drying in argon, they were immersed into a 5% acetone solution of APS for 1 h. Then they were washed in acetone several times and dried again at 120 ºC for 30 min. After that 30 µL of a 1 mg/mL solution of anti-human IgG in PBS buffer, containing 5 mM EDC/sulfo-NHS, were placed on the membrane filtering side and left there overnight at 4 ºC. The same procedure was followed for the immobilization of the anti-PTHrP antibodies, using in this case an antibody concentration of 20 µg/mL.

After thoroughly washing with PBS buffer, the immunoassay was performed by incubating 30 µL of a human IgG solution on the membrane filtering side during 1 hour. Finally the membranes were thoroughly washed and stored in Milli-Q water before electrochemical measurements. The same experimental procedure was followed for PTHrP antigen containing sample, Figure 5-1 show the schematic representation (not in scale) of the antibody immobilization and immunoassay formed in the wall of nanoporous membrane.

Blank assays were performed by following the same experimental procedure, but using goat IgG instead of human IgG and BSA instead of PTHrP respectively.

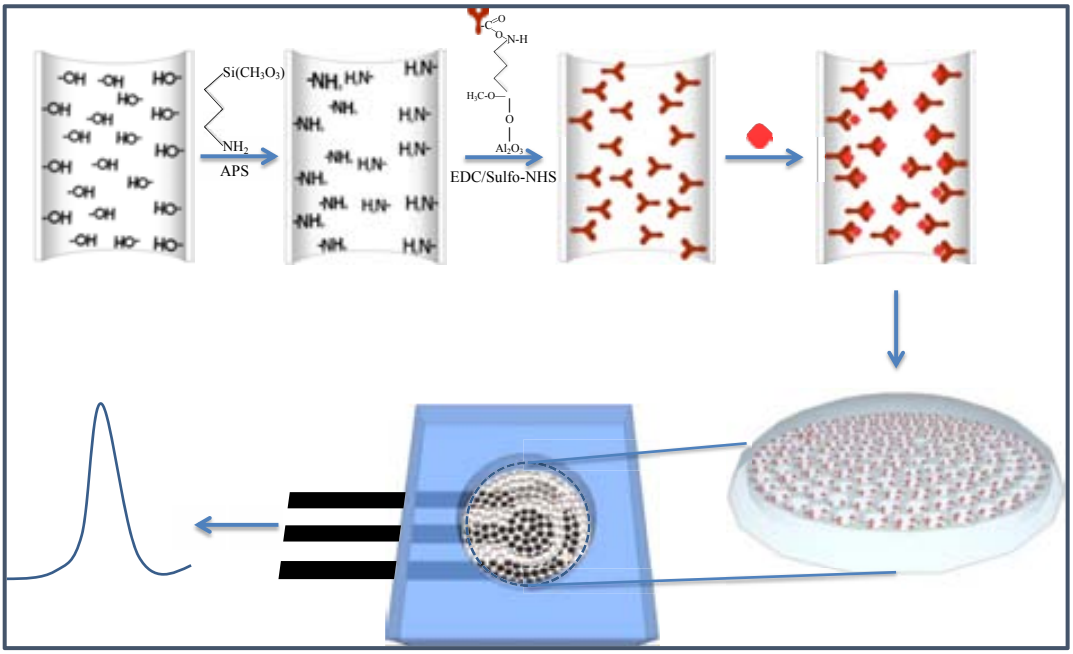

Figure 5-1. Schematic (not in scale) of the chemical reactions inside the AAO membranes for their functionalization and antibodies immobilization.

5.3.7. Cell set-up and electrochemical detection

AAO membranes were fixed onto the screen-printed carbon electrodes (SPCEs) by a physical attachment inside a methacrylate cell (as shown in Figure 5-2) and the electrochemical cell was filled with 100 µL of a 10 µg/mL PBNPs suspension. A pre-treatment at -550 mV was applied for 30 s and immediately after, a differential pulse voltammetric (DPV) scan from -550 mV to +700 mV (step potential 10 mV, modulation amplitude 50 mV) was applied resulting in an analytical signal due to oxidation of PB Prussian blue (PB) to Berlin green (BG) at approximately +500 mV. The measurements were carried out at room temperature under no stirring conditions. Each measurement was performed with a new membrane and a new SPCE using a thoroughly washed with Milli-Q water methacrylate cell.

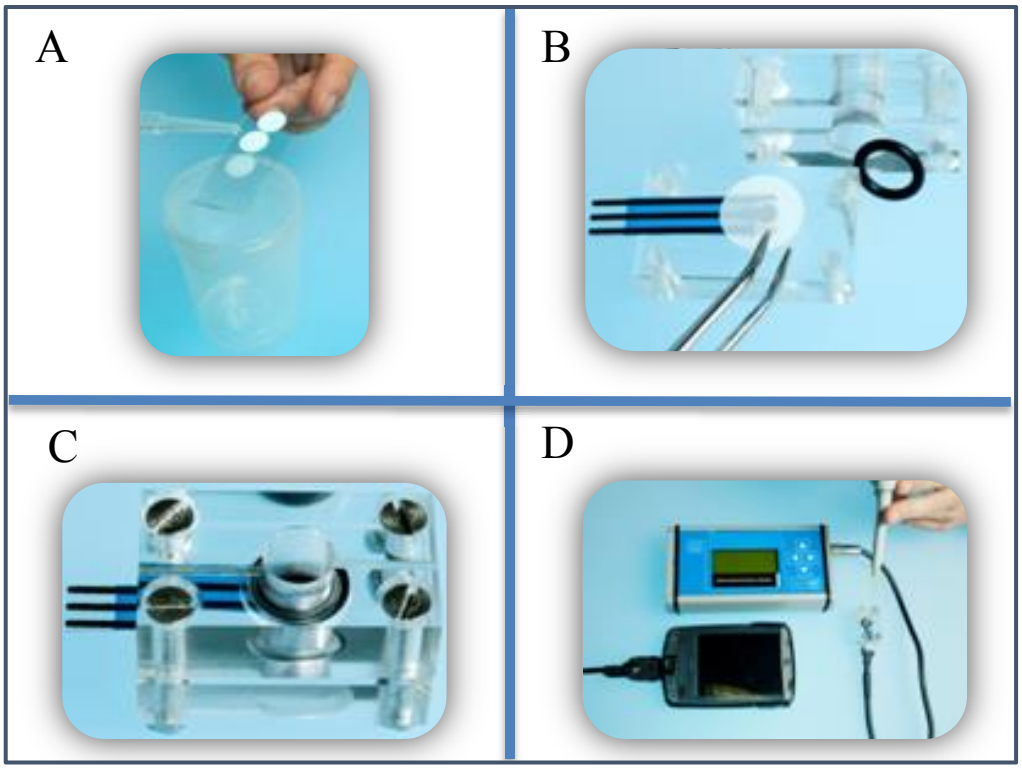

Figure 5-2. Process of membranes washing (A), fixing on the SPCE and assembling with two methacrylate blocks (B), cell set-up (C) and final measurement system using a portable potentiostat (D).

5.4. Results and discussion

5.4.1. Optimization / characterization of Prussian blue nanoparticles

PVP was used as stabilizer to produce PBNPs of approximately 4 nm in diameter. Different characterizations of the obtained PBNPs were performed to evaluate size distribution, dispersion and surface charge. UV–Vis absorption spectrum of PBNPs was first recorded (Figure 5-3A). The characteristic absorption band of PB observed at approximately 690 nm is attributed to the charge transfer from Fe^{2+} to Fe^{3+} in Prussian blue (Miao and Liu, 2009).

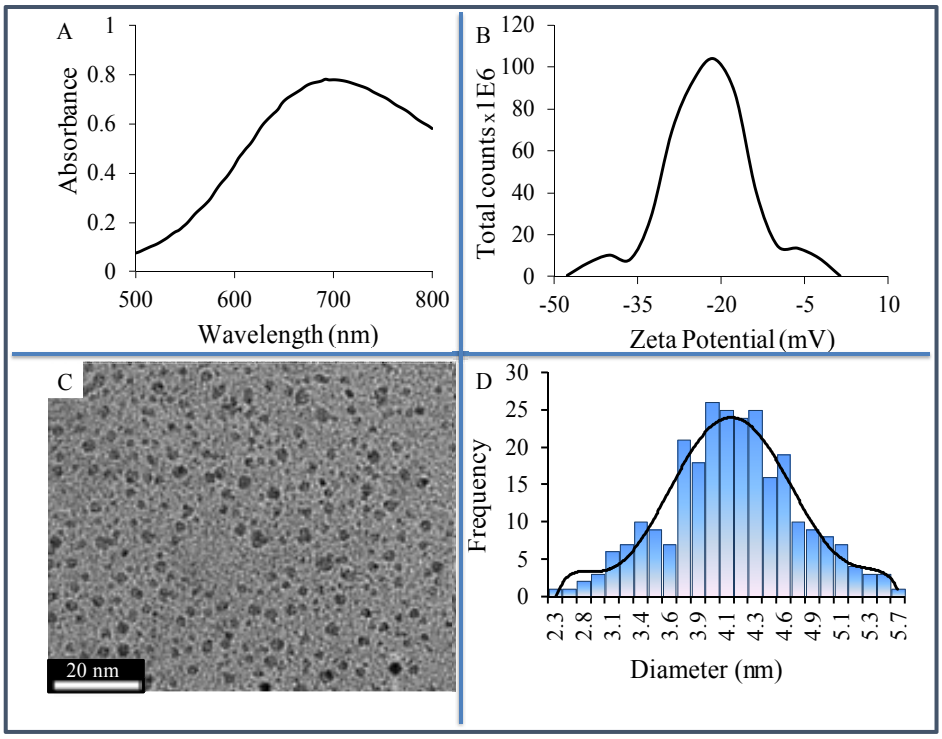

Figure 5-3. (A) UV–Vis absorbance spectrum obtained for a 2.5 µg/mL PBNPs suspension; (B) Z-potential diagram as distribution versus total counts obtained for 2.5 µg/mL PBNPs suspension; (C) Transmission electron micrograph (TEM) of a 20 µg/mL of PBNPs suspension and the corresponding size-distribution diagram.

The Z-potential technique was also used for the estimation of the surface charge of the PBNPs as well as for the evaluation of the NPs suspension stability. It is known that a high zeta potential (positive or negative) confers stability since the dispersion resists aggregation [26]. When the absolute value of the Z-potential is low, attraction exceeds repulsion and the dispersion breaks and flocculates. Thus, it has been defined that nanoparticle suspension stability is reached at absolute zeta potential values higher than 10 mV [27]. As shown in Figure 5-3B, the zeta potential value of the PBNPs suspensions was around -21.30 mV. This would indicate a negative surface charge value that provides a good stability. The size and shape of the PBNPs were determined by transmission electron microscopy (TEM) analysis. Figure 5-3C and Figure 5-3D show the obtained TEM images and the corresponding size distribution respectively. Well-defined spherical NPs, with a narrow size distribution (adjusted to a Gaussian curve) were obtained being the mean diameter value of 4.1 ± 0.7 nm (obtained measuring 360 nanoparticles).

Cyclic voltammograms in the range from +200 mV to +800 mV were recorded for different concentrations of PBNPs (2, 4, 6, 10 and 15 µg/mL) (Figure 5-4A) to evaluate their electrochemical behavior with interest for further use as red-ox indicator. The current intensity of both peaks increases with the concentration of PBNPs, reaching a plateau at 10 µg/mL (Figure 5-4A) which is chosen as optimum concentration for analytical applications. A well-defined redox peaks at approximately + 590 mV and + 460 mV attributed to the conversion of Prussian blue (PB) to Berlin green (BG) can be observed.

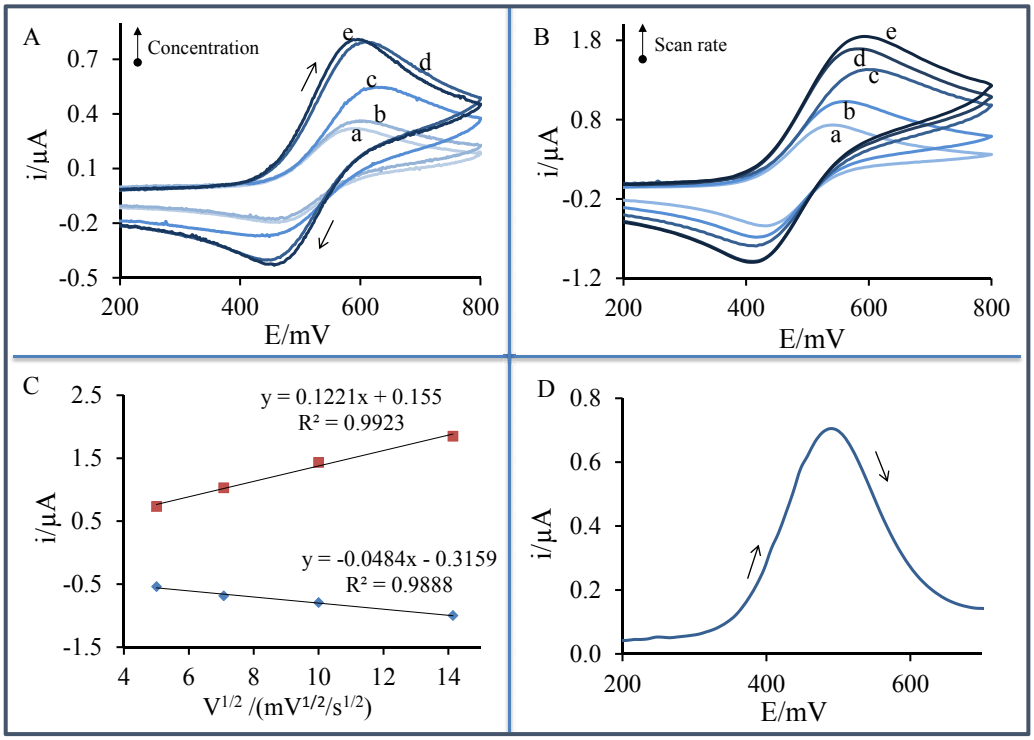

Figure 5-4. (A) Cyclic voltammograms recorded from -200 mV to +800 mV for different concentrations of PBNPs suspension (from down to up): 2, 4, 6, 10 and 15 µg/mL. Scan rate: 50 mV/s, electrolyte: 1M HCl; (B) Cyclic voltammograms recorded from -200 mV to +800 mV at different scan rates (from down to up): 25, 50 100, 150 and 200 mV/s. PBNPs concentration: 10 µg/mL, electrolyte: 1M HCl; (C) Linear relationship between the peak currents (anodic – squares; cathodic - circles) and the square root of scan rate obtained from the cyclic voltammograms at different scan rates;(D)Differential pulse voltammogram (DPV) recorded from +200 mV to +700 mV for a PBNPs concentration of 10 µg/mL. Step potential 10 mV, modulation amplitude 50 mV, electrolyte; 1M HCl.

The effect of the potential scan rate (v) on the peak current (both anodic and cathodic) was investigated in the range of 25 - 200 mV/s. The voltammograms in Figure 5-4B show that both peak currents increase with increasing scan rates. The relationship between peak currents and square root of the scan rate ($v^{1/2}$) for the redox reaction is adjusted to a linear equation suggesting a diffusion red-ox process (Figure 5-4C). The values of the currents (ip) were

obtained from the software employed to obtain the voltammograms. It was found that both anodic and cathodic peak currents increased linearly with the square root of scan rate between 25 and 200 mV/s, suggesting a diffusion redox process. The oxidation process of PB to BG obtained for a 10 μg/mL suspension of PBNPs was chosen for the evaluation of the response of the PBNPs as red-ox indicator. Furthermore, differential pulse voltammetry (DPV) was selected as a more convenient technique for quantitative use (better defined peaks and shorter analysis time) than cyclic voltammetry for the monitoring of this process. Figure 5-4D shows the DPV recorded from +200 mV to +700 mV for the above mentioned suspension of PBNPs, where a peak of current at approximately +500 mV which is chosen as analytical signal is observed.

The sensing principle for the detection of human IgG (chosen as model protein) together with a picture of the electrochemical cell set-up and SEM images of the AAO membranes are shown in Figure 5-5. The formation of the immunocomplex inside the pores produces a partial blockage in the diffusion of the electroactive species through the nanoporous membranes to the electrochemical transducer surface, which results in a decrease in the voltammetric signal. This approach was previously reported by our group but using the $[Fe(CN)_6]^{4-/3-}$ ionic system as red-ox indicator reaching detection limits of around 200 μg/mL of human IgG using AAO membranes with 20 nm pores [9]. This poor sensitivity was attributed to the low steric blockage that the immunocomplex exerts toward the diffusion of the small $[Fe(CN)_6]^{4-}$ ions (size below 1 nm). Thus, sandwich immunoassays with labels such as AuNP including Ag enhancement acting as additional enhancers of the steric nanochannels blocking were used [10].

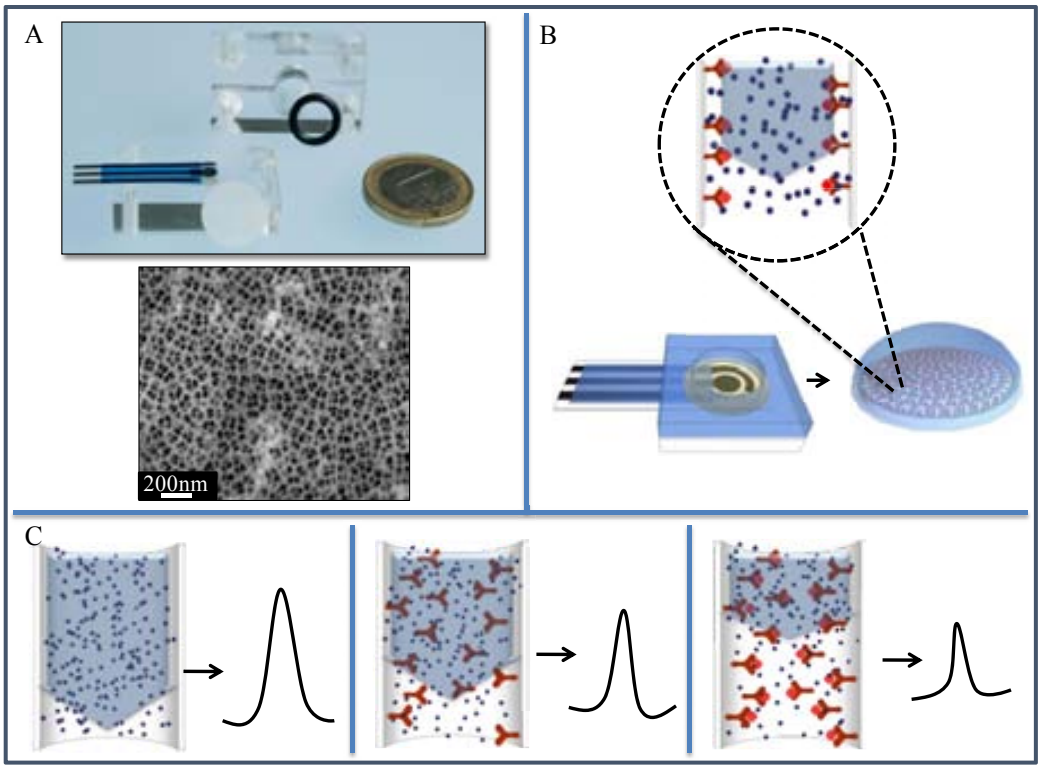

Figure 5-5. (A) Picture of the electrochemical cell set-up: the AAO membrane (white circular piece) is placed covering the working area of the SPCE and closed between 2 methacrylate blocks with a hole defining the electrochemical cell; a SEM top-view of the AAO membrane containing pores of 20 nm is also shown. (B) Schematic representation of the process occurring on the nanochannel modified electrode (PBNPs are represented as blue spheres). (C) Schematic representation of the sensing principle: the voltammetric signal of the PBNPs decrease with the subsequent AAO membranes modification.

However, these sandwich immunoassays have inherent disadvantages related to the time of assay and consumption of reagents together with their limitation to proteins of relative large size. For this reason, we explore now the use of PBNPs of 4 nm size as an alternative red-ox indicator to increase the sensitivity of the label-free immunoassay. Results obtained for both red-ox indicators is schematized Figure 5-6. In the $[Fe(CN)_6]^{4-/3-}$ system ($[Fe(CN)_6]^{4-}$ ions represented as small yellow spheres), a concentration of 200 µg/mL IgG was necessary to observe a 20% decrease in the voltammetric signal. However, in the case of the PBNPs (represented as bigger blue spheres); up to a 60% decrease in the signal is observed for IgG at levels as low as 1 ng/mL.

These results are in agreement with the hypothesis of the stronger hindering of the diffusion of the electroactive species due to steric effects in the nanochannels of 20 nm in diameter. As schematized in Figure 5-6 the size of the antibodies can be approximated to a sphere of a

radius of around 6 nm [28]. So, in the absence of an antigen, both the small $[Fe(CN)_6]^{4-}$ ions and the bigger PBNPs can freely flow through the channel to the electrode. However, in the presence of an antigen, the formed immunocomplex of around 12 nm largely hinders the flow of the 4 nm spheres of PBNPs. As result of all this, low quantities of antigen produce a remarkable decrease in the signal, allowing for a sensitive label-free immunosensing system.

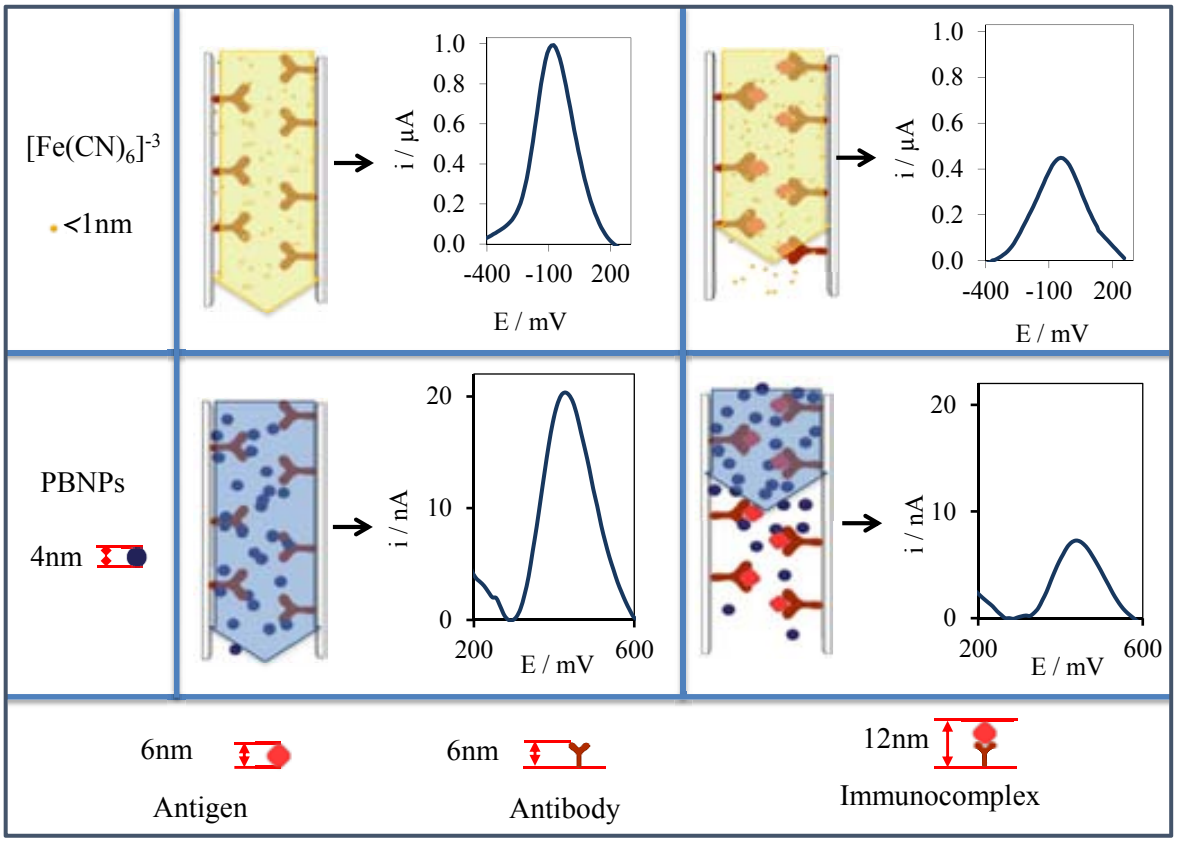

Figure 5-6. Schematic representation of the effect of the immunocomplex formation towards the voltammetric signal using $[Fe(CN)_6]^{3-}$ (top) and PBNPs (bottom) as red-ox indicator. DPV signals correspond to blank samples (left) and samples containing the antigen (HIgG) (right) at levels of 200 µg/mL and 100 ng/mL and respectively. DPV parameters as detailed in previous figures.

The ability of the developed system for quantitative analysis was then evaluated. As shown in Figure 5-7A, the analytical signal decreases by increasing human IgG concentrations. Both parameters adjusted to a logarithmic relationship (inset curve) in the range between 0.1 - 1000 ng/mL, with a correlation coefficient of 0.999, according to the following equation: ip (nA) = -1.43ln [human IgG] (ng/mL) + 16.18.

The reproducibility of the method shows a RSD of 5 % (n= 3) for a human IgG concentration of 0.1 ng/mL. Regarding the selectivity of the method, when goat IgG was evaluated as control, no signal decrease was observed even for concentrations as high as 500 µg/mL (data not shown). A limit of detection (LOD) (calculated as the analyte concentration giving a signal equal to the blank signal + three times its standard deviation) of around 34 pg/mL of human IgG is estimated. This sensitivity fits in the required one for application in diagnostics, since the protein levels of clinical interest are usually in the order of nanograms per milliliter [29]. The obtained LOD is seven order of magnitude better than the one obtained using the $[Fe(CN)_6]^{4-/3-}$ system as indicator, as summarized in the graphic of Figure 5-7B. For comparison purposes, the LOD obtained using membranes with 200 nm pore size are also included, evidencing the better results achieved with the smaller size pores and the bigger size indicator, which strongly suggests that the steric effects are the key factor responsible for the analytical performance of this sensing system.

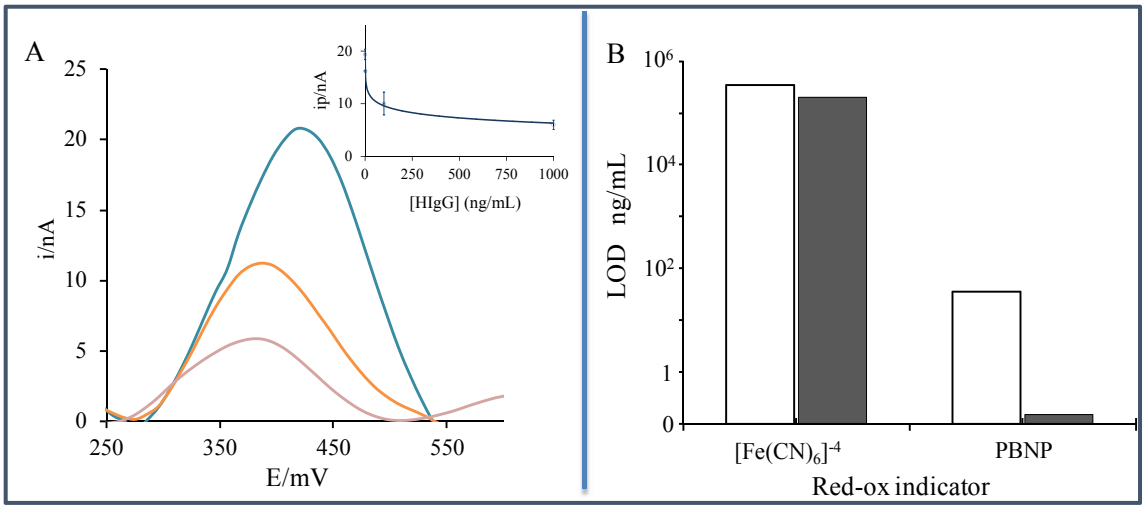

Figure 5-7. (A) DPV obtained using PBNPs and following the experimental procedure detailed at experimental section for different concentrations of human IgG, from top to bottom: 0, 100, 1 000 ng/mL. In set curve shows the logarithmic relationship obtained. (B) Comparison of the limit of detection (LOD) of human IgG obtained for $[Fe(CN)_6]^{3-}$ and PBNPs as red-ox indicators, using AAO membranes with pores of 20 nm (grey bars). The values obtained using membranes containing pores of 200 nm (white bars) are also shown for comparison purposes.

As explained before, the use of 4 nm sized PBNPs as indicator in the developed sensing system allows detecting very low concentrations of human IgG, chosen as model analyte,

thanks to a strong steric blockage of the nanochannels. But the advantages of using this large sized nanochannel blocking indicator should be related not only to a better sensitivity for the detection of a big protein (human IgG: 150 kDa; 6 nm approx.) but also for the detection of small proteins which would not produce any blockage for ionic red-ox indicators such as $[Fe(CN)_6]^{4-/3-}$. In this context, the developed label-free methodology appears as a very advantageous alternative for the detection of small proteins, which are not easily detected using sandwich immunoassays.

This is the case of PTHrP, a small protein of 173 aminoacids (MW: 18 kDa). The most challenging issue in the detection of this protein using a biosensing system is to find a pair of antibodies that recognize different aminoacids sequences and, consequently, are suitable to form a sandwich immunoassay. In our approach, a single antibody was used to capture the protein followed by its label-free detection avoiding the use of the sandwich format. Table 5.1 shows three different antibodies evaluated using indirect ELISA tests.

Antibody	Supplier	Epitope (PTHrP)	Origen/mono-poly	Results
PC09	Merck Millipore	34 – 53	Rabbit polyclonal	High affinity to PTHrP
Ab40642	AbCam	1 – 35	Rabbit polyclonal	Low affinity to PTHrP
SC H137	Santa Cruz	41-177	Rabbit polyclonal	No affinity to PTHrP

Table 5.1 Antibodies anti-PTHrP evaluated in an indirect ELISA assay.

Figure 5-8A show a schematic representation of the indirect ELISA assay used to determine which antibody offers higher affinity to recognize PTHrP, what is evaluated by measuring the maximum of UV-Vis absorbance of the enzymatic product (oxidized TMB) generated by the action of the HRP enzyme. Figure 5-8B shows a summary of the obtained results for the different antibodies evaluated (all the experiments were performed by triplicate).

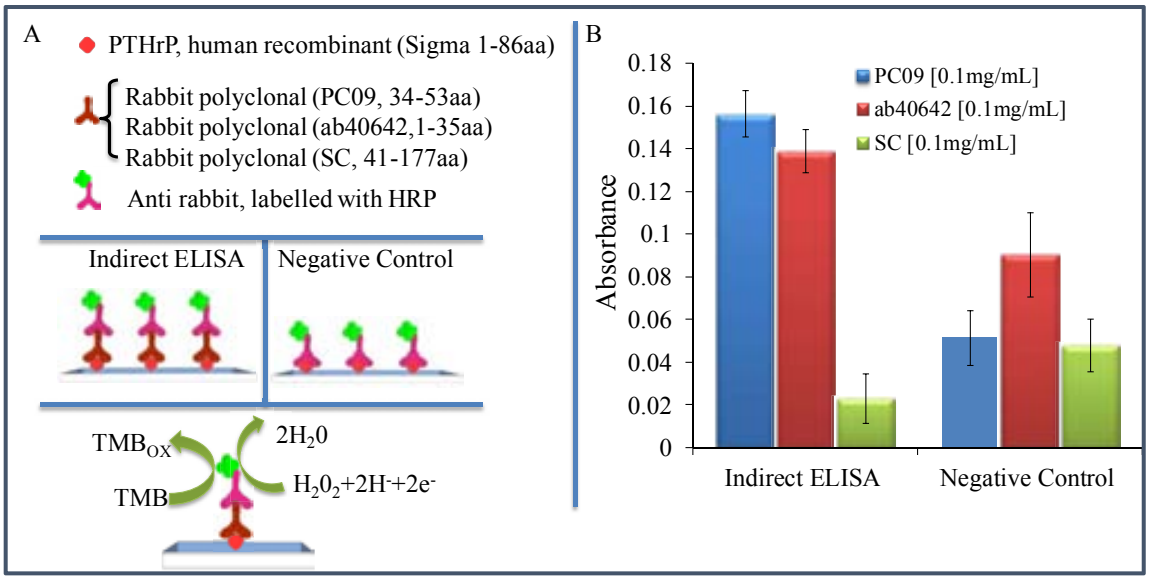

Figure 5-8. (A) Scheme of the indirect ELISA assay performed for the evaluation of 3 different antibodies. (B) Summary of the results obtained for a PTHrP concentration of 20 ng/mL.

The best results were achieved with an antibody that recognizes the aminoacids sequence 34-53 of PTHrP (see details in Chemicals and instruments).

This antibody was immobilized inside the inner walls of the nanochannels and used for the selective capturing of PTHrP through the blockage of the PBNP, diffusion evaluated via the decrease of its DPV signal (analytical signal). As shown in Figure 5-9, it was found that the PBNP-NC system responds to protein levels of 50 ng/mL, being this response proportional to protein concentrations up to 1000 ng/mL. Regarding the selectivity of the method, Bovine Serum Albumin (BSA; MW: 66 kDa) was evaluated in this case as control, not observing any signal decrease for concentrations as high as 2000 ng/mL (data not shown).

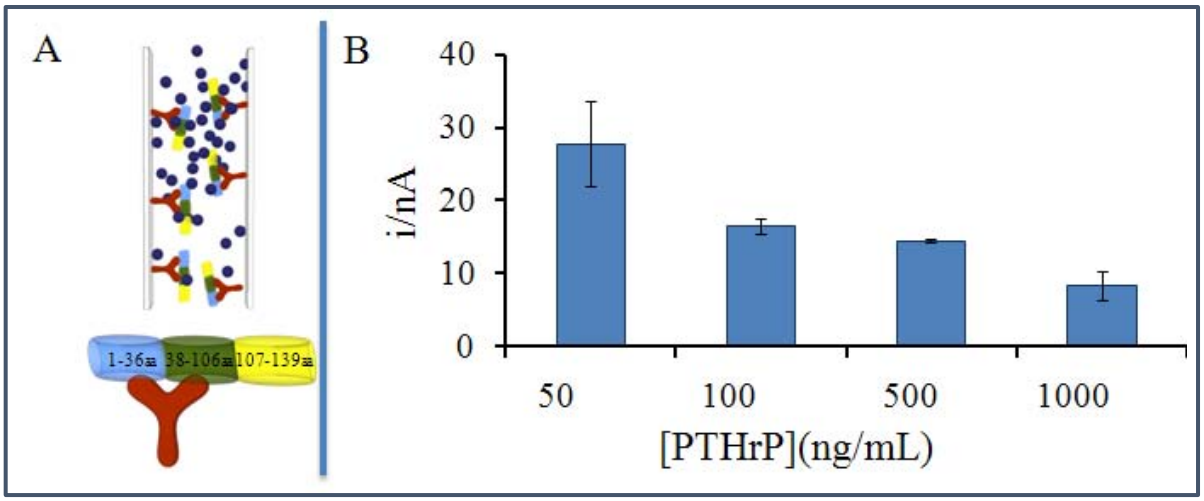

Figure 5-9. (A) Schematic representation of the parathyroid hormone-related protein (PTHrP) capturing on the inner walls of the nanochannels and its blocking effect on the diffusion of the PBNPs to the electrode. (B) Effect of the PTHrP concentration on the analytical signal.

5.5. Conclusions

In summary, we have developed a novel and highly sensitive nanochannel based immunosensing system that uses Prussian blue nanoparticles (PBNPs) as red-ox indicator instead of ionic based one. These PBNPs novel red-ox indicator improves the sensitivity of a label-free electrochemical immunosensing system based on nanoporous platforms. The stable and narrow-sized (around 4 nm) PBNPs, protected by Polyvinylpyrrolidone, exhibited well-defined and reproducible red-ox pairs, successfully applied for the voltammetric evaluation of the nanochannels blockage due to the immunocomplex formation. The bigger size of the PBNPs compared with ionic indicators such as the $[Fe(CN)_6]^{4-/3-}$ system and the consequent increase in the steric effects that hinder their diffusion to the electrodes is probably the main factor that allowed to improve the detection limits of model human IgG from 200 µg/mL to 34 pg/mL levels. Given the sensitivity of the developed system toward small proteins captured inside the nanochannels it was successfully applied for the detection of a cancer biomarker (parathyroid hormone-related protein, PTHrP) at levels of 50 ng/mL. Although the

detection limit of the developed device does not allow for the measurement of this factor in the clinical setting yet, these promising results pave the way for future applications potentially useful in basic research laboratories. These might include monitoring of the secretion of PTHrP not only in cell lysates but also in situ, directly on cells that may be growing on nanoporous membranes that can simultaneously act as sensing platform and filter of the complex matrix samples.

5.6. References

(1) Coulter, W. H. Means for Counting Particles Suspended in a Fluid. 2,656,508, 1953.

(2) Coulter, W.; Coulter, J. High Speed Automatic Blood Cell Counter and Cell Size Analyzer. Proc. Natl. El. Conf 1956, 12, 1034–1040.

(3) Sisson, A.; Shah, M. R.; Bhosale, S.; Matile, S. Synthetic Ion Channels and Pores (2004-2005). Chem. Soc. Rev. 2006, 35, 1269–86.

(4) Hou, X.; Guo, W.; Jiang, L. Biomimetic Smart Nanopores and Nanochannels. Chem. Soc. Rev. 2011, 40, 2385–2401.

(5) Siwy, Z. S.; Howorka, S. Engineered Voltage-Responsive Nanopores. Chem. Soc. Rev. 2010, 39, 1115–32.

(6) Bayley, H.; Cremer, P. S. Stochastic Sensors Inspired by Biology. Nature 2001, 413, 226–230.

(7) Kasianowicz, J. J.; Robertson, J. W. F.; Chan, E. R.; Reiner, J. E.; Stanford, V. M. Nanoscopic Porous Sensors. Annu. Rev. Anal. Chem. 2008, 1, 737–66.

(8) De la Escosura-Muñiz, A.; Merkoci, A. Nanochannels Preparation and Application in Biosensing. Am. Chem. Soc. 2012, 6, 7556–7583.

(9) De la Escosura-Muñiz, A.; Merkoçi, A. Label-Free Voltammetric Immunosensor Using a Nanoporous Membrane Based Platform. Electrochem. Commun. 2010, 12, 859–863.

(10) De la Escosura-Muñiz, A.; Merkoçi, A. A Nanochannel/nanoparticle-Based Filtering and Sensing Platform for Direct Detection of a Cancer Biomarker in Blood. Small 2011, 7, 675–682.

(11) De la Escosura-Muñiz, A.; Mekoçi, A. Nanoparticle Based Enhancement of Electrochemical DNA Hybridization Signal Using Nanoporous Electrodes. Chem. Commun. 2010, 46, 9007–9.

(12) Lundgren, C. A.; Murray, R. W. Observations on the Composition of Prussian Blue Films and Their Electrochemistry. Inorg. Chem 1988, 27, 933–939.

(13) Karyakin, A. A. Prussian Blue and Its Analogues : Electrochemistry and Analytical Applications. Electroanalysis 2001, 13, 813–819.

(14) Uemura, T.; Kitagawa, S. Prussian Blue Nanoparticles Protected by Poly(vinylpyrrolidone). J. Am. Chem. Soc. 2003, 125, 7814–5.

(15) Miao, Y.; Chen, J.; Wu, X. Electrochemical Characterization of Prussian Blue Nanoparticles. Colloid J. 2007, 69, 334–337.

(16) Ghasdian, N.; Liu, Y.; McHale, R.; He, J.; Miao, Y.; Wang, X. Synthesis of Prussian Blue Metal Coordination Polymer Nanocubes via Cyanoferrate Monomer Design. J. Inorg. Organomet. Polym. Mater. 2012, 23, 111–118.

(17) Liang, G.; Xu, J.; Wang, X. Synthesis and Characterization of Organometallic Coordination Polymer Nanoshells of Prussian Blue Using Miniemulsion Periphery Polymerization (MEPP). J. Am. Chem. Soc. 2009, 131, 5378–5379.

(18) Miao, Y.; Liu, J. Assembly and Electroanalytical Performance of Prussian Blue/polypyrrole Composite Nanoparticles Synthesized by the Reverse Micelle Method. Sci. Technol. Adv. Mater. 2009, 10, 025001.

(19) Suva, L. J.; Winslow, G. A.; Wettenhall, R. E.; Hammonds, R. G.; Moseley, J. M.; Diefenbach-Jagger, H.; Rodda, C. P.; Kemp, B. E.; Rodriguez, H.; Chen, E. Y. A Parathyroid Hormone-Related Protein Implicated in Malignant Hypercalcemia: Cloning and Expression. Science. 1987, 237, 893–6.

(20) McCauley, L. K.; Martin, T. J. Twenty-Five Years of PTHrP Progress: From Cancer Hormone to Multifunctional Cytokine. J. Bone Miner. Res. 2012, 27, 1231–9.

(21) Burtis, W. J.; Fodero, J. P.; Gaich, G.; Debeyssey, M.; Stewart, A. F. Preliminary Characterization of Circulating Amino- and Carboxy-Terminal Fragments of Parathyroid Hormone-Related Peptide in Humoral Hypercalcemia of Malignancy. J. Clin. Endocrinol. Metab. 1992, 75, 1110–4.

(22) Grill, V.; Ho, P.; Body, J. J.; Johanson, N.; Lee, S. C.; Kukreja, S. C.; Moseley, J. M.; Martin, T. J. Parathyroid Hormone-Related Protein: Elevated Levels in Both Humoral Hypercalcemia of Malignancy and Hypercalcemia Complicating Metastatic Breast Cancer. J. Clin. Endocrinol. Metab. 1991, 73, 1309–15.

(23) Burtis, W. J.; Brady, T. G.; Orloff, J. J.; Ersbak, J. B.; Warrell, R. P.; Olson, B. R.; Wu, T. L.; Mitnick, M. E.; Broadus, A. E.; Stewart, A. F. Immunochemical Characterization of Circulating Parathyroid Hormone-Related Protein in Patients with Humoral Hypercalcemia of Cancer. N. Engl. J. Med. 1990, 322, 1106–12.

(24) Hiraki, A.; Ueoka, H.; Bessho, A.; Segawa, Y.; Takigawa, N.; Kiura, K.; Eguchi, K.; Yoneda, T.; Tanimoto, M.; Harada, M. Parathyroid Hormone-Related Protein Measured at the Time of First Visit Is an Indicator of Bone Metastases and Survival in Lung Carcinoma Patients with Hypercalcemia. Cancer. 2002, 95, 1706–13.

(25) Lu, C. M.; Burton, W. D. W.; Fitzgerald, R. L.; Deftos, L. J.; Buchholz, B. A.; Vogel, J. S.; Herold, D. A. Mass Spectrometric Immunoassay for Parathyroid Hormone-Related Protein. Anal. Chem. 2002, 74, 5507–12.

(26) Thielbeer, F.; Donaldson, K.; Bradley, M. Zeta Potential Mediated Reaction Monitoring on Nano and Microparticles. Bioconjugate Chem. 2011, 22, 144–150.

(27) Green, A. J.; J, J. C.; L, A. K.; H, B. J. Mathematical Model of Antibody Targeting : Important Parameters Defined Using Clinical Data. Phys. Med. Biol. 2001, 46, 1679–1693.

(28) De la Escosura-Muñiz, A.; Merkoçi, A. Electrochemical Detection of Proteins Using Nanoparticles: Applications to Diagnostics. Expert Opin. Med. Diagn. 2010, 4, 21–37.

(29) Butt, H.-J.; Graf, K.; Kappl, M. Physics and Chemistry of Interfaces; John Wiley & Sons, 2003; Vol. 2003, p. 361.

Chapter 6.

General conclusions and future perspectives

General conclusions and future perspectives

6.1. General conclusions

The development of novel and improved electrochemical biosensing systems for protein and bacteria detection, exploiting novel properties of nanoparticles (gold nanoparticles and Prussian blue nanoparticles) and of nanoporous materials have been achieved as planned in this PhD thesis.

Considering the detailed objectives described in Chapter 2 and the obtained results described in Chapters 3, 4 and 5, the conclusions are detailed as follows:

1. A simple electrochemical theranostic platform based on the use of gold nanoparticles with interest for the study of the effect of k-casein derived peptides as inhibitors of bacterial adhesion is developed. Peptide modified gold nanoparticles were successfully prepared, thoroughly characterized and finally used for the evaluation of the interaction between the peptides and the K88 fimbriae bacteria (K88). The hydrogen evolution reaction induced by gold nanoparticles (used as carriers of bacteria adhesion inhibitors) was registered by a simple chronoamperometric measurement at an applied fixed potential. The efficiency of the developed theranostic system was evaluated using another class of bacteria (NF; as control) that do not present fimbriae onto its surface. The obtained results show that gold nanoparticles can be easily loaded with k-casein derived, drive toward fimbria bacteria and electrochemically detected distinguishing the fimbriae (K88) from non-fimbriae (NF) bacteria.

2. A novel nanochannels-based biosensing platform using a cheap, disposable and single-use screen-printed ITO electrodes (SPIEs) was developed. Homogeneous monolayers

of assembled polystyrene nanospheres (PS) were successfully deposited onto the working surface of the SPIEs by dip coating, creating well-ordered nanochannels in the inter-particle spaces. Antibodies were efficiently immobilized on the carboxy-modified PS through covalent binding, allowing the capturing of specific antigens and further quantification by voltammetric evaluation of the nanochannels blockage due to the immunocomplex formation. The limit of detection obtained with such a label-free approach was lower when smaller was the PS diameter, and consequently the nanochannels size, reaching values as low as 580 ng/mL for human IgG, chosen as model protein.

3. Nanoimprint lithography (NIL) was applied for the formation of nanochannels onto ITO/PET substrates, using PDMS stamps and a photocurable polymer. Areas of around 40 x 40 μm were successfully printed with nanochannels of around 350 nm in diameter and 200 nm in depth. Residual photocurable polymer layers have also been successfully removed by RIE treatment, allowing to obtain open nanochannels.

4. Some preliminary testing as proof of concept nanochannel-based platform for direct measurement of biomarkers (PTHrP) in the presence of cancer cells are carried out opening the way to future studies with interest for real sample applications.

6.2. Future perspectives

The developed proof of concept theranostic system related to the use of AuNP as label/carrier of peptides for bacteria detection may open the way to therapeutic and biosensing applications

with interest for various fields including food, health and pharmaceutical ones, given its simplicity and fast development possibility.

Regarding the approach based on the use of PBNPs in combination with nanochannels, although the detection limit of the developed device does not allow for the measurement of the assayed biomarker (PTHrP) in the clinical setting yet, these promising results pave the way for future applications potentially useful in basic research laboratories. These might include monitoring of the secretion of PTHrP not only in cell lysates but also *in-situ*, directly on cells that may be growing on nanoporous membranes that can simultaneously act as sensing platform and filter of the complex matrix samples. In this context, the preliminary studies demonstrating the ability of HaCat cells (cells chosen as model due to their continuous production of PTHrP) to grow and adhere onto the silanized AAO nanoporous membranes opened the way to the *in-situ* detection of the PTHrP secreted by the HaCaT cells cultured onto AAO nanoporous membranes. This work is now in progress in our laboratories.

On the other hand, the approach based on the nanochannel formation onto the electrotransducer surface by nanoparticle assembling overcome many of the limitations of previously reported approaches based on commercial anodic aluminum oxide (AAO) membranes in terms of integration and sensitivity, representing a really disposable biosensing devices for a one-step sensing procedure. Moreover, this approach brings new opportunities in terms of robustness and mass production toward various applications for protein, DNA, and cell sensing.

Finally, the alternative methodology for nanochannels creation based on nanoimprint lithography may also open the way to novel integrated biosensing systems. However, the defects obtained, probably due to small dust, particles trapped between the photocurable

polymer are avoiding the obtaining of large homogeneous printed areas. For this reason, alternative methodologies are currently being optimized in our laboratory to obtain larger printed areas, which could allow its use as real integrated biosensing platforms.

Annex 1.
In-situ electrochemical detection of PTHrP secreted by cells cultured on nanoporous membranes

Annex 1. In-situ electrochemical detection of PTHrP secreted by cells cultured on nanoporous membranes

A1.1. Introduction

In this annex, preliminary results related to the application of the biosensing system developed in Chapter 5 for the detection of Parathyroid hormone-related protein (PTHrP) in cell cultures are shown. This protein is highly expressed in normal skin keratinocytes and classically known as mediator of the humoral hypercalcemia of malignancy syndrome [1,2]. The interest in the detection of PTHrP relies in the fact that it shares some amino-terminal sequence identity with the parathyroid hormone (PTH) and it is able to activate the PTH/PTHrP receptor, producing classical PTH-like effects in the bone and kidney (for calcemia of malignancy) [3]. In case of hypercalcemia, PTHrP is secreted by tumor cells and circulates in the bloodstream to the bone [4]. Measuring the levels of circulating PTHrP was initially reported to be a useful marker to monitor the state of malignant-associated hypercalcemia and the effectiveness of treatment in cancer patients [5], evidencing the clinical relevance of PTHrP detection.

Current methods for the detection of PTHrP (i.e. Westerrn-blot [6], ELISA [7], Radio-immuno assay (RIA) [8], nuclear run-on assay [9], RNase protection assays [10]) don't fulfil the needs of early diagnosis of hypercalcemia with the required sensitivity and/or at a cost compatibility with large scale screening, so alternative methodologies are highly required. Immortalized human keratinocyte (HaCaT) cell lines are commonly used to study the mechanisms involved in PTHrP production by keratinocytes due to their continuous production of PTHrP [11].

As detailed in **Chapter 5**, the electrochemical immunodetection of standards of PTHrP was accomplished through the blockage in nanochannels (anodized aluminum oxide -AAO- membranes, 20 nm-sized pores) produced by the immunocomplex formation, which was

monitored through the decrease in the voltammetric signal coming from Prussian blue nanoparticles as red-ox indicator. However, the detection limit of this system (50 ng/mL) yet does not allow the measurement of this factor in the clinical setting, where levels starting from around 19 pg/mL are needed to be detected [8].

In this context, a method for in-situ monitoring of PTHrP secreted in live cell cultures would be ideal for the sensitive determination of this protein and the evaluation of cells carcinogenicity.

A1.2. Objective

The main objective of this work consists in the design and evaluation of a novel integrated system for the detection of PTHrP secreted by HaCaT cells directly cultured on top of AAO nanoporous membrane-modified screen-printed carbon electrodes (SPCEs). Anti-PTHrP antibodies have to be previously immobilized in the inner walls of the nanochannels for the in-situ capturing of the secreted PTHrP protein and the later detection based on the sensing principle detailed in **Chapter 5**. A scheme of the proposed sensing system is shown in Figure A1.1.

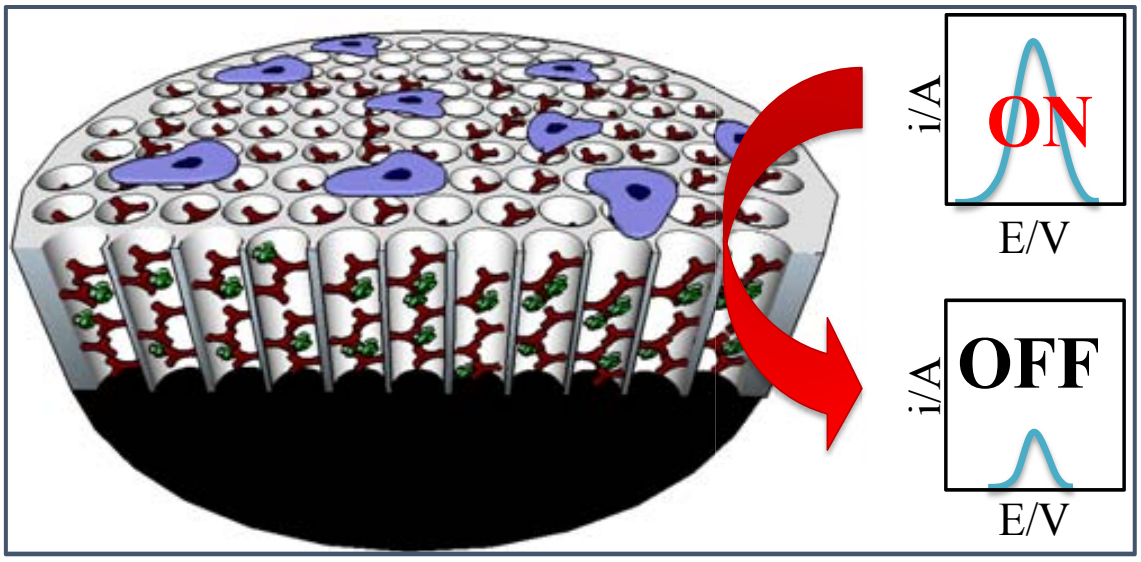

Figure A 1.1 Schematic (not in scale) of the proposed sensing system. HaCaT cells are cultured on AAO nanoporous membranes previously modified anti-PTHrP antibodies. Secreted PTHrP is selectively captured and detected through the decrease in the electrochemical signal of PBNPs due to their blockage.

A1.3. Experimental section

A1.3.1. Aparatus and electrodes

Thermostatic bath ISOTEMP was purchase from Fisher Scientific. Incubator NU-5100E/GCO_2 was purchase from Nuaire (USA). A BIOII A/P biosecurity cabinet (from Telstar, Spain) was used. TC Flask 75 cm^2, Multiple Well Cluster Plate, TC-Treated, Sterile, Stripettes individual 25, 10, 5, 2 mL were purchased from Cultek (Spain). Screen-printed carbon electrodes (SPCEs) used as transducers were fabricated following the experimental procedure detailed in **Chapter 3**. SPCEs consist of three electrodes: working electrode, reference electrode and counter electrode in a single strip fabricated with a semi-automatic screen-printing machine DEK248 (DEK International, Switzerland). The reagents used for this process were: Autostat HT5 polyester sheet (McDermid Autotype, UK) and Electrodag 423SS carbon ink, Electrodag 6037S Sil ver/silver chloride ink and Minico 7000 blue insulating ink (Acheson Industries, The Netherlands). A new model of homemade

methacrylate electrochemical cell set-up for six samples was developed and used for electrochemical measurements that were performed with an Autolab 20 (Eco-chemie, The Netherlands) connected to a PC. All the measurements were carried out at room temperature with a working volume of 200 μL, which was enough to cover the three electrodes contained in the SPCEs connected to the potentiostat by a homemade edge connector module. Anodized alumina oxide filter membranes (Whatman anodisc AAO filters, 13 mm diameter; 60 μm thickness; containing 20 nm pores) were purchased from Scharlab (Spain). Olympus IX71 (Spain) inverse microscope and Scanning Electrochemical Microscopy FEI Quanta 650 FEG ESEM (The Netherlands) were used for the optical characterizations.

A1.3.2. Reagents and solutions

The HaCaT cell lines were provided from *Hospital Sant Joan de Deú*, (Barcelona, Spain). Anti-PTHrP (PC09; 34-53; polyclonal antibody developed in rabbit) was purchased from Calbiochem (Spain). Aliquots of this antibody were prepared in 0.01 M PBS buffer pH 7.4, containing 5 mM EDC/sulfo-NHS. Bottle of CO_2 was purchased from Carburos Metálicos (Spain). Parathyroid Hormone-Related Peptide (PTHrP) (SRP4651; human recombinant, expressed in E.coli) was purchased from Sigma-Aldrich (Spain). $FeCl_2 \cdot 4H_2O$ and $K_3[Fe(CN)]_6$) were purchased from *Panreac Química* SA (Spain). Polyvinylpyrrolidone (PVP) (average MW 40 KDa), 3-aminopropyltrimethoxysilane (APS), [N -(3-dimethylamino) propyl)]-N-ethylcarbodimide (EDC), sulfo N-hydroxysuccinimide (sulfo-NHS), phosphate buffer solutions tablets (PBS) were purchased from Sigma-Aldrich (Spain). RPMI-1640 w/o l-glutamine (CE), Fetal Bovine Serum EU approved (south amer.), L-glutamine 200MM (100X), penicillin streptomycin sol, trypsin 0.25% and EDTA were purchase from Fisher Scientific (Spain). All chemicals were of analytical grade and used as received. All aqueous solutions were prepared in Milli-Q water.

Prussian blue nanoparticles (PBNPs) were synthetized following the experimental procedure described in **Chapter 5**.

A1.4. Methods

A1.4.1. HaCaT cell cultures

Gibco® RPMI medium used for the cell culture was supplemented with glutamine 2mM, 10 % of fetal bovine serum and penicillin streptomycin solution. All the cell manipulations were carried out in a biosafety cabinet with laminar flow, using sterile materials and specific waste containers. The cells were incubated in TC Flask at 37 °C in humidified atmosphere of 95% air and 5% CO_2. The medium was renovated every 3 days, and the cells were subcultured every week. All the mediums were pre-warmed at 37 °C (in a thermostatic bath) before using.

A1.4.2. AAO nanoporous membranes modification and in-situ cell culturing

Anodic aluminum oxide (AAO) nanoporous membranes (20 nm-sized pores) were first boiled in Milli-Q water for 1 h and then silanized by immersing into a 5% acetone solution of APS for 1 h. Then they were washed in acetone several times and dried at 120 ºC for 30 min. After this pre-treatment, AAO membranes were placed in a multi-well plate and 1.5 mL of 6 x 10^5 HaCaT cells/mL were placed on each well and incubated at 37 °C in humidified atmosphere of 95% air and 5% CO_2 during 36 hours.

A1.4.3. Evaluation of different materials for the preparation of the electrochemical cell set-up

Both the main component of the electrochemical cell set-up (rigid polymer) and the flexible ring (used to prevent the liquid leakage) were evaluated. The different materials are detailed in Table A1.1.

Rigid polymer	Abbreviation
Nylon	Nylon
Polyethylene terephthalate glycol-modified	PETG
Poly(methyl Methacrylate)	(PMMA)
Flexible ring	
Red Silicone	RS
Natural Silicone	NS
Nitrile rubber	NBR

Table A1.1 Different materials evaluated for the building of the electrochemical cell set-up.

This study was carried out in a multi-well plate, and the normal growth and adherence of the cells were verified using an inverse microscope. Small pieces of the rigid polymer (3 x 5 mm) and of the flexible ring (around 11 mm) were placed into multi-well plates followed by the addition of 2 mL of a 75 x 10^3 HaCaT cells/mL suspension. Cell culture controls were done in a multi-well plate without introducing any of these materials. Optical Microscopy images of the cell cultures were obtained just after the cells addition and after 3 h and 9 h.

A1.4.4. Electrochemical detection of PTHrP in cell culture medium

Preliminary studies for the evaluation of the ability of the developed sensing system for the determination of PTHrP in a complex matrix such as the cell culture medium were performed. The medium was extracted from the cell culture, prepared as detailed in section A1.4.1, and placed in Eppendorf tubes where different quantities of standard solutions of PTHrP were

spiked. After that, 50 µL of this solution were placed onto the membranes (with the anti-PTHrP antibody previously immobilized) and incubated during 2 h at room temperature. After washing with PBS buffer, the AAO membranes were fixed onto the SPCEs by a physical attachment and the cell set-up was closed (same set-up as detailed in **Chapter 5**), and filled with 200 µL of a 10 µg/mL PBNPs suspension. A pre-treatment at -550 mV was applied during 30 s and immediately after, a differential pulse voltammetric (DPV) scan from -550 mV to +700 mV (step potential 10 mV, modulation amplitude 50 mV) was applied resulting in an analytical signal due to oxidation of Prussian blue (PB) to Berlin green (BG) at approximately +500 mV. The measurements were carried out at room temperature under non-stirring conditions.

A1.5. Results and discussion

A1.5.1. Evaluation of HaCaT cell culture adhesion on AAO nanoporous membranes

The ability of the HaCaT cells to grow and adhere on the AAO nanoporous membrane, before and after the membrane silanization (a process necessary for the immobilization of antibodies in the inner walls of the nanochannels) was evaluated, as shown in the optical microscope images of Figure A1.2. First of all, bare membranes were evaluated (Figure A1.2B) observing that the cells grew and adhered well on the membranes, keeping their normal morphology which is corroborated by comparison with the control images corresponding to the cell culture on multi-well plates (Figure A1.2A). After the membranes silanization, no detrimental effects were observed, as evidenced in Figure A1.2C, suggesting that cell culturing can be performed without affecting their normal physiology, included the PTHrP secretion.

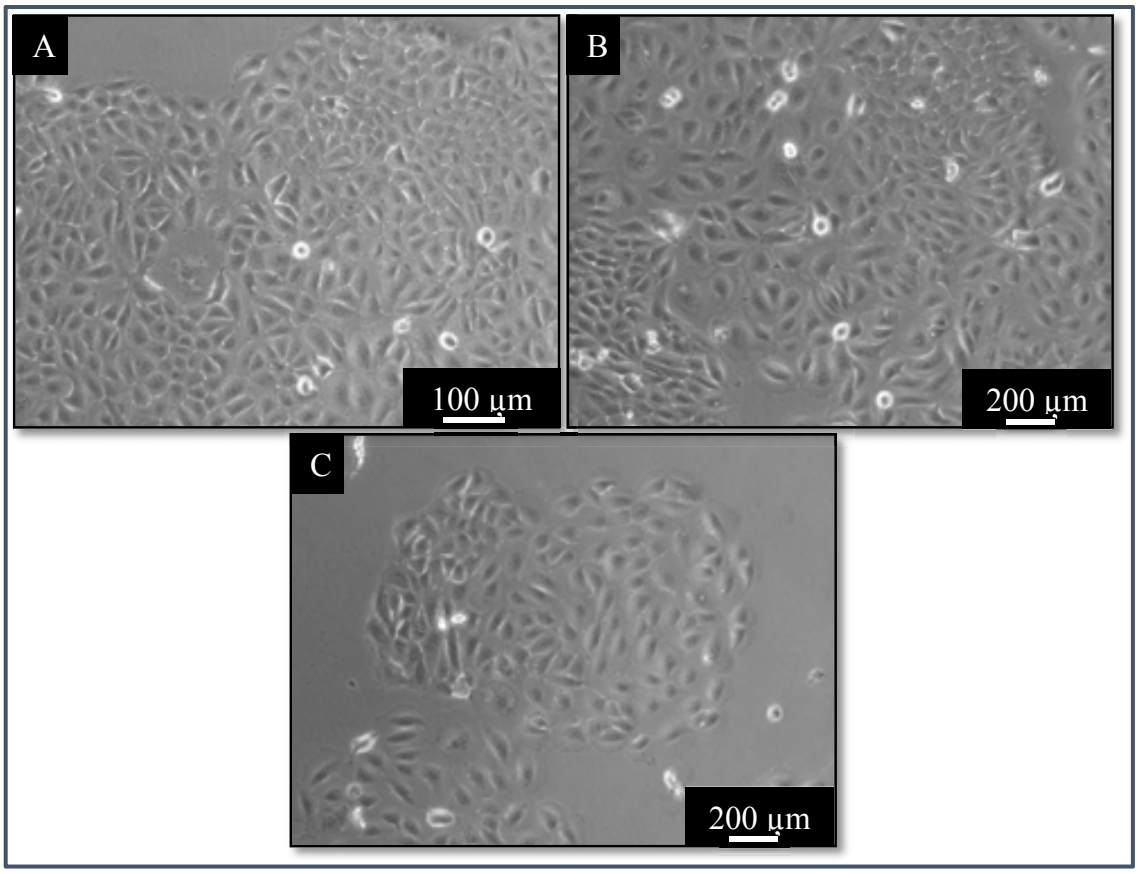

Figure A1.2 Optical microscope images (top view) of HaCaT cell cultures on: (A) multi well plate, (B) bare AAO nanoporous membrane and (C) silanized AAO nanoporous membrane. Cultures performed at 37 ºC in humidified atmosphere of 95% air and 5% CO_2.

SEM analysis was used for a more accurate evaluation of the cultured cells on the silanized membranes. As shown in Figure A1. 3, cells are adhered on the membranes through their filamental appendixes, keeping the nanochannels free for the PTHrP entering and capturing by the antibodies immobilized inside the channels.

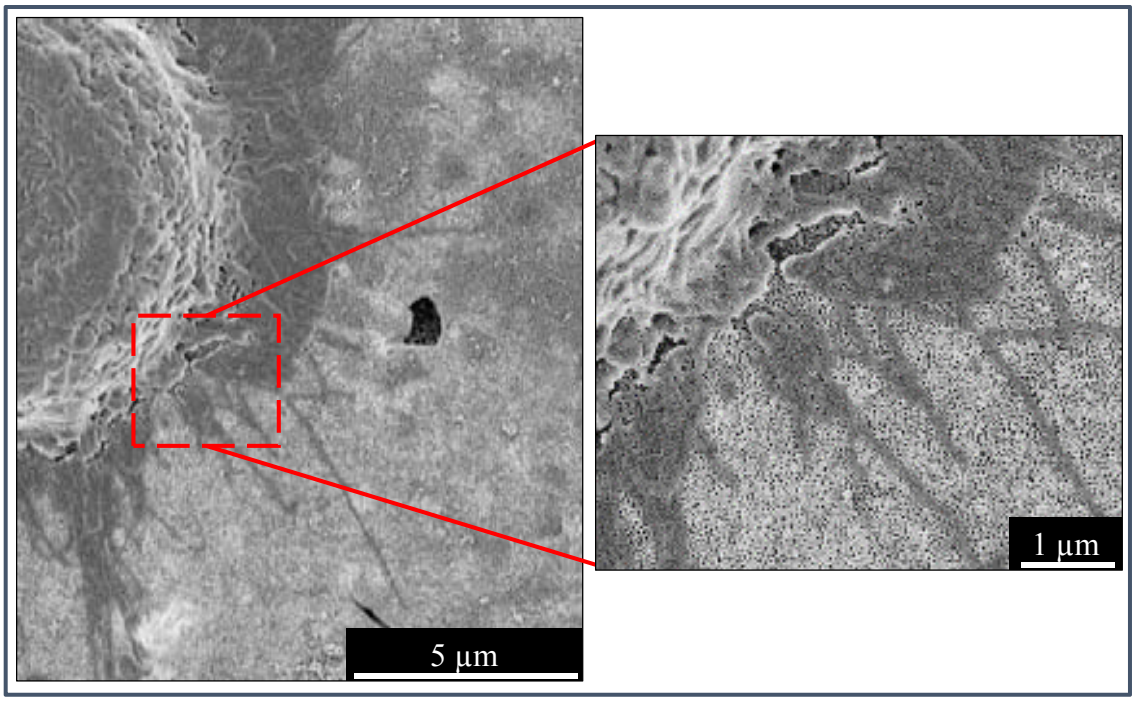

Figure A1.3. SEM images (top view) of the HaCaT cells cultured onto the surface of a silanized AAO nanoporous membrane. Culture performed at 37 ºC in humidified atmosphere of 95% air and 5% CO_2.

A1.5.2. Optimization of the set-up for the in-situ cell culture/electrochemical detection

The proposed design of the set-up for the in-situ cell culture/electrochemical detection is detailed in Figure A1.4.

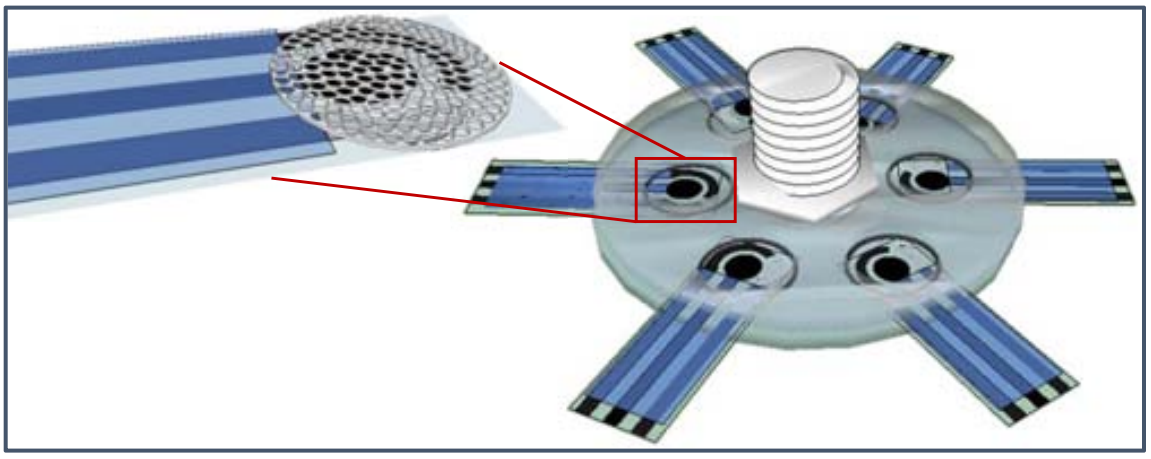

Figure A1.4 Pictures of the proposed set-up for the in-situ cell culture/electrochemical detection. Homemade methacrylate parts and the whole electrochemical cell set-up for six samples are shown.

Different materials were evaluated for the building of this electrochemical cell set-up (AAO membranes assembled to SPCEs) so as to find the best conditions, which allow the cell culture to grow normally, without exerting any toxic effect.

The compatibility of the different materials listed in Table A1.1, with the normal cell growth was evaluated. Optical microscope images of the cell cultures obtained under the conditions detailed in section A.1.4.3 are shown in Figure A1.5. Just after adding the cells (time 0), their presence in suspension is observed in all cases. After 3 hours, the cells begin to adhere on the multi-well plate in the presence of nylon and PETG, while in presence of PMMA cell adhesion was not observed at all, suggesting the non-compatibility of this material with the normal cell grow and adhesion.

After 9 hours, cells adhesion was only observed in the presence of nylon and PETG. These results suggest that an electrochemical cell made of nylon or PETG is required to perform the cell culture on the AAO nanoporous membranes assembled to the SPCE.

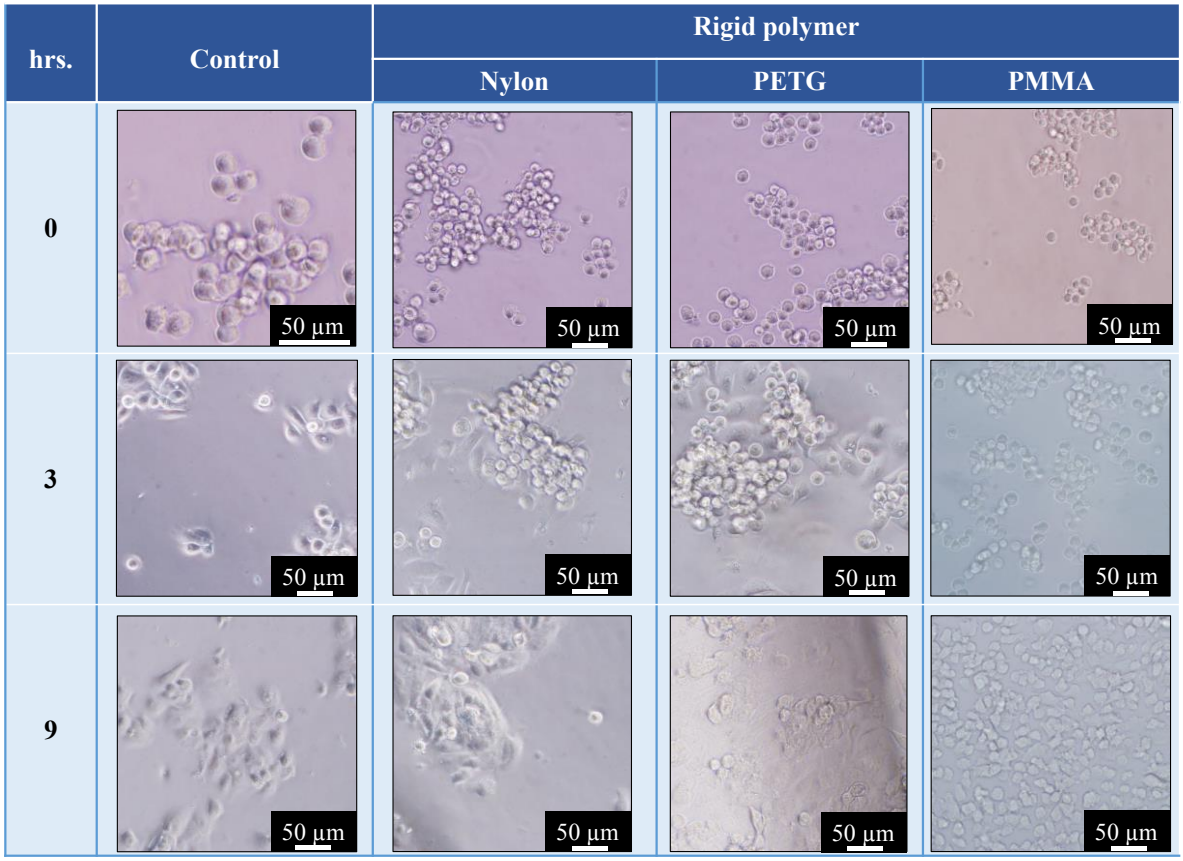

Figure A1.5 Optical microscopy images of HaCaT cell cultures in multi-well plates in the absence (control) and the presence of different rigid polymers for different culture times (0, 3 and 9 hours). Cultures were performed at 37 ºC in humidified atmosphere of 95% air and 5% CO_2.

In the case of the flexible rings, as shown in Figure A1.6, RS and NS were found as the best materials, suggesting that the ring used for defining the working area of the electrode and avoiding liquid leakage must be made of one these materials.

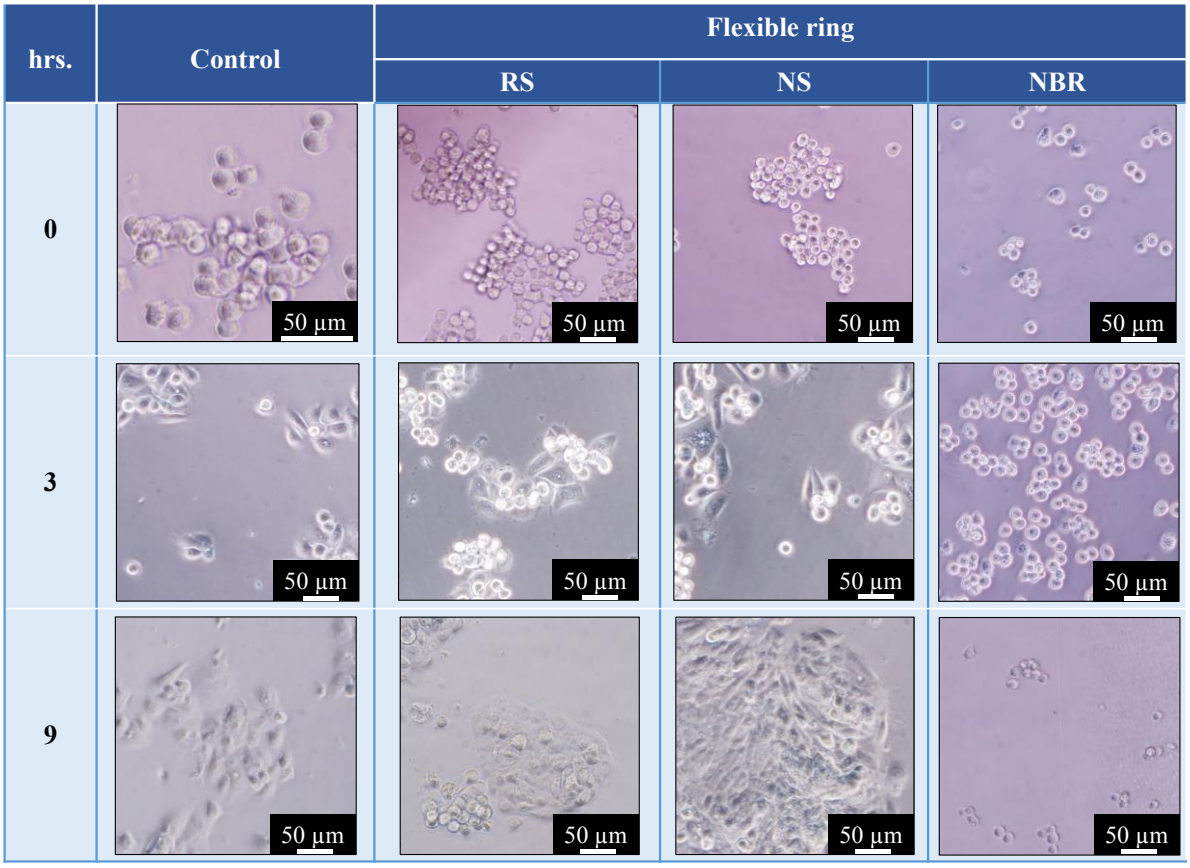

Figure A1.6. Optical microscopy images of HaCaT cell cultures in multi-well plates in the absence (control) and the presence of different flexible rings for different culture times (0, 3 and 9 hours). Cultures were performed at 37 ºC in humidified atmosphere of 95% air and 5% CO_2.

A1.5.3. Electrochemical detection of PTHrP in cell culture medium

As previously explained, preliminary experiments so as to evaluate the ability of our sensing system to detect the presence of PTHrP in the complex matrix of the cell culture medium were performed. Standards of PTHrP suspensions were spiked in such a medium as detailed in section A.1.4.4. The electrochemical measurements were performed using the same set-up as the detailed in **Chapter 5**.

As shown in Figure A1.7, it was found that this system responds to protein levels of 50 ng/mL, being this response proportional to protein concentrations up to 500 ng/mL. These results are similar to those obtained in PBS buffer medium, suggesting that the matrix of the cell culture is not affecting the biosensing response. This could be mainly thanks to the

filtering effect of the nanoporous membranes which allow to remove interferences that could affect the analytical signal.

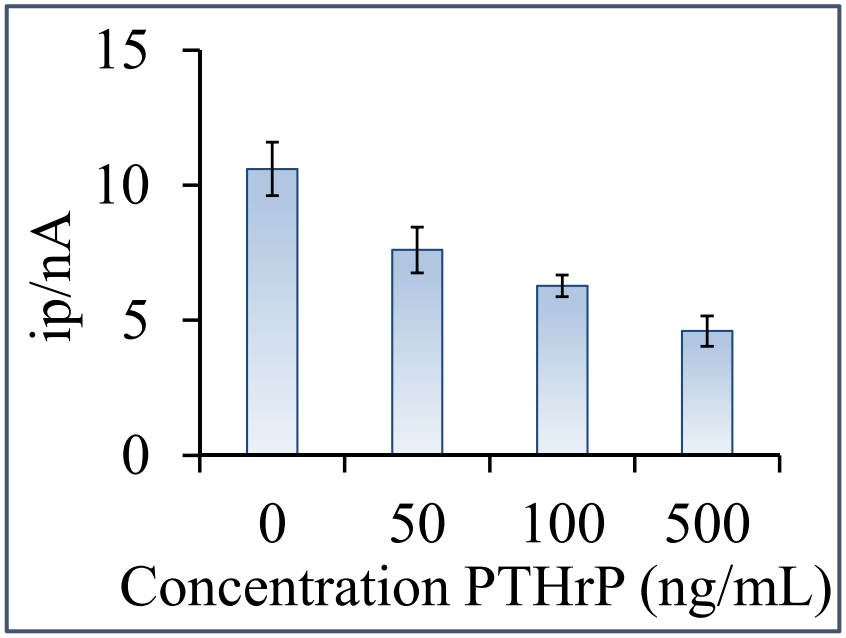

Figure A 1.7. Analytical signals obtained for different standard PTHrP concentrations spiked into HaCaT cell culture medium.

A1.6. Conclusions and futures perspectives

Preliminary studies for the future application of the biosensing system based on the use of nanochannels for the *in-situ* detection of biomarkers secreted by cell cultures have been performed. The ability of HaCaT cells (chosen as model due to their continuous production of PTHrP) to grow and adhere on the silanized AAO nanoporous membranes has been demonstrated.

Furthermore, the compatibilities of different materials with the cell culture so as to find the optimum for building the in-situ cell culture/electrochemical detection set-up system, without damaging the cells have been evaluated.

Finally, PTHrP spiked in cell culture medium has been detected using the previously developed nanochannels-based sensing system, obtaining a similar performance as in PBS buffer, demonstrating the ability of the developed sensing system to detect the presence of this biomarker in a real clinical scenario.

This work is in progress in our laboratories. This consists in the *in-situ* detection of the PTHrP secreted by the HaCaT cells cultured onto AAO nanoporous membranes, using the set-up optimized in this chapter, based on a PETG polymer-based electrochemical cell using natural silicone (NS) rings.

A1.7. References

(1) Lam, M. H.; Olsen, S. L.; Rankin, W. a; Ho, P. W.; Martin, T. J.; Gillespie, M. T.; Moseley, J. M. PTHrP and Cell Division: Expression and Localization of PTHrP in a Keratinocyte Cell Line (HaCaT) during the Cell Cycle. J. Cell. Physiol. 1997, 173, 4334–4346.

(2) Suva, L. J.; Winslow, G. A.; Wettenhall, R. E.; Hammonds, R. G.; Moseley, J. M.; Diefenbach-Jagger, H.; Rodda, C. P.; Kemp, B. E.; Rodriguez, H.; Chen, E. Y. A Parathyroid Hormone-Related Protein Implicated in Malignant Hypercalcemia: Cloning and Expression. Science. 1987, 237, 893–896.

(3) Luparello, C. Parathyroid Hormone-Related Protein (PTHrP): A Key Regulator of Life/Death Decisions by Tumor Cells with Potential Clinical Applications. Cancers (Basel). 2011, 3, 396–407.

(4) Burtis, W. J.; Fodero, J. P.; Gaich, G.; Debeyssey, M.; Stewart, A. F. Preliminary Characterization of Circulating Amino- and Carboxy-Terminal Fragments of Parathyroid Hormone-Related Peptide in Humoral Hypercalcemia of Malignancy. J. Clin. Endocrinol. Metab. 1992, 75, 1110–1114.

(5) Burtis, W. J.; Brady, T. G.; Orloff, J. J.; Ersbak, J. B.; Warrell, R. P.; Olson, B. R.; Wu, T. L.; Mitnick, M. E.; Broadus, A. E.; Stewart, A. F. Immunochemical Characterization of Circulating Parathyroid Hormone-Related Protein in Patients with Humoral Hypercalcemia of Cancer. N. Engl. J. Med. 1990, 322, 1106–1112.

(6) Hopyan, S.; Gokgoz, N.; Poon, R.; Gensure, R. C.; Yu, C.; Cole, W. G.; Bell, R. S.; Jüppner, H.; Andrulis, I. L.; Wunder, J. S.; Alman, B. a. A Mutant PTH/PTHrP Type I Receptor in Enchondromatosis. Nat. Genet. 2002, 30, 306–310.

(7) Lu, Y.; Xiao, G.; Galson, D. L.; Nishio, Y.; Mizokami, A.; Keller, E. T.; Yao, Z.; Zhang, J. PTHrP-Induced MCP-1 Production by Human Bone Marrow Endothelial Cells and Osteoblasts Promotes Osteoclast Differentiation and Prostate Cancer Cell Proliferation and Invasion in Vitro. Int. J. cancer. 2007, 121, 724–733.

(8) Grill, V.; Ho, P.; Body, J. J.; Johanson, N.; Lee, S. C.; Kukreja, S. C.; Moseley, J. M.; Martin, T. J. Parathyroid Hormone-Related Protein: Elevated Levels in Both Humoral Hypercalcemia of Malignancy and Hypercalcemia Complicating Metastatic Breast Cancer. J. Clin. Endocrinol. Metab. 1991, 73, 1309–1315.

(9) Heath, J. K.; Southby, J.; Fukumoto, S.; O'Keeffe, L. M.; Martin, T. J.; Gillespie, M. T. Epidermal Growth Factor-Stimulated Parathyroid Hormone-Related Protein Expression Involves Increased Gene Transcription and mRNA Stability. Biochem. J. 1995, 307, 159–167.

(10) Nakchbandi, I.; Weir, E.; Insogna, K.; Philbrick, W.; Broadus, A. Parathyroid Hormone-Related Protein Induces Spontaneous Osteoclast Formation via a Paracrine Cascade. Proc. Natl. Acad. Sci. 2000, 97, 7296–7300.

(11) Bíró, T.; Szabo, I.; Kovács, L.; Hunyadi, J.; Csernoch, L. Distinct Subpopulations in HaCaT Cells as Revealed by the Characteristics of Intracellular Calcium Release Induced by Phosphoinositide-Coupled Agonists. Arch. Dermatol. Res. 1998, 270–276.

Annex 2.

Nanoimprint lithography for nanochannels creation on ITO/PET electrodes

Annex A2. Nanoimprint lithography for nanochannels creation on ITO/PET electrodes

A2.1. Introduction

Solid-state nanochannel arrays for molecular sensing can be easily prepared with great control using nanoimprint lithography (NIL). Well-established lithographic techniques have been used to create negative masters of the pores, which are subsequently cast into polymeric slabs [1]. Improved approaches have also been reported based on the fabrication of well-defined nanostructures for nanopatterning using self-assembly of block copolymers [2] (BCPs), which is of great interest due to the flexibility, simplicity, and low-cost of the process together with the possibility of tuning the dimensions and chemical properties [3–8].

Furthermore, the recent advances and improvements in the soft lithographic molding in terms of both the absolute sizes and aspect ratios of molded features that it can generate have made this technique an interesting alternative for the production of nanochannel arrays [9,10]. The most representative example of soft lithographic molding is the so called Nanoimprint lithography (NIL). It is a low cost nanolithography process with high resolution and high throughput which allows to create patterns in the nanoscale by modification of a thin polymer film (mechanical deformation of the resist) using a template (mold, stamp) containing the micro/nanopattern (typically made of PDMS, silicon or quartz) followed by a thermo-mechanical or UV curing process [11,12]. In other words, NIL uses the direct contact between the mold and the thermoplastic or UV-curable resist to imprint (or replicate) the pattern so unlike optical lithography, it doesn't require expensive and complex optics and light sources to print nanostructures.

This technology is ideal for nanochannels formation onto flexible substrates, such as ITO/PET electrodes with the objective of obtaining an integrated biosensing system based on the sensing principle detailed in C**hapters 4 and 5**.

A2.2. Objective

The main objective of this work consists on the design and development of an integrated sensing platform based on ITO/PET electrodes modified with nanochannels using nanoimprint lithography (NIL). The three-electrode system would be completed using screen-printing technology for the printing of counter and reference electrodes **(see Chapter 4**).

The as-prepared sensing platform would overcome most of the limitations of the previously developed nanochannels-based sensing systems (**see Chapter 5**) since it would be: 1) more integrated: nanochannels will be directly created onto the electrotransducer surface; 2) more sensitive: thickness of nanochannels will range in the nanoscale.

A2.3. Experimental section

A2.3.1. Reagents and materials

Indium tin oxide coated polyethylene terephthalate (ITO/PET) sheets (surface resistivity 60 Ω/sq) and acetone were purchased from Sigma-Aldrich (Spain). mr-UVcur21-300 nm photocurable polymer was purchased from Micro resist technology GmbH (Germany). Poly(dimethylsiloxane) (PDMS) was purchased from Santa Cruz Biotechnology (Germany).

Stamps made of silicon with pillar of diameter 350 nm and pitch 700 nm geometry were prepared at the Centre Nacional de Microelectrónica (CNM-CSIC) (Barcelona, Spain).

A2.3.2. Apparatus

A 60 W plasma cleaner (Harrick Plasma, United States) was used for the pre-treatment of the ITO/PET substrates. A DELTA 20 model BLE spin coater (England) was used with the aim of depositing a thin film of photocurable polymer on ITO/PET substrates. A scanning electron microscope (FEI Quanta 650 FEG ESEM) was used for the optical characterization of the printed substrates, without any pre-treatment.

A homemade stainless-steel chamber with a quartz window was used for the imprinting applying pressure and irradiating UV-light. For this purpose, a compressed air machine and a UV-lamp were coupled to the chamber.

A2.4. Methods

A2.4.1. Polymer deposition on ITO/PET

ITO/PET substrate was pre-treated with oxygen plasma (2 minutes, 18W) to make it more hydrophilic and facilitate the photocurable polymer deposition. After that, 2 mL of photocurable polymer were placed onto the surface of a 4 x 4 cm piece of ITO/PET substrate and homogeneously spread by spin coating during 1 min at 2000 rpm. Under these conditions, a photocurable polymer thin layer of around 300 nm was obtained.

A2.4.2. Nanoimprinting procedure

The experimental procedure followed for printing channels is schematized in Figure A2.1. The ITO/PET substrate modified with the photocurable polymer thin layer (A) is placed inside the curing chamber together with the PDMS stamp (B). After closing the chamber, a pressure of 2 bar is first applied during 1 minute, followed by UV-light irradiation (365 nm of wavelength) during 1 minute (while applying the pressure). Finally the stamp was removed (C) and the photocurable polymer residual layer was later removed by reactive-ion etching (RIE) at 50 W during 1 minute (D).

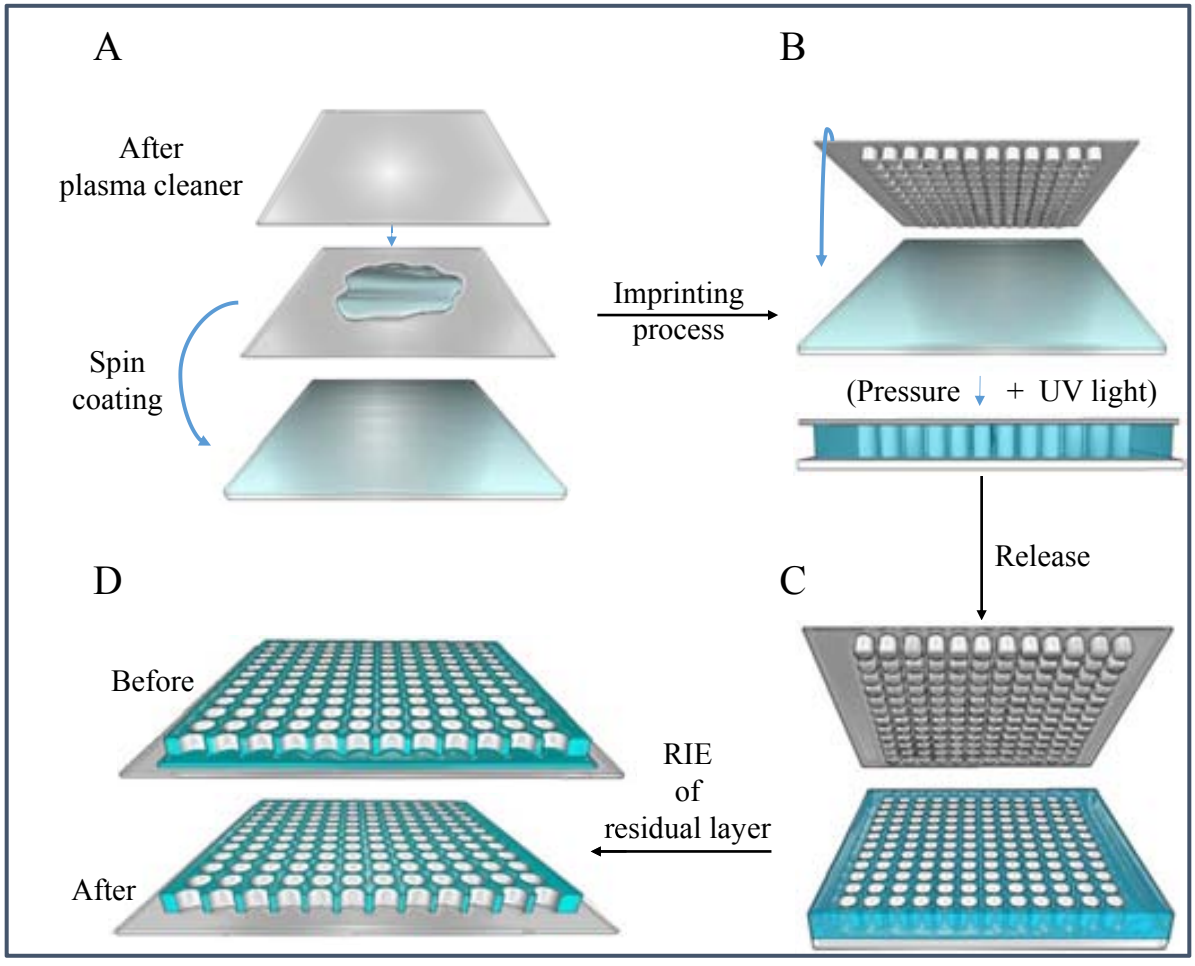

Figure A2.1 Schematic representation of the Nanoimprinting lithography procedure. (A) Photocurable polymer deposition onto ITO/PET substrate. (B) Imprinting of the stamp motives applying pressure and irradiating UV-light. (C) Demolding step. (D) Removing of the residual layer by reactive ion etching (RIE).

A2.5. Results and discussion

Different stamp materials (i.e. PDMS, Quarz, Silicon) and geometries (i.e. channels and holes) in combination with the use of a photocurable polymer (mr-UVcur21-300nm) were evaluated. Furthermore, the main parameters related to the photocurable polymer deposition on the ITO/PET substrate (pretreatment, spin coating velocity/time, baking of the substrate) and the nanoimprint process (pressure, time) so as to obtain an homogenous printing of nanochannels on the substrate were optimized (data not shown).

The best results were obtained using the materials and conditions detailed in methods section and summarized in Table A2.1.

Stamp	Substrate	Plasma Pretreatment Time/power	Pre baking	Velocity of spin coater/rpm	Pressure	UV/time
PDMS/pillars	ITO/PET	2 min/18 W	No	2000	4 bar.	2 min

Table A2.1 Optimized conditions and materials for the photocurable polymer deposition and nanoimprinting processes.

A PDMS stamp with pillars geometry was found as optimum for printing large areas of nanochannels as observed in the SEM images shown in Figure A2.2

Areas of around 40 X 40 µm without any defect with a minimum residual layer of approximately 55 ± 3 nm were obtained. The diameter of the nanochannels was of around 350 ± 3nm with a thickness of 200 ± 3 nm (see Figure A2.2A).

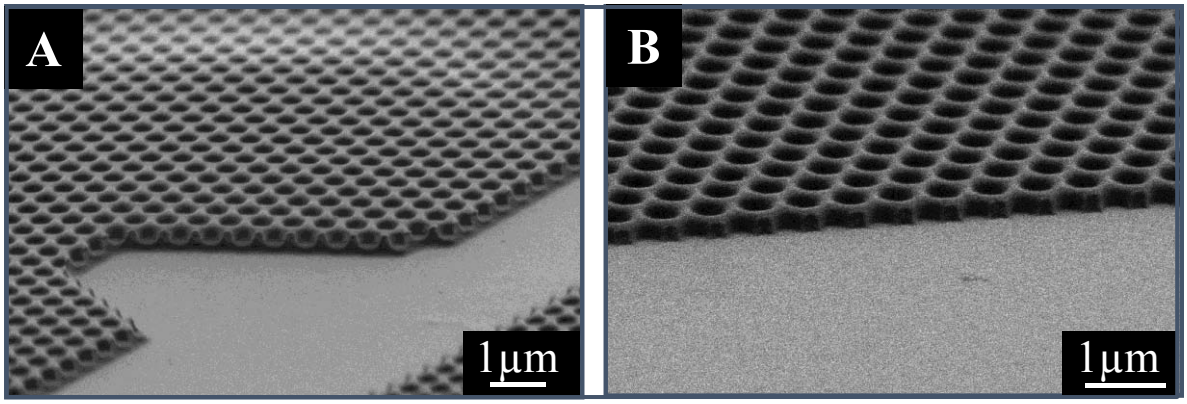

Figure A2.2 SEM images of (A) Nanochannels printed on the ITO/PET substrate and (B) the same sample after RIE treatment to remove the photocurable polymer residual layer. Experimental conditions are detailed in Table A2.1.

A crucial point for the further application of these nanochannel-modified electrodes in biosensing consists in the removing of the residual layer, so as to open the nanochannels and be able to allow electroactive species to be in contact with the electrode in future applications. This was performed by reactive ion etching (RIE) technology used in microfabrication. It uses chemically reactive plasma to remove the material deposited onto wafers. The plasma is generated under low pressure (vacuum) by an electromagnetic field. High-energy ions from the plasma attack the wafer surface and react with it. In our approach, the plasma power was 50w.

Under the above mentioned optimized conditions, the photocurable polymer residual layer was successfully removed, as shown in Figure A2.2B. These strict conditions are critical, so as to only remove a thin layer of polymer, keeping the nanochannels structure unaltered.

In spite of some promising results, large areas with defects in the imprinting are obtained, as shown in Figure A2. 3.

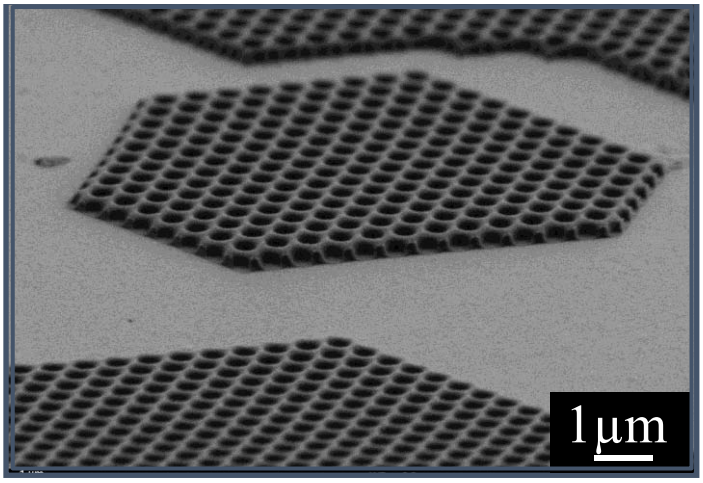

Figure A2. 3 SEM image of an ITO/PET area with defects after the nanoimprint process.

These large areas without printed channels represent a key limitation for the intended use as biosensing platform. These defects can be mainly due to small dust particles trapped between the photocurable polymer. It is also important to optimize the set-up to prevent the air bubbles formation. Finally, the use of smaller stamps could also facilitate the homogeneity of the printed nanochannels.

A2.6. Conclusions and future perspectives

Nanoimprint lithography (NIL) has been applied for the creation of nanochannels on ITO/PET substrates, using PDMS stamps and a photocurable polymer. Areas of around 40 x 40 µm have been successfully printed with nanochannels of around 350 nm in diameter and 200 nm in depth. Residual photocurable polymer layers have also been successfully removed by RIE treatment, allowing to obtain open nanochannels.

However, large areas with defects are still obtained probably due to to small dust particles trapped between the photocurable polymer. Air bubbles were also formed, avoiding the

obtaining of large homogeneous printed areas. Alternative methodologies are currently being optimized in our laboratory so as to obtain larger printed areas which could allow its use as integrated biosensing platforms.

A2.7. References

(1) Saleh, O. a.; Sohn, L. L. An Artificial Nanopore for Molecular Sensing. Nano Lett. 2003, 3, 37–38.

(2) Simao, C.; Khunsin, W.; Kehagias, N.; Salaun, M.; Zelsmann, M.; Morris, M. A.; Sotomayor Torres, C. M. Order Quantification of Hexagonal Periodic Arrays Fabricated by in Situ Solvent-Assisted Nanoimprint Lithography of Block Copolymers. Nanotechnology. 2014, 25, 175703.

(3) Cheng, J. Y.; Ross, C. a.; Smith, H. I.; Thomas, E. L. Templated Self-Assembly of Block Copolymers: Top-Down Helps Bottom-Up. Adv. Mater. 2006, 18, 2505–2521.

(4) He, J.; Sill, K.; Xiang, H. Self-Directed Self-Assembly of Nanoparticle / Copolymer Mixtures. 2005, 55–59.

(5) Park, S.; Kim, B.; Wang, J.-Y.; Russell, T. P. Fabrication of Highly Ordered Silicon Oxide Dots and Stripes from Block Copolymer Thin Films. Adv. Mater. 2008, 20, 681–685.

(6) Olson, D. a.; Chen, L.; Hillmyer, M. a. Templating Nanoporous Polymers with Ordered Block Copolymers. Chem. Mater. 2008, 20, 869–890.

(7) Yang, S. Y.; Yang, J.-A.; Kim, E.-S.; Jeon, G.; Oh, E. J.; Choi, K. Y.; Hahn, S. K.; Kim, J. K. Single-File Diffusion of Protein Drugs through Cylindrical Nanochannels. ACS Nano 2010, 4, 3817–3822.

(8) Chao, C.; Wang, T.; Ho, R.; Georgopanos, P.; Avgeropoulos, A.; Thomas, E. L. Robust Block Copolymer Mask for Nanopatterning Polymer Films. ACS Nano 2010, 4, 2088–2094.

(9) Pokroy, B.; Epstein, A. K.; Persson-Gulda, M. C. M.; Aizenberg, J. Fabrication of Bioinspired Actuated Nanostructures with Arbitrary Geometry and Stiffness. Adv. Mater. 2009, 21, 463–469.

(10) Lipomi, D. J.; Kats, M. A.; Kim, P.; Kang, S. H.; Aizenberg, J.; Capasso, F.; Whitesides, G. M. Fabrication and Replication of Arrays of Single- or Multicomponent Mechanical Sectioning. ACS Nano 2010, 4, 4017–4026.

(11) Lan, H.; Ding, Y. Nanoimprint Lithography. In Lithography; Wang, M., Ed.; In Tech: Croatia, 2010; pp. 458–494.

(12) Guo, L. J. Nanoimprint Lithography: Methods and Material Requirements. Adv. Mater. 2007, 19, 495–513.